JGP Journal of General Physiology

ARTICLE

Synchrony of sarcomeric movement regulates left ventricular pump function in the in vivo beating mouse heart

Fuyu Kobirumaki-Shimozawa[1*], Togo Shimozawa[2*], Kotaro Oyama[1,3*], Shunsuke Baba[4], Jia Li[5], Tomohiro Nakanishi[1], Takako Terui[6], William E. Louch[5,7], Shin'ichi Ishiwata[8], and Norio Fukuda[1]

Sarcomeric contraction in cardiomyocytes serves as the basis for the heart's pump functions. It has generally been considered that in cardiac muscle as well as in skeletal muscle, sarcomeres equally contribute to myofibrillar dynamics in myocytes at varying loads by producing similar levels of active and passive force. In the present study, we expressed α-actinin–AcGFP in Z-disks to analyze dynamic behaviors of sequentially connected individual sarcomeres along a myofibril in a left ventricular (LV) myocyte of the in vivo beating mouse heart. To quantify the magnitude of the contribution of individual sarcomeres to myofibrillar dynamics, we introduced the novel parameter "contribution index" (CI) to measure the synchrony in movements between a sarcomere and a myofibril (from −1 [complete asynchrony] to 1 [complete synchrony]). First, CI varied markedly between sarcomeres, with an average value of ∼0.3 during normal systole. Second, when the movements between adjacent sarcomeres were asynchronous (CI < 0), a sarcomere and the ones next to the adjacent sarcomeres and farther away moved in synchrony (CI > 0) along a myofibril. Third, when difference in LV pressure in diastole and systole (ΔLVP) was lowered to <10 mm Hg, diastolic sarcomere length increased. Under depressed conditions, the movements between adjacent sarcomeres were in marked asynchrony (CI, −0.3 to −0.4), and, as a result, average CI was linearly decreased in association with a decrease in ΔLVP. These findings suggest that in the left ventricle of the in vivo beating mouse heart, (1) sarcomeres heterogeneously contribute to myofibrillar dynamics due to an imbalance of active and passive force between neighboring sarcomeres, (2) the force imbalance is pronounced under depressed conditions coupled with a marked increase in passive force and the ensuing tug-of-war between sarcomeres, and (3) sarcomere synchrony via the distal intersarcomere interaction regulates the heart's pump function in coordination with myofibrillar contractility.

Introduction

Myocardial sarcomeres repeat shortening and lengthening in vivo at a heart rate (HR) that is dependent on the animal species. A sarcomere length (SL) change of merely ∼100 nm dramatically changes the heart's pump functions, indicating the importance of high-precision tracking of individual sarcomere movements along myofibrils in the in vivo beating heart (Kobirumaki-Shimozawa et al., 2014, 2016; Shimozawa et al., 2017).

Recent advances in optical fluorescence technologies have enabled measurements of SL at high spatial and temporal resolution in cardiac cells by using various techniques, such as expression of GFP derived from *Aequorea coerulescens* (AcGFP; Shintani et al., 2014) or Cameleon-Nano140 (Tsukamoto et al., 2016) in Z-disks, binding of quantum dots to Z-disks (Serizawa et al., 2011), and fluorescence staining of the T-tubules (Bub et al., 2010; Botcherby et al., 2013; Ibarra et al., 2013; Inoue et al., 2013). To our knowledge, Aguirre et al. (2014) were the first to visualize the motions of the fluorescence-labeled T-tubules in the mouse heart upon external electric stimulation under two-photon microscopy

[1]Department of Cell Physiology, The Jikei University School of Medicine, Tokyo, Japan; [2]Technical Division, School of Science, The University of Tokyo, Tokyo, Japan; [3]Quantum Beam Science Research Directorate, National Institutes for Quantum and Radiological Science and Technology, Gunma, Japan; [4]Department of Pediatrics, The Jikei University School of Medicine, Tokyo, Japan; [5]Institute for Experimental Medical Research, Oslo University Hospital and University of Oslo, Oslo, Norway; [6]Department of Anesthesiology, The Jikei University School of Medicine, Tokyo, Japan; [7]K.G. Jebsen Center for Cardiac Research, University of Oslo, Oslo, Norway; [8]Department of Physics, Faculty of Science and Engineering, Waseda University, Tokyo, Japan.

*F. Kobirumaki-Shimozawa, T. Shimozawa, and K. Oyama contributed equally to this work; Correspondence to Norio Fukuda: noriof@jikei.ac.jp; Fuyu Kobirumaki-Shimozawa: kobirumaki@jikei.ac.jp.

following reconstruction of the original images. However, large movements of the contracting heart per se hindered nanoscale analyses of inter–T-tubular distances. Moreover, T-tubule positions may deviate from Z-disks when the heart is at work, especially in diseased conditions (see Guo et al., 2013 and references therein). To solve these problems, we previously developed a high-precision in vivo real-time cardiac nanoimaging system for use in the left ventricle of mice via expression of AcGFP in Z-disks, enabling SL analyses at 20-nm (100 frames per s [fps]) precision during the cardiac cycle, simultaneous with electrocardiogram (ECG) and left ventricular (LV) pressure measurements (Kobirumaki-Shimozawa et al., 2016). In this previous work, we reported that (1) the working range of SL exists on the shorter resting distribution side (i.e., ∼1.7–1.9 µm) and (2) the difference in LV pressure in diastole and systole (ΔLVP) is a linear function of sarcomere shortening that occurs on the order of only 100 nm. These data have provided a novel insight into the role of sarcomere dynamics in the regulation of ventricular function in vivo.

It has been perceived that sarcomeres in myofibrils of striated muscle contribute uniformly to the dynamic behavior of muscles under various loaded conditions by generating a similar level of active force (most notably, see Huxley, 1957; Gordon et al., 1966; Huxley and Simmons, 1971). Under this premise, the developed force of a myofibril is simply in proportion to the sum of force-generating cross-bridges in a sarcomere, formed via either Ca^{2+} binding to troponin C or the binding of strongly bound cross-bridges to thin filaments or both (e.g., Fukuda et al., 1998; Kobirumaki-Shimozawa et al., 2014). However, it remains to be elucidated whether sarcomeres along a myofibril do in fact operate uniformly during repeated contractions, especially in the in vivo beating heart. We previously demonstrated that (1) a large variation in SL of as much as ∼300 nm existed along myofibrils (five sarcomeres in two myofibrils analyzed) in both diastole and systole, and (2) although a typical SL waveform (consisting of rapid shortening followed by slow lengthening) appeared after averaging the individual SL signals, individual sarcomeres moved in a rather asynchronous fashion (Kobirumaki-Shimozawa et al., 2016). This finding appears to be consistent with observations made in the tibialis anterior muscle of living mice because SL distribution was observed to become broader (i.e., indicating greater SL nonuniformity) upon electric stimulation at both short (90° ankle flexion) and long (180° ankle flexion) SL (Moo et al., 2017). SL nonuniformity has likewise been reported at the cardiomyocyte level. For example, Sarai et al. (2002) reported that SL distribution is inhomogeneous in isolated rat cardiomyocytes even under the resting condition. Weiwad et al. (2000) showed, in isolated skinned rat cardiomyocytes, that SL nonuniformity is increased upon an increase in the Ca^{2+} concentration at SL >2.5 µm. Most recently, by taking advantage of SL nanometry, we demonstrated that although Ca^{2+} transients are synchronized in single sarcomeres along a myofibril, timings of individual SL shortening and lengthening vary markedly in rat cultured myocytes expressed with Cameleon-Nano140 in Z-disks (Tsukamoto et al., 2016).

In the present study, we focused on the dynamic behaviors of sarcomeres and systematically investigated how individual sarcomere movements generate organized contractions of a myofibril in an LV myocyte in the in vivo beating mouse heart. We analyzed sequentially connected individual sarcomeres (up to 35) in mice with varying levels of ΔLVP. Accordingly, we found that ΔLVP was a function of the magnitude of sarcomere synchrony caused via distal interactions along a myofibril. Physiological implications, focusing on the role of titin (connectin), are discussed.

Materials and methods

This study was performed in accordance with the Guidelines on Animal Experimentation of The Jikei University School of Medicine. The study protocol was approved by the Animal Care Committee of The Jikei University School of Medicine and the Recombinant Gene Research Safety Committee of The Jikei University School of Medicine. All experiments were performed at The Jikei University School of Medicine.

α-Actinin–AcGFP expression in the heart of living mice in vivo

Adenovirus vector (ADV) was constructed based on our previous studies (Kobirumaki-Shimozawa et al., 2016, 2018, 2020). In brief, recombinant adenoviruses encoding mouse α-actinin-3–AcGFP (Genbank/European Molecular Biology Laboratory/DNA Data Bank of Japan accession no. NM_013456) were constructed using the AdMax ADV creation kit (Microbix Biosystems). The ADV was then purified using the Vivapure AdenoPACK 20 purification kit (Sartorius) and concentrated by ultrafiltration to yield 1×10^{11} to 1×10^{12} viral particles/ml in PBS (−) (as in Kobirumaki-Shimozawa et al., 2016). ADV was stored at −80°C for up to 2 mo. ADV was injected into the surface of the left ventricle of male BALB/c mice (aged 3–8 wk) anesthetized with ∼2% isoflurane during ventilation (Kobirumaki-Shimozawa et al., 2016). In brief, left thoracotomy was performed in order to visualize the anterior surface of the left ventricle under ventilation (first surgery). The animal body temperature was maintained at 38°C. PBS (−) containing ADV at various viral titers was injected into the epicardial surface of the central region of the left ventricle (10 µl in ∼3 × 3 mm^2; ∼10 spots) using a 1-ml syringe pump with a 32-gauge needle. To analyze the movements of individual single sarcomeres at the highest possible precision in a target myocyte, we decreased the number of α-actinin-AcGFP–expressing myocytes to a minimum, based on our previous study (Kobirumaki-Shimozawa et al., 2018). We previously reported that an ADV injection at 1×10^{11} to 1×10^{12} viral particles/ml does not cause distortion or swelling of the sarcolemma, disarrangement of the T-tubules, or sarcomere shortening (Kobirumaki-Shimozawa et al., 2018). 2 d after chest closure, the mouse was anesthetized again with ∼2% isoflurane and ventilated, and the anterior thoracic wall was removed by cutting the ribs, muscles, and intercostal arteries with an electric scalpel for in vivo cardiac sarcomere nanoimaging (second surgery; see Kobirumaki-Shimozawa et al., 2016 for details). Throughout the present study, mice were euthanized after experiments with an isoflurane overdose (greater than ∼5%).

CellMask treatment

The heart was treated with the plasma membrane stain CellMask Orange (CellMask; Thermo Fisher Scientific) based on our previously published treatment method (Kobirumaki-Shimozawa et al., 2018). See Materials and methods in the supplemental text at the end of the PDF for details.

Echocardiography

Noninvasive transthoracic echocardiograms were performed based on previous reports (Nadadur et al., 2016; Lindsey et al., 2018; see Materials and methods in the supplemental text for details). Also see Results and discussion I in the supplemental text, Fig. S1, and Table S1.

Microscopic system

Our microscopic system for in vivo nanoimaging was described in detail in our previous studies (Kobirumaki-Shimozawa et al., 2016; Shimozawa et al., 2017). In brief, an upright microscope (BX-51WI; Olympus Co.) combined with a Nipkow confocal scanner (CSU21; Yokogawa Electric Co.) and an electron-multiplying charge-coupled device camera (iXonEM+; Andor Technology Ltd.) were used at a 512 × 170–pixel resolution at an exposure time of 9.8 ms. A 60× water immersion lens (LUMPLFLN 60×W, numerical aperture 1.00; Olympus Co.) was used to visualize the LV surface. α-Actinin-AcGFP–expressing myocytes in the left ventricle were excited by a 488-nm laser light (HPU50211-PFS; Furukawa Electric Co.), and the resultant fluorescence signals were detected by using a BA510–550 bandpass emission filter (Olympus Co.).

In vivo nanoimaging

Nanoimaging was performed in accordance with our previous studies (Kobirumaki-Shimozawa et al., 2016, 2018, 2020; Shimozawa et al., 2017). Briefly, an open-chest mouse anesthetized with ∼2% isoflurane was placed on a custom-made microscope stage (250 × 350 mm) while ventilated, and the animal was warmed to 38°C throughout the cardiac nanoimaging procedure. ECG lead III was recorded by using an amplifier (JB-611J/MEG-6108/AB-611J; Nihon Kohden), and LVP was recorded by a pressure catheter (FTH-1211B-0018; Transonic Systems, Inc.) inserted through the apex of the heart. The ECG and LVP signals and image acquisition timing from the camera were simultaneously recorded by the LabScribe software (iWorx Systems, Inc.) at 5 kHz. ΔLVP was defined as systolic LVP minus diastolic LVP. A coverslip (0.04–0.06-mm thickness, 12-mm diameter, no. 000; Matsunami Glass Ind.) was gently placed on the surface of the central part of the left ventricle (see Fig. S2) using glue (∼2 mm apart, KrazyGlue; Toagosei Co.). The field of view was large enough to allow examination of several myocytes expressing α-actinin-AcGFP (as in Kobirumaki-Shimozawa et al., 2018). The position of the coverslip was carefully controlled using a custom-made micromanipulator (Sigmakoki Co.). The LVP change caused by the coverslip setting procedure is <5%, as addressed in our previous study (Kobirumaki-Shimozawa et al., 2016). The ventilator was turned off during imaging. The precision value for the single SL measurement with the present optical system was 11 nm (100 fps) at a depth of up to ∼150 µm in the α-actinin-AcGFP–expressing left ventricle of the mouse heart in vivo (Fig. S3 and Video 1; cf. Kobirumaki-Shimozawa et al., 2016). In some experiments, mice were anesthetized with ∼5% (or ∼1.5%) isoflurane to depress (or enhance) the heart's pump function (compare Kobirumaki-Shimozawa et al., 2018, 2020); nanoimaging was performed at low (or high) systolic condition. Individual sarcomere movements were analyzed from two to three myofibrils in a myocyte of a mouse. Six mice with various ΔLVP values were used. Cardiac arrest was defined by the absence of an ECG signal.

Analyses

SL analysis was performed in accordance with our previous studies (Kobirumaki-Shimozawa et al., 2016, 2018, 2020; Shimozawa et al., 2017). All data were analyzed using ImageJ software (National Institutes of Health). In brief, SL profiles were analyzed using multipeak Gaussian fitting with a linear function of offset ($Y = aX + b$), based on the Levenberg-Marquardt algorithm, and the lengths of individual sarcomeres were calculated as the distance between the centers of two adjacent peaks (indicating the positions of Z-disks; for details, see Kobirumaki-Shimozawa et al., 2016). The lengths of sequentially connected sarcomeres in a myofibril of interest were measured frame by frame, and, during each cardiac cycle, the time course of changes was obtained for each sarcomere. By using the R statistical analysis software, we obtained correlation coefficient matrices for (1) the average time series of all sarcomeres (average SL) and (2) the time series of each sarcomere (expressed as "no." from left to right along a myofibril), which were shown in heat maps ranging from full positive correlation (dark blue; 1) to full negative correlation (dark red; −1). Throughout the present study, "contribution index" (CI) is defined as the R value (i.e., the correlation coefficient).

Statistics

Linear regression analyses were performed by OriginPro 8.6 (OriginLab). Dunnett's test was performed using the R software (3.6.3, 2020-02-29). Student's two-tailed unpaired t test was performed using Microsoft Excel 2016 MSO (16.0.14026.20304) only for the echocardiographic experiments. Data are expressed as mean ± SD.

Online supplemental material

Fig. S1 shows echocardiographic evaluation of the LV structure and function in mice with and without the first open-chest surgery. Fig. S2 shows the coverslip setting for nanoimaging of sarcomeres on the LV surface in an open-chest mouse. Fig. S3 shows the fluctuation analysis for the length of a single sarcomere in a myocyte in an in vivo mouse heart at rest. Fig. S4 shows the representative data of SL changes in an LV myocyte in a mouse with normal systolic function. Fig. S5 shows scatter plots between average and individual SLs in an LV myocyte of a mouse with normal systolic function (myofibril 1 [M1]). Fig. S6 shows the in vivo tracking of individual sarcomeres in LV myocytes of mice with low systolic function. Fig. S7 shows scatter plots between adjacent sarcomeres in an LV myocyte of a mouse with normal systolic function. Fig. S8 shows the representative

data of time course of changes in individual versus average SLs in an LV myocyte of a mouse with normal systolic function. Fig. S9 shows the representative data of time course of changes in individual SL versus LVP in an LV myocyte of a mouse with normal systolic function. Fig. S10 shows scatter plots between sarcomeres at the same longitudinal positions in neighboring myofibrils in an LV myocyte of a mouse with normal systolic function. Fig. S11 shows scatter plots between average and individual SLs in an LV myocyte of a mouse with normal systolic function (myofibril 2 [M2]). Fig. S12 shows triangular heat maps of the correlation between sarcomeres in sequential cardiac cycles in a mouse with normal systolic function. Fig. S13 shows the fluctuation analysis for the T-tubular distance in a myocyte in an in vivo mouse heart at rest. Fig. S14 shows the in vivo analysis of individual T-tubular distances in an LV myocyte of a mouse. Fig. S15 shows the in vivo tracking of individual sarcomeres along myofibrils in an LV myocyte of a mouse with high systolic function. Fig. S16 shows individual SL distributions in LV myocytes of mice with various systolic functions. Fig. S17 shows the time course of changes in LVP and average SL in an LV myocyte in a mouse under deep anesthesia. Fig. S18 shows the in vivo tracking of individual sarcomeres in a LV myocytes of mice under deep anesthesia. Fig. S19 shows the interplay between sarcomeres connected in series in an LV myocyte of a mouse under deep anesthesia. Fig. S20 shows the in vivo tracking of individual sarcomeres along myofibrils in LV myocytes of mice at various systolic states. Table S1 summarizes echocardiographic data of mice with and without the first open-chest surgery. Table S2 summarizes the average values of CI in sequential cardiac cycles under various contractile conditions. Table S3 summarizes CI, LVP, and HR with CellMask treatment. Table S4 summarizes CI, LVP, and HR under physiological and near-physiological contractile conditions. Video 1 shows an image sequence of a myocyte in the left ventricle of a mouse at rest. Video 2 shows an image sequence of a myocyte in the left ventricle of a mouse with normal systolic function. Videos 3 and 4 show image sequences of a myocyte in the left ventricle of a mouse with low systolic function. Video 5 shows an image sequence of a CellMask-stained myocyte in the left ventricle of a mouse at rest. Video 6 shows an image sequence of a CellMask-stained myocyte in the left ventricle of a mouse. Video 7 shows an image sequence of a myocyte in the left ventricle of a mouse with high systolic function. Videos 8 and 9 show image sequences of a myocyte in the left ventricle of a mouse under deep anesthesia. Additional text at the end of the PDF provides additional information about the methods used in our research.

Results and discussion

First, we analyzed the dynamic behaviors of individual sarcomeres in a myofibril in an LV myocyte of the mouse heart with normal systolic function in vivo. As in our previous studies (Kobirumaki-Shimozawa et al., 2016, 2018, 2020), an ADV injection effectively expressed α-actinin-AcGFP in Z-disks along myofibrils, enabling visualization of clear striation patterns in a myocyte (Fig. 1 A and Video 2). The fluorescent Z-disks were subjected to our multipeak fitting program (see Kobirumaki-Shimozawa et al., 2016) to yield the lengths of individual sarcomeres along a myofibril at various time points during cardiac cycles (Fig. S4). See Results and discussion II in the supplemental text for details.

Fig. 1 B, top, shows the time course of changes in average SL from 30 sequentially connected sarcomeres along a myofibril (i.e., M1 in the yellow-lined rectangle in Fig. 1 A). Average SL measures showed cyclical shortening and lengthening during each of six consecutive cardiac cycles in a manner inversely related to changes in LVP (Fig. 1 B, bottom; ΔLVP, 96.4 ± 4.7 mm Hg; HR, 469 ± 2.9 beats per minute [bpm]; see Table 1). Average diastolic and systolic SLs during six cardiac cycles were 1.85 ± 0.02 μm and 1.70 ± 0.04 μm, respectively (compare 1.97 ± 0.10 μm and 1.72 ± 0.07 μm in diastole and systole, respectively; Kobirumaki-Shimozawa et al., 2016). This is consistent with our previous observation that the working SL range in the central part of the left ventricle exists within the shorter range of the resting SL distribution (1.97 ± 0.20 μm; Kobirumaki-Shimozawa et al., 2016; compare Aschar-Sobbi et al., 2015). We observed a large variation in SL (SD, ∼0.16–0.47 μm) during cardiac cycles, larger than the precision of the single SL measurement under our microscopic system (i.e., 11 nm; see above). We consider that the variation results from asynchronous behaviors of individual sarcomeres (as found in cardiomyocytes; Shintani et al., 2014; Tsukamoto et al., 2016) and not from a lack of resolution (see below for details on asynchronous behaviors of individual sarcomeres).

Fig. 1 C shows the time course of changes in the lengths of 30 individual sarcomeres in M1. Typical examples of plot profiles from confocal images and time-dependent changes in the lengths of sequential sarcomeres are shown in Fig. S4 (sarcomere nos. 1–6; from 0.42 to 0.46 s). Even along the same myofibril, (1) the absolute SL in diastole or systole, as well as the magnitude of change, varied between sarcomeres; (2) individual sarcomere movements did not occur in synchrony; and (3) some sarcomeres (e.g., nos. 3 and 6) moved in opposite directions (see Fig. S4).

Next, in order to investigate whether individual sarcomere movements vary depending on the location in a myofibril (i.e., proximal or distal to the edge [intercalated disc] of a myocyte; cf. Kobirumaki-Shimozawa et al., 2020), we analyzed correlations of individual versus average SLs for M1 on the basis of scatter plots in Fig. S5. Typical examples illustrated in Fig. 1 D show that although most correlations were positive (e.g., no. 1; CI, 0.59), indicating that the sarcomere shortened and lengthened with the same pattern as the overall change in SL, other sarcomeres showed no correlation (no. 8; CI, 0.06) or a negative correlation (no. 20; CI, −0.17). We found that CI varied markedly between sarcomeres, and its magnitude did not depend on the longitudinal position along a myofibril. Because the P value for the slope was <0.05 when CI was >0.2 in Fig. S5, with the exception of sarcomere no. 5 (CI, 0.22; P = 0.066), in the present study, we define the sarcomeres with CI > 0.2 as "contributing sarcomeres" (i.e., sarcomeres that contribute to myofibrillar dynamics).

To summarize the correlation of individual sarcomere movements versus myofibrillar dynamics, we converted scatter

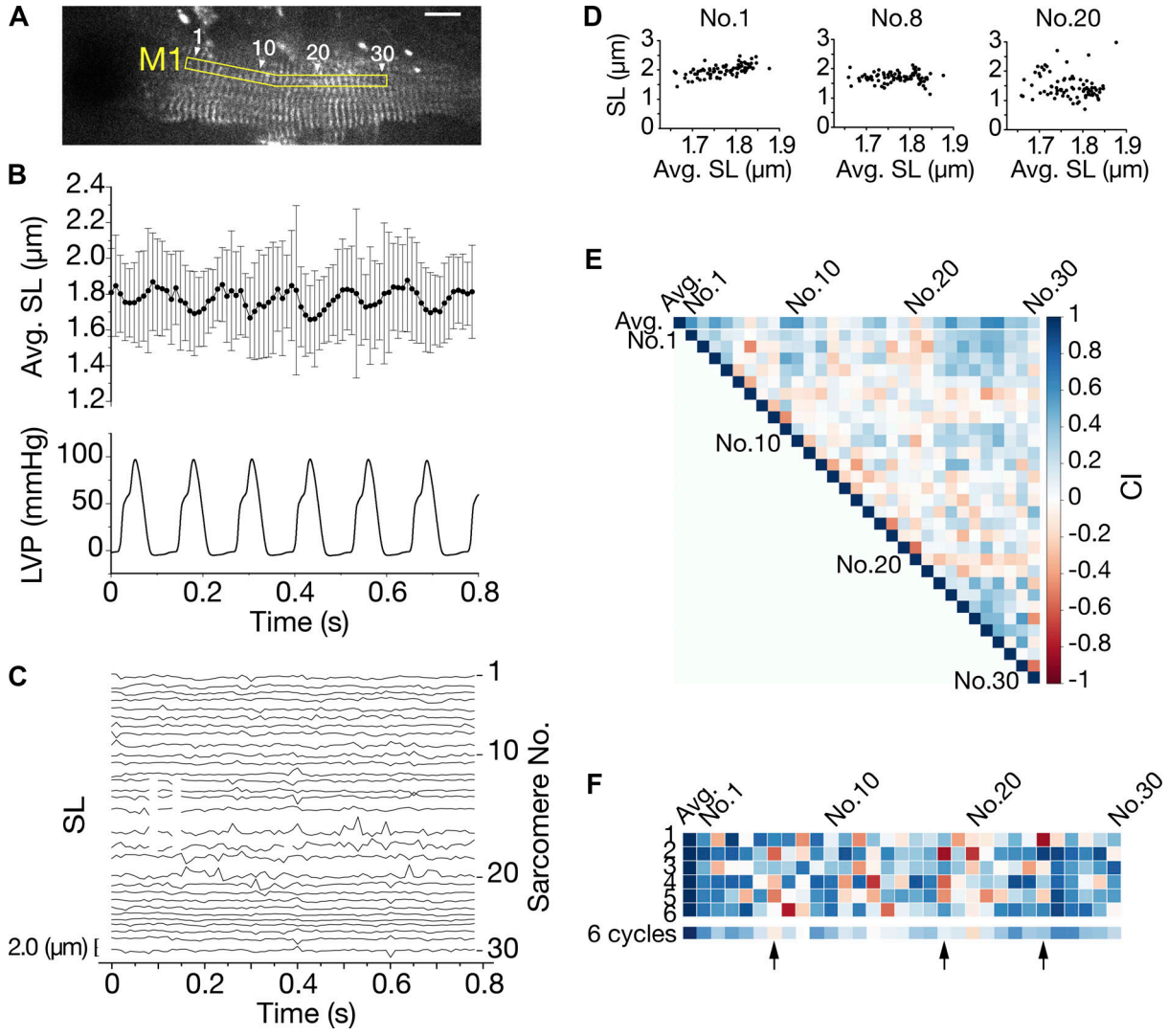

Figure 1. **In vivo tracking of individual sarcomeres along a myofibril in an LV myocyte. (A)** Confocal image of a myocyte expressing α-actinin-AcGFP. Note clear striation patterns along myofibrils. In the yellow-outlined rectangle (M1), 30 sequentially connected sarcomeres in a myofibril were analyzed. Numbers on top of the myofibril indicate longitudinal positions of sarcomeres (i.e., nos. 1–30). Scale bar, 10 µm. See Video 2. **(B)** Time course of changes in average SL (top) and LVP (bottom) during six cardiac cycles (cardiac cycle determined based on LVP recording). Average SL indicates the average of the lengths of 30 sarcomeres in M1. During six cardiac cycles, HR was 469 ± 2.9 bpm, and ΔLVP (systolic LVP minus diastolic LVP) was 96.4 ± 4.7 mm Hg. Error bars for average SL indicate the SD of 30 sarcomeres. **(C)** Time course of changes in the lengths of sarcomere nos. 1–30 (from top downward for sarcomere nos. 1–30; see right) in M1. Note that large, abrupt length changes (e.g., in sarcomere no. 20) are due to irregular movements of the target myocyte and do not reflect SL changes. **(D)** Typical examples of scatter plots showing a positive correlation (no. 1), no correlation (no. 8), and a negative correlation (no. 20) between changes in average and individual SLs during six cardiac cycles in B. CI values are 0.59, 0.06, and −0.17 for nos. 1, 8, and 20, respectively. See Fig. S5 for data on all sarcomeres. **(E)** Triangular heat map showing correlation between average and individual SLs (top row) and between an individual sarcomere and other sarcomeres in M1 (second row and below). Sarcomere number (i.e., from nos. 1 to 30; or average) is indicated on top and at the left end of each row. CI is illustrated on a color scale, as indicated on right (i.e., from 1 [dark blue] to −1 [dark red]). **(F)** Color diagram showing CI between average and individual SLs from nos. 1 to 30 during six cardiac cycles for M1. Sarcomere numbers are indicated on top, and cardiac cycle numbers on left. Bottom: Average of six cycles (i.e., same as top row in E). Arrows indicate sarcomeres at nos. 6, 18, and 25 showing marked changes in CI during consecutive cardiac cycles.

plots to a triangular heat map (Fig. 1 E). The top row (denoted by Avg.) in this map indicates CI between each sarcomere (from no. 1 to no. 30; Fig. S5) and the average of 30 sarcomeres. Irregular color configurations in the top row were consistent with the notion that CI does not depend on the longitudinal position of a sarcomere along a myofibril in a myocyte. The fraction of contributing sarcomeres was ∼67% for M1 (Table 1). Analyses in mice with somewhat lower systolic function are shown in Fig. S6 (see Videos 3 and 4); namely, the fractions of contributing sarcomeres were ∼57% and ∼64% (average of two myofibrils for both mice) when ΔLVP values were 60.5 ± 4.2 mm Hg and 40.6 ± 2.5 mm Hg, respectively (HR, 581 ± 6.6 bpm and 347 ± 7.9 bpm in mice with 60.5 mm Hg and 40.6 mm Hg, respectively; see Table 1).

The rows below the top row in Fig. 1 E indicate CI between each sarcomere (nos. 1–30) and others (average CI, 0.30 ± 0.22). For instance, the second row shows CI between no. 1 and nos. 2–30, and the third row CI between no. 2 and nos. 3–30. Similar

Table 1. **Summary showing CI, LVP, and HR under various contractile conditions**

Myofibril	Frequency			Total number of sarcomeres	CI	Avg. CI	Diastolic LVP (mm Hg)	Systolic LVP (mm Hg)	ΔLVP (mm Hg)	HR (bpm)
	CI > 0.2	0.2 > CI > 0	CI < 0							
M1	5	0	0	5	0.51 ± 0.06	0.48 ± 0.24	−3.8 ± 0.1	131.9 ± 1.4	135.7 ± 1.5	496 ± 0.4
M2	5	1	0	6	0.42 ± 0.12					
M3	4	0	1	5	0.54 ± 0.43					
M1	20	7	3	30	0.30 ± 0.22	0.29 ± 0.20	−4.5 ± 1.2	88.6 ± 3.1	96.4 ± 4.7	469 ± 2.9
M2	23	5	2	30	0.29 ± 0.19					
M1	8	4	4	16	0.20 ± 0.24	0.26 ± 0.25	−0.5 ± 0.1	61.2 ± 1.1	60.5 ± 4.2	581 ± 6.6
M2	9	4	1	14	0.33 ± 0.25					
M1	21	5	6	32	0.32 ± 0.36	0.27 ± 0.33	0.5 ± 0.1	42.1 ± 0.4	40.6 ± 2.5	347 ± 7.9
M2	22	5	8	35	0.22 ± 0.31					
M1	5	4	0	9	0.25 ± 0.16	0.23 ± 0.16	13.3 ± 0.1	20.2 ± 0.1	7.2 ± 0.1	159 ± 45.4
M2	4	4	1	9	0.21 ± 0.17					
M1	2	4	1	7	0.17 ± 0.27	0.17 ± 0.24	9.9± 0.1	14.6 ± 0.2	4.7 ± 0.2	80 ± 14.2
M2	3	2	2	7	0.17 ± 0.24					
M3	3	3	1	7	0.20 ± 0.23					

Data were taken from Fig. S15 (135.7 mm Hg), Fig. 3 (96.4 mm Hg), Fig. S6 (60.5 and 40.6 mm Hg), and Fig. S18 (7.2 and 4.7 mm Hg). Two or three myofibrils were analyzed in one mouse, each of which provided the fraction of CI (two myofibrils, 96.4, 60.5, 40.6, and 7.2 mm Hg; three myofibrils, 135.7 and 4.7 mm Hg). Avg. CI indicates the average value of CI of individual sarcomeres in analyzed myofibrils (see Fig. 4 D).

to the data in the top row, color configurations were disordered in each row (see below for quantitative analysis). Comparing each sarcomere with its immediate neighbor (i.e., one position right of the leftmost edge of the heat map) revealed that a positive correlation (CI > 0.2) was observed in only 7 of 29 cases (~24%), while no correlation (0.2 > CI > 0) was observed in 6 cases (~21%) and a negative correlation (CI < 0) in 16 cases (~55%; see Fig. S7 for scatter plots between adjacent sarcomeres). The scatter plots between adjacent sarcomeres in Fig. S7 (from 1 versus 2 to 29 versus 30) correspond to the diagonal portion of the triangular heat map in Fig. 1 E. This finding suggests that in a heart with normal systolic function, only ~24% of adjacent sarcomeres exhibit synchronized movements, while more than half (~55%) exhibit shortening or lengthening in opposite directions. This is likely to account, at least in part, for a certain level of asynchronous sarcomere movements along a myofibril (fraction of contributing sarcomeres, ~67% for M1; Table 1).

We further analyzed whether CI between individual and average SLs varies during the course of cardiac cycles (i.e., cycles 1–6; Fig. 1 F; see Fig. S8 for examples of sarcomeres with high or low CI, corresponding to Fig. 1 C). We found that (1) CI for each sarcomere changed between cardiac cycles (see marked changes in color, especially, nos. 6, 18, and 25); and (2) sarcomeres showing a positive correlation (in blue) in one cardiac cycle could show either no correlation (in white) or a negative correlation (in red) during the next cardiac cycle; and, despite (1) and (2), (3) average CI was similar in each cardiac cycle in order, presumably to maintain LV contractility (Table S2). These findings demonstrate clearly that in the left ventricle under normal systolic function, sarcomeres that contribute to myofibrillar dynamics change from one cardiac cycle to another, with the fraction of contributing sarcomeres of ~50–73% in each cardiac cycle (~67% for the average of six cardiac cycles). Similarly, we investigated whether the dynamics of individual sarcomeres along the same myofibril correlate with the LV pump function by analyzing the correlation between individual sarcomere movements and −LVP (i.e., LVP × −1) during each cardiac cycle. Although some sarcomeres showed a high correlation with −LVP, such as no. 3, others showed no correlation with −LVP, such as no. 20 (Fig. S9). Thus, as observed for average sarcomere dynamics in Fig. 1 F, CI for each sarcomere varied markedly between cardiac cycles, indicating that sarcomeres contributing to the ventricular pump function change from one cardiac cycle to the next.

We next analyzed the relationship between CI, the difference in SL in diastole and systole (ΔSL; i.e., sarcomere dynamics; see Kobirumaki-Shimozawa et al., 2016), and diastolic and systolic SL, by using the average values for 30 sarcomeres in M1 obtained during the course of six consecutive cardiac cycles (Fig. 1 B). First, we observed a positive linear relationship between CI and ΔSL (R = 0.66; $P < 0.001$; Fig. 2 A) and between CI and diastolic SL (R = 0.41; $P < 0.05$; Fig. 2 B), but not between CI and systolic SL (R = −0.12; $P > 0.05$; Fig. 2 C). Likewise, there was a positive linear relationship between diastolic SL and ΔSL (R = 0.71; $P < 0.001$) in the range between ~1.6 and ~2.2 µm (Fig. 2 D), but not between systolic SL and ΔSL (R = −0.06; $P > 0.05$; Fig. 2 E). We previously reported that a positive linear relationship

exists between ΔSL and ΔLVP in data from 13 individual mice (Kobirumaki-Shimozawa et al., 2016), demonstrating an important role of sarcomere dynamics in the regulation of LV pump function. Therefore, the above findings, obtained from 30 sequential sarcomeres from a myofibril in the same mouse, suggest that CI, ΔSL, and diastolic SL are interrelated such that under conditions where sarcomeres along a myofibril repeat contractions with a certain magnitude of synchrony (CI, ∼0.3; fraction of contributing sarcomeres, ∼67%) in vivo, ΔSL increases as a function of diastolic SL, and, as a result, systolic LVP increases.

What is the mechanism underlying the correlation between diastolic SL and ΔSL? We consider that when SL becomes longer than ∼1.85 µm (i.e., slack length in intact mouse ventricular myocytes; see King et al., 2011) along a myofibril, titin-based passive force reduces the thick–thin filament spacing in individual sarcomeres; this promotes myosin binding to actin and the ensuing thick–thin filament sliding under auxotonic conditions, as in the in vivo beating heart (SL-dependent activation as a basis of the Frank-Starling mechanism; e.g., Cazorla et al., 2001; Fukuda et al., 2003, 2005a; Terui et al., 2008, 2010; Kobirumaki-Shimozawa et al., 2014). This scenario is likely to operate in the range of ∼1.6–2.2 µm for diastolic SL (Fig. 2 D) because the mouse ventricle almost exclusively expresses the stiff N2B titin isoform rather than the compliant N2BA (e.g., Cazorla et al., 2000; Wu et al., 2000; Inoue et al., 2013). This relationship, however, likely varies between individual mice with differing levels of ventricular contractility (i.e., ΔLVP) due to a variance in the SL range (compare Kobirumaki-Shimozawa et al., 2016). We suggest that under normal physiological conditions, (1) this titin-based mechanism operates stochastically on a beat-to-beat basis at the single-sarcomere level along a myofibril (see Fig. 1 F) due presumably to a relatively large magnitude of freedom for the length of each sarcomere at physiological partial activation (see Kobirumaki-Shimozawa et al., 2014 and references therein), and (2) ΔLVP, as a function of ΔSL (Kobirumaki-Shimozawa et al., 2016), is related to the fraction of contributing sarcomeres within each myofibril.

It has been reported that in adult myocardial cells of mammals, Z-disks are connected by structural proteins, such as desmin (e.g., Lockard and Bloom, 1993; Zhang et al., 2001; Epstein and Davis, 2003; Conover and Gregorio, 2011). It is therefore expected that although the fraction of contributing sarcomeres along a myofibril is ∼67% under the normal systolic condition (Fig. 1, E and F; and Table 1), sarcomeres at the same longitudinal positions in neighboring myofibrils move in synchrony. We analyzed this correlation in individual sarcomeres at the same longitudinal positions in neighboring myofibrils (i.e., M1 and M2 in Fig. 3 A). The average lengths of 30 sarcomeres in 2 myofibrils changed with time in synchrony during the course of 6 cardiac cycles. However, at the single-sarcomere level, we observed that some moved in synchrony with those in the parallel myofibril (see longitudinal position no. 2), whereas others showed asynchrony (see no. 20; Fig. 3 B). Converting the time courses to scatter plots allowed quantification of the correlation in SL dynamics; that is, sarcomeres at no. 2 exhibited a positive correlation (CI, 0.46), and those at no. 20 exhibited a

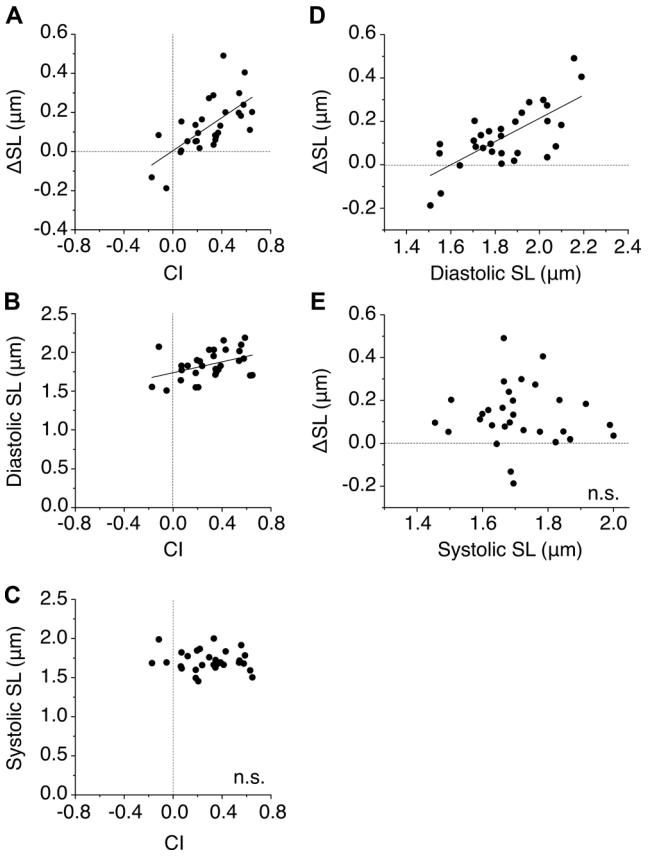

Figure 2. **Relationship between CI, ΔSL, and diastolic or systolic SL.** **(A)** Plots of ΔSL (diastolic SL minus systolic SL) versus CI. A significant linear relationship was observed (R = 0.66; $P < 0.001$). Diastolic and systolic SLs were obtained for 30 sarcomeres in M1 (Fig. 1, A and B) at which average SL became maximal and minimal, respectively, during each of six consecutive cardiac cycles. Resultant ΔSL values, as well as diastolic and systolic SL values, were averaged for six cardiac cycles; CI was quantified from Fig. 1 E, top (Fig. 1 F, bottom). **(B)** Plots of diastolic SL versus CI revealed a significant linear relationship (R = 0.41; $P < 0.05$). **(C)** Plots of systolic SL versus CI showed no significant correlation (n.s.). **(D)** Plots of ΔSL versus diastolic SL, using values in A and B, revealed a significant linear relationship (R = 0.71; $P < 0.001$). **(E)** Plots of ΔSL versus systolic SL, using values in A and C, showed no significant relationship (n.s.). In A–E, dashed lines indicate 0 values.

negative correlation (CI, −0.18; Fig. 3 B; see Fig. S10 for all sarcomeres). To summarize parallel interactions between sarcomeres, we performed correlation analyses for individual sarcomeres in M1 and M2 (Fig. 3 C). The top row in the heat map shows the correlation between the average of 30 sarcomeres in M1 (denoted as M1 Avg.) and each individual sarcomere in M2 (i.e., nos. 1–30, or the average of 30 sarcomeres in M2; right end; M2 Avg.). As is apparent from the time-course data in Fig. 3 B, a high correlation (CI, 0.82) was observed for the average movements between two myofibrils (note dark blue for M2 Avg. in the top row). For the lower rows in the heat map, the left edge in each row indicates the CI between sarcomeres located at the same longitudinal position, from 1 to 30 (compare Fig. 3 C and Fig. S10). The inconsistent colors of these blocks illustrate the lack of regularity of the sarcomeric function in neighboring myofibrils. Indeed, the average of the numbers in the left edges

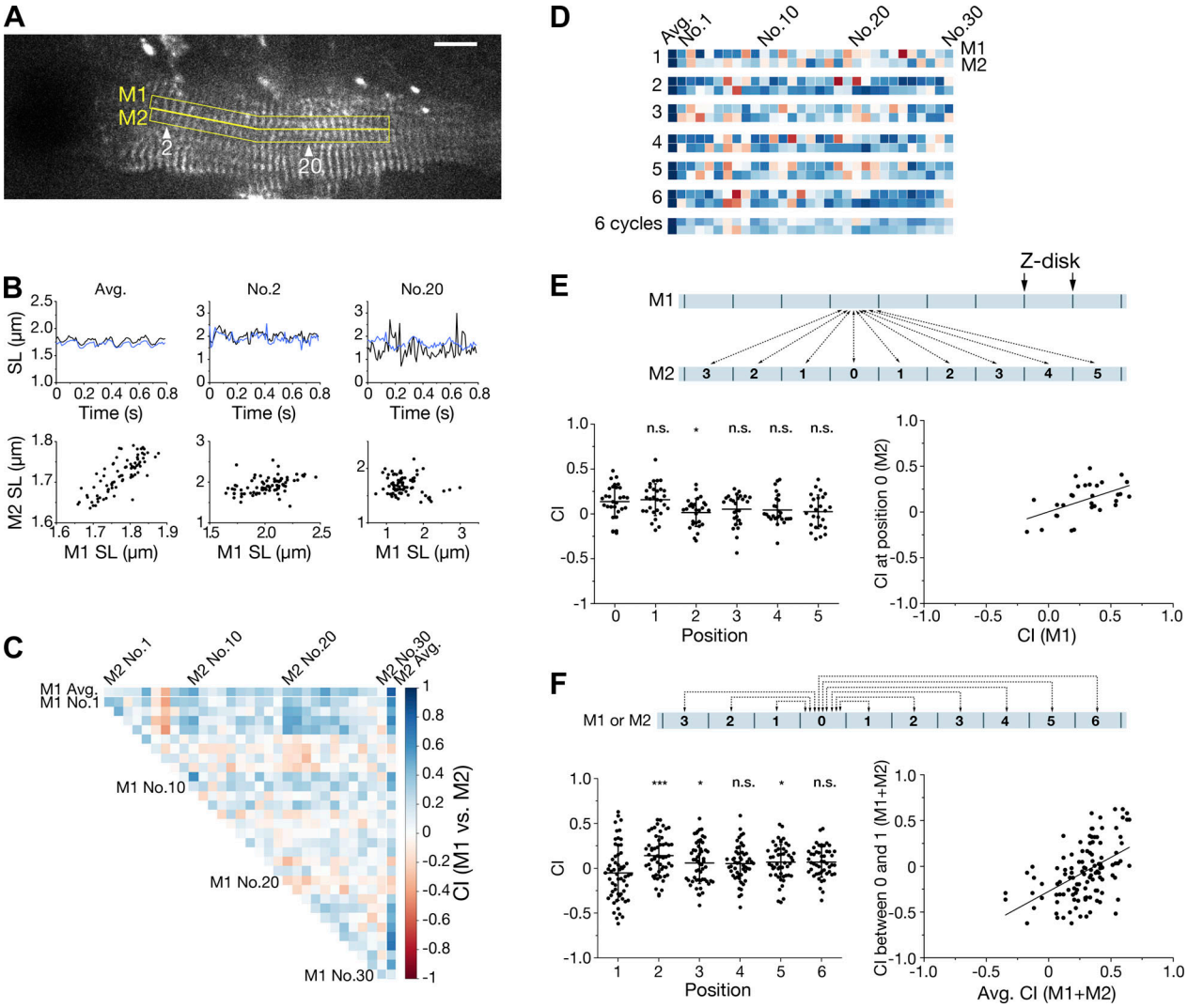

Figure 3. **In vivo tracking of individual sarcomeres along parallel myofibrils in an LV myocyte. (A)** Confocal image of a myocyte expressing α-actinin-AcGFP (same as in Fig. 1 A). 30 sarcomeres, in yellow-outlined rectangles, were analyzed for M1 and M2 were analyzed. Scale bar, 10 μm. See Video 2. **(B)** Top: Time course of changes in the lengths of averaged 30 sarcomeres (left), and examples of sarcomeres at the same longitudinal positions showing a positive correlation (middle, no. 2) or a negative correlation (right, no. 20). Data were obtained from six cardiac cycles. Black line, M1; blue line, M2. Average diastolic and systolic SLs for M1 were 1.85 ± 0.02 μm and 1.70 ± 0.04 μm, respectively (as in text; see Fig. 2, B–E, for plots of 30 sarcomeres). Average diastolic and systolic SLs for M2 were 1.77 ± 0.02 μm and 1.66 ± 0.02 μm, respectively. Average shortening ratios were 8.0% and 6.5% for M1 and M2, respectively (compare Kobirumaki-Shimozawa et al., 2016). Bottom: Scatter plots for dynamics between sarcomeres in M1 (x axis) and M2 (y axis). Left: Averaged 30 sarcomeres (CI, 0.82); middle, sarcomeres at no. 2 (CI, 0.46); right, sarcomeres at no. 20 (CI, −0.18). **(C)** Triangular heat map showing correlation between the average of 30 sarcomeres in M1 and each sarcomere in M2 or the average of 30 sarcomeres in M2 (right end). Sarcomere numbers are indicated on top. Underlying rows show correlations between sarcomere nos. 1–30 in M1 and each sarcomere in M2, or the average of 30 sarcomeres in M2. In this diagram, CI is displayed on a color scale, as indicated on right (i.e., from 1 [dark blue] to −1 [dark red]). **(D)** Color diagram showing CI between sarcomeres in M1 and M2 at the same longitudinal positions during six cardiac cycles. Sarcomere numbers are indicated on top. The diagram on bottom indicates average CI along myofibrils during six cardiac cycles. Data for M1 are the same as in Fig. 1 F. **(E)** Top: Illustration showing the numbering of sarcomeres in M1 and M2. In this analysis, six positions (i.e., 0–5) in M2 in relation to M1 are defined. Position 0 is defined as the same longitudinal position along M2. Position 1 is adjacent to position 0 on both sides, and positions 2–5 are defined as illustrated. Bottom left: Graph showing CI for sarcomeres located at positions 0–5 in M2. *, $P < 0.05$ compared with position 0. Bottom right: Relationship between average CI for individual sarcomeres along M1 (x axis) and CI at position 0 in M2 (y axis). A significant linear relationship was present ($R = 0.51$; $P < 0.01$). **(F)** Top: Illustration showing the numbering of sarcomeres in a myofibril (either M1 or M2). In this analysis, seven positions (i.e., 0–6) in series are defined. Position 1 is adjacent to position 0 on both sides, and positions 2–6 are defined as illustrated. Bottom left: Graph showing CI for sarcomeres located at positions 1–6. Data from M1 and M2 are pooled. *, $P < 0.05$; ***, $P < 0.001$ compared with position 1. Bottom right: Relationship between average CI for individual sarcomeres along a myofibril (x axis) and CI between neighboring sarcomeres (i.e., at positions 0 and 1; y axis). A significant linear relationship was present ($R = 0.50$; $P < 0.001$). Data from M1 and M2 are pooled in this graph. In B–D and F, Avg. indicates average.

of sarcomeres nos. 1–30 was 0.13 ± 0.17, and the fraction of CI >0.2 along myofibrils was only ∼37%.

Fig. 3 D compares changes in CI for individual versus average sarcomeres in M1 and M2 during six cardiac cycles (i.e., cycles 1–6; see scatter plots showing correlations of individual versus average SL for M2 in Fig. S11). CI for each sarcomere varied between cardiac cycles in both myofibrils (see triangular heat maps in each cardiac cycle; i.e., cycles 1–6 for M1 and M2 in Fig. S12), with differing magnitudes at the same longitudinal positions during each cardiac cycle, and this tendency held true for the average of six cardiac cycles (see row on bottom in Fig. 3 D). It should be pointed out, however, that average CI, as well as the fraction of contributing sarcomeres, was similar in each cardiac cycle in both myofibrils (see Table 1).

One may point out that the apparently low values of CI in Table 1, even under the normal physiological condition, result from the surgeries and α-actinin-AcGFP expression in myocytes via adenovirus infection (see Materials and methods). However, the experiment with T-tubule staining by CellMask yielded a similar value of CI of ∼0.3 (see Figs. S13 and S14, Table S3, and Videos 5 and 6). Because the CellMask experiment does not require the first open-chest surgery and adenovirus infection for nanoimaging, it is unlikely that the asynchronous sarcomere movements in the in vivo beating heart observed via α-actinin-AcGFP expression are caused by our experimental procedures (see Results and discussion III in the supplemental text for details).

We next quantified whether CI varies depending on the geometrical position of a sarcomere relative to the one in a neighboring myofibril (i.e., M1 versus M2 in Fig. 3 A; see also illustration for sarcomere positions in Fig. 3 E, top). First, the average value of CI for sarcomeres at the same longitudinal positions, nos. 1–30, was 0.13 ± 0.17 (see data for position 0 in Fig. 3 E, bottom left). The positive value shows that the sarcomeres at the same longitudinal positions in neighboring myofibrils tend to move, albeit weakly, interacting with each other. Our analysis revealed that although CI at position 1 was similar to that at position 0 with a value of 0.15 ± 0.16 ($P > 0.05$ compared with the value at position 0), that at position 2 and farther (analyzed up to position 5) was lower than that at position 0 with a value close to 0 (values significantly different at positions 0 versus 2). Therefore, a sarcomere in a myofibril affects the movements of sarcomeres in neighboring myofibrils at the same longitudinal position or those that are one position removed. We likewise found that a significant linear relationship ($R = 0.51$; $P < 0.01$) was present for the values between average CI for individual sarcomeres along M1 (x axis) and CI at position 0 in M2 (y axis; Fig. 3 E, bottom right). This correlation indicates that the sarcomeres synchronizing with the ones in a neighboring myofibril contribute to the average dynamics of the myofibril.

Previous works by others have indicated that transitional junctions, located at the end of myofibrils in a myocardial cell, are easily distorted upon movements of myofibrils due to their immature structure (e.g., Bennett et al., 2006; Bennett, 2018). In contrast, our own work has shown that Z-disks have a solid structure with little or no distortions during cardiac cycles in the in vivo mouse heart (Kobirumaki-Shimozawa et al., 2020). The present findings (Fig. 3 E) indicate that protein connections between aligned Z-disks may play a role in synchronizing the movements of sarcomeres in neighboring myofibrils in the in vivo heart.

Longitudinal intersarcomere interactions may fine-tune the imbalance of movements between sarcomeres along a myofibril in the in vivo beating heart (compare de Souza Leite and Rassier, 2020 [and references therein] in isolated skeletal myofibrils). To investigate whether this mechanism operates along a myofibril in a myocyte in the in vivo beating heart, we quantified the magnitude of correlation for sequentially connected sarcomeres (see illustration for geometrical sarcomere positions in Fig. 3 F, top). As found in Fig. S7 in that the fractions of pairs of adjacent sarcomeres with no correlation and negative correlation were ∼21% and ∼55%, respectively, in M1, CI between a sarcomere and its immediate neighbors (see position 1 in Fig. 3 F, top) showed a negative value of −0.06 ± 0.31 (Fig. 3 F, bottom left; data from M1 and M2 pooled in this graph). This finding shows that during systole in the in vivo beating heart, a sarcomere tends to move in directions opposite to its immediate neighbors due presumably to the imbalance of force between them along a myofibril. It is interesting that the sarcomeres at position 2 (i.e., just beyond the immediate neighbors) showed a positive correlation with a value of 0.13 ± 0.22 ($P < 0.001$ compared with the value at position 1). The values for the sarcomeres at positions 3, 4, 5, and 6 were likewise positive, but with a lesser magnitude than that at position 2. In Fig. 3 F (bottom right) is the relationship between average CI for individual sarcomeres along a myofibril (x axis) and CI between neighboring sarcomeres (i.e., sarcomeres at positions 0 and 1 in Fig. 3 F, top; data from M1 and M2 pooled in this graph; y axis), providing a significant linear relationship ($R = 0.50$; $P < 0.001$; i.e., sarcomere synchronization).

Should longitudinal intersarcomere interactions be at play in regulating the heart's pump function, more synchronized individual sarcomere movements will be observed at a higher contractile state. We therefore investigated whether and how sarcomere synchrony is altered in a mouse under shallow anesthesia (∼1.5% isoflurane). This is because the well-known positive inotropy via stimulation of β receptors affects the local Ca^{2+} signaling at/around the T-tubules in myocytes, and therefore individual sarcomeric movements as well as synchronization behaviors along myofibrils may be affected accordingly (see, e.g., Tsukamoto et al., 2016). Fig. S15 A shows a typical example of an α-actinin-AcGFP–expressing myocyte in the left ventricle of a mouse anesthetized with ∼1.5% isoflurane (Video 7), in which ΔLVP was 135.7 mm Hg (HR, 496 ± 0.4 bpm; Table 1). The individual SL distribution was similar to that at ΔLVP 96.4 mm Hg (1.74 ± 0.24 μm) with the value of 1.76 ± 0.18 μm (Fig. S16); similar maximal and minimal SL values were likewise obtained, with 1.97 ± 0.17 μm and 1.54 ± 0.16 μm, respectively (as compared with 2.03 ± 0.26 μm and 1.46 ± 0.22 μm, respectively, at ΔLVP 96.4 mm Hg). We then analyzed SL correlations for individual sarcomeres. In five to six sequential sarcomeres, the CI values were 0.51 ± 0.06, 0.42 ± 0.12, and 0.54 ± 0.43 for M1, M2, and M3, respectively (Fig. S15 B and Table 1). The average CI value was 0.48 ± 0.24, which was significantly

($P < 0.05$) greater than that obtained at ΔLVP 96.4 mm Hg (0.29 ± 0.20; see below). As observed under the normal physiological condition (Fig. 1 F), CI for each sarcomere changed between seven cardiac cycles (Fig. S15 C).

We previously reported that in open-chest mice, an increase in the isoflurane concentration from ∼2% to ∼5% markedly depresses ventricular contractility accompanied by a decrease in HR (Kobirumaki-Shimozawa et al., 2016). By taking advantage of these effects (see Materials and methods), we investigated whether the individual sarcomere movements are altered under low contractile conditions. Fig. 4 A, top left, shows a typical example of an α-actinin-AcGFP–expressing myocyte in the left ventricle of a mouse anesthetized with ∼5% isoflurane (Video 8), in which SL varied between ∼2.0 and ∼2.2 µm with ΔLVP 7.2 ± 0.1 mm Hg (HR, 159 ± 45.4 bpm; Fig. S17). The individual SL distribution was shifted to the longer side with the average value of 2.11 ± 0.24 µm as compared with 1.74 ± 0.24 µm under the normal physiological condition (Fig. S16); the maximal and minimal SL values were 2.03 ± 0.26 µm and 1.46 ± 0.22 µm, respectively, at ΔLVP 96.4 mm Hg, and 2.70 ± 0.45 µm and 1.60 ± 0.28 µm, respectively, at ΔLVP 7.2 mm Hg. We then analyzed SL correlations for individual sarcomeres. In nine sequential sarcomeres, individual sarcomeres showed some positive correlation with the average movements (average CI, 0.23 ± 0.16 during eight cardiac cycles; Table 1 and Fig. 4 A, bottom left); however, more than half of the interactions between individual sarcomeres were asynchronous (as indicated by dominant white and red colors in Fig. 4 A, bottom left).

Occasionally, ∼5% isoflurane dramatically depressed the LV pump function, finally leading to cardiac arrest. Fig. 4 A, top right, shows an example of an α-actinin-AcGFP–expressing myocyte in the left ventricle just before cardiac arrest (ΔLVP, 4.7 ± 0.2 mm Hg; HR, 80 ± 14.2 bmp; Video 9). As in the case of ΔLVP 7.2 mm Hg, the individual SL distribution was shifted to the longer side with the average value of 2.03 ± 0.17 µm (Fig. S16); the maximal and minimal SL values were 2.37 ± 0.20 µm and 1.67 ± 0.18 µm, respectively. Even under this condition in which the heart's pump function was markedly depressed, some correlation was observed between individual sarcomeres and the average movements (average CI, 0.17 ± 0.24 during three cardiac cycles; Table 1 and Fig. 4 A, bottom right). However, most of the interactions between individual sarcomeres were asynchronous, as dominated by white and red colors in rows below the top (Fig. 4 A, bottom right). It should be stressed that when ΔLVP was markedly depressed to <10 mm Hg, the movements between neighboring sarcomeres became negatively correlated, as shown by dominant red colors in the diagonal portion of the triangular heat map for ΔLVP of 7.2 or 4.7 mm Hg (Fig. 4 A, bottom left and right). See Results and discussion IV in the supplemental text for the possible effects of isoflurane on cardiac excitation–contraction coupling and the ensuing sarcomere dynamics in the in vivo beating heart.

Fig. 4 B compares the CI values of individual versus average sarcomere movements in mice with various levels of ΔLVP (see Fig. S18 for analyzed myofibrils in mice with ΔLVP 7.2 and 4.7 mm Hg). Under the physiological condition of ΔLVP 96.4 mm Hg, the fractions of contributing (CI > 0.2 in blue) and noncontributing (0.2 > CI > 0 and CI < 0 in white and red, respectively) sarcomeres were ∼72% and ∼28%, respectively (see Table 1). In association with an increase in ΔLVP to 135.7 mm Hg, the fraction of contributing sarcomeres increased (∼88%), accompanied by a decrease in noncontributing sarcomeres (∼12%). Conversely, as ΔLVP decreased, the fraction of contributing sarcomeres decreased, whereas noncontributing sarcomeres increased. Indeed, the fractions of contributing and noncontributing sarcomeres were ∼38% and ∼62%, respectively, at ΔLVP 4.7 mm Hg. Our analysis revealed that a significant positive linear relationship ($R = 0.90$; $P < 0.001$) existed between ΔLVP and the fraction of contributing sarcomeres (Fig. 4 C).

Fig. 4 D shows the CI values for individual versus average SLs at various ΔLVP (six mice were analyzed as in Fig. 4, B and C; see Table 1). At ΔLVP 96.4 mm Hg, CI was positive (0.29 ± 0.20), indicating that sarcomere synchronization generates organized myofibrillar dynamics, and it was significantly ($P < 0.05$) increased at ΔLVP 135.7 mm Hg (0.48 ± 0.24). CI tended to be decreased as ΔLVP was reduced from 96.4 mm Hg (i.e., 0.26 ± 0.25, 0.27 ± 0.33, and 0.23 ± 0.16 at ΔLVP 60.5, 40.6, and 7.2 mm Hg, respectively). At ΔLVP 4.7 mm Hg, CI was significantly ($P < 0.05$) decreased with a value of 0.17 ± 0.24. Accordingly, there existed a linear relationship ($R = 0.93$; $P < 0.01$) between ΔLVP and CI over the range of ΔLVP tested (Fig. 4 E). Interestingly, the intersarcomere interaction between a sarcomere and those distal to it operated even at low ΔLVP conditions (Fig. S19); that is, the CI values between a sarcomere and the ones at position 2 and farther away were significantly higher than that with its neighbors (i.e., position 1; −0.25 ± 0.13 and −0.43 ± 0.13 at ΔLVP 7.2 and 4.7 mm Hg, respectively; see Fig. 3 F, top for sarcomere geometry along a myofibril). These findings suggest that (1) distal intersarcomere interactions operate along myofibrils in LV myocytes regardless of the contractile state and (2), reduced sarcomere synchrony exacerbates disorganized myofibrillar movements and underlies, at least in part, a decrease in the myocardial contractile force in the in vivo beating heart.

We further investigated CI in myocytes from the mice of ΔLVP 96.4 and 60.5 mm Hg, but at different pressure points in the physiological and near-physiological levels (Fig. S20 and Table S4). The inclusion of these data confirmed that there exists a significant positive linear relationship between ΔLVP and CI (see Results and discussion V in the supplemental text for details).

Finally, we investigated how CI between neighboring sarcomeres or individual ΔSL varies as a function of ΔLVP. Fig. 5 A compares CI between immediate neighbors along a myofibril (i.e., position 1 in Fig. 3 F) in mice with various ΔLVP. As stated above, the value was −0.06 ± 0.28 under the normal physiological condition at 96.4 mm Hg, −0.03 ± 0.35 ($P > 0.05$ compared with the value at 96.4 mm Hg) at 135.7 mm Hg, and 0.10 ± 0.27 ($P < 0.05$ compared with the value at 96.4 mm Hg) at 60.5 mm Hg, and it was decreased to −0.22 ± 0.32 ($P < 0.01$ compared with the value at 96.4 mm Hg) at 40.6 mm Hg. At 7.2 and 4.7 mm Hg, the values were further decreased to −0.25 ± 0.13 and −0.43 ± 0.13, respectively (values at 7.2 and 4.7 mm Hg, $P < 0.05$ and $P < 0.001$, respectively, compared with that at

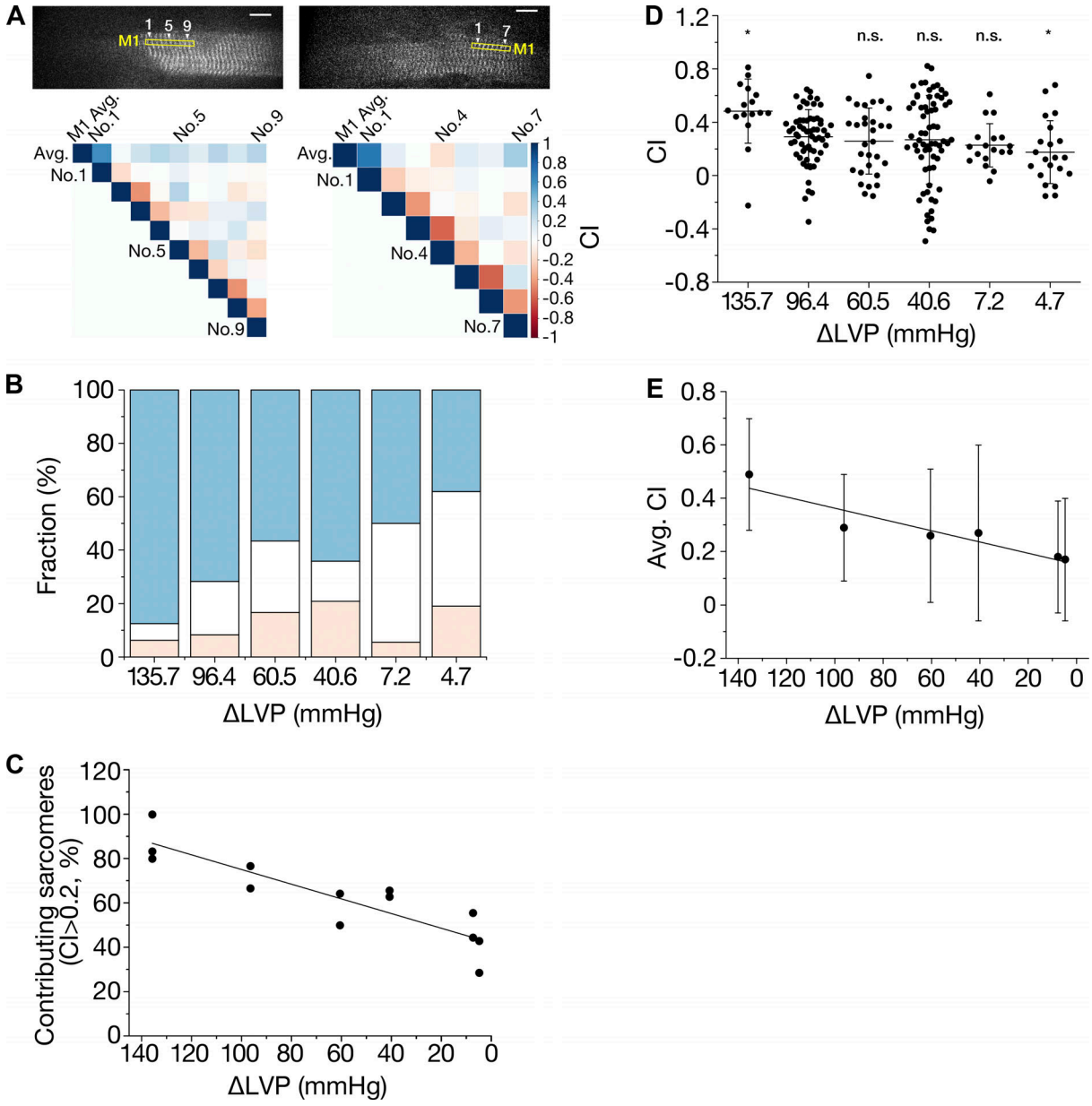

Figure 4. **Analyses of individual sarcomeric movements in the left ventricle with varying levels of contractility. (A)** Top left: Confocal image of an α-actinin-AcGFP–expressing LV myocyte in a heart with depressed cardiac function during deep anesthesia (~5% isoflurane). ΔLVP, 7.2 ± 0.1 mm Hg; HR, 159 ± 45.4 bpm (see Fig. S18 A). In the yellow-outlined rectangle, nine sequentially connected sarcomeres were analyzed for M1. Scale bar, 10 µm. See Video 8. Bottom left: Triangular heat map showing correlation between average and individual SLs (top row) and between an individual sarcomere and other sarcomeres in M1 (second row and below). Sarcomere number (i.e., from nos. 1 to 9 [or average]) is indicated on top and left of each row. Top right: Confocal image of an α-actinin-AcGFP–expressing myocyte in the left ventricle just before cardiac arrest under deep anesthesia with ~5% isoflurane. ΔLVP, 4.7 ± 0.2 mm Hg; HR, 80 ± 14.2 bpm (see Fig. S18 B). In the yellow-outlined rectangle, seven sequentially connected sarcomeres were analyzed for M1. Scale bar, 10 µm. See Video 9. Bottom right: Triangular heat map showing the correlation between average and individual SLs (top row) and between an individual sarcomere and other sarcomeres in M1 (second row and below). Sarcomere number (i.e., from nos. 1 to 7 [or average]) is indicated on top and left of each row. In bottom left and right, CI is shown based on a color scale (i.e., from 1 [dark blue] to –1 [dark red]). **(B)** Bar graph showing the fractions of CI between average and individual SLs at various levels of ΔLVP. Data at 135.7, 96.4, 60.5, 40.6, 7.2, and 4.7 mm Hg are shown. CI was categorized into the following three groups: blue (CI > 0.2 [positive correlation]), white (0.2 > CI > 0 [no correlation]), and red (CI < 0 [negative correlation]). **(C)** Relationship between ΔLVP and the fraction of contributing sarcomeres in myofibrils from mice with varying contractile conditions. Contributing sarcomeres are defined as those with CI >0.2 in the average data of three to eight cardiac cycles. Each plot indicates a myofibril (i.e., sequentially connected sarcomeres). A significant relationship was observed (R = 0.90; $P < 0.001$). **(D)** Plots of CI between average and individual SLs at various levels of ΔLVP. A significant difference (*, $P < 0.05$) was observed between ΔLVP 96.4 mm Hg and 135.7 mm Hg and between ΔLVP 96.4 mm Hg and 4.7 mm Hg, but not between ΔLVP 96.4 mm Hg and 60.5, 40.6, or 7.2 mm Hg (n.s.). Horizontal bars, average; vertical bars, SD. **(E)** Relationship between ΔLVP and the average values of CI (Avg. CI) in D. A significant linear relationship (R = 0.93; $P < 0.01$) was observed. In B–E, two myofibrils were analyzed for ΔLVP 96.4, 60.5, 40.6, and 7.2 mm Hg (Figs. 3, S6, and S18), and three myofibrils were analyzed for 135.7 and 4.7 mm Hg (Figs. S15 and S18).

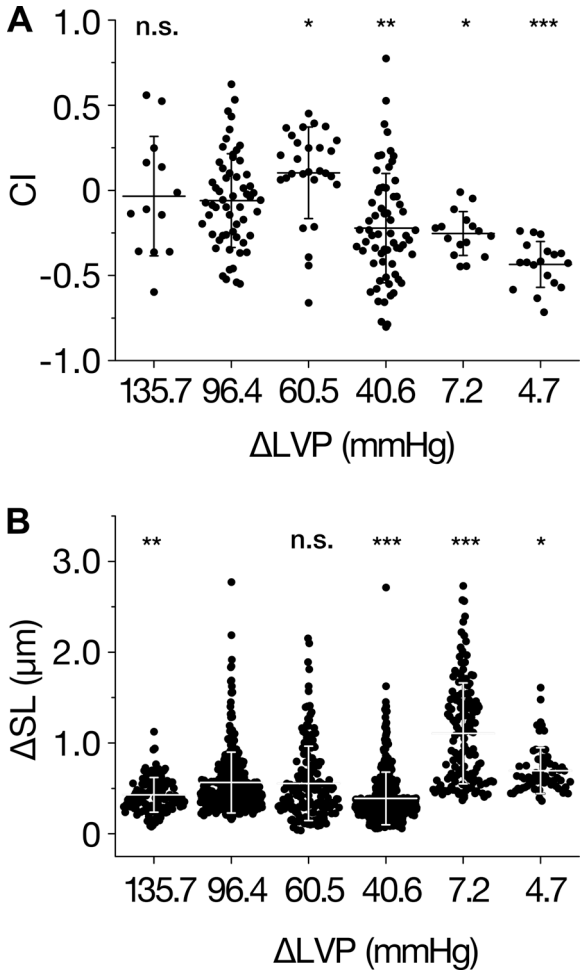

Figure 5. **Sarcomere dynamics and interplay between adjacent sarcomeres at various levels of LV contractility. (A)** CI between adjacent sarcomeres at various levels of ΔLVP (i.e., between position 0 and 1 in Fig. 3 F, top). CI, −0.03 ± 0.35, −0.06 ± 0.28, 0.10 ± 0.27, −0.22 ± 0.32, −0.25 ± 0.13, and −0.43 ± 0.13 at 135.7, 96.4, 60.5, 40.6, 7.2, and 4.7 mm Hg, respectively. Horizontal bars, average; vertical bars, SD. *, P < 0.05; **, P < 0.01; and ***, P < 0.001 compared with 96.4 mm Hg. **(B)** Individual ΔSL at various levels of ΔLVP. ΔSL (maximal SL minus minimal SL): 0.43 ± 0.19, 0.56 ± 0.33, 0.55 ± 0.41, 0.39 ± 0.29, 1.11 ± 0.56, and 0.69 ± 0.25 μm at 135.7, 96.4, 60.5, 40.6, 7.2, and 4.7 mm Hg, respectively (compare Fig. S16). Horizontal bars, average; vertical bars, SD. *, P < 0.05; **, P < 0.01; and ***, P < 0.001 compared with 96.4 mm Hg. In A and B, data from two myofibrils were pooled for 96.4, 60.5, 40.6, and 7.2 mm Hg (Figs. 3, S6, and S18), and three myofibrils were pooled for 135.7 and 4.7 mm Hg (Figs. S15 and S18).

96.4 mm Hg). Therefore, similar to the finding for average CI (Fig. 4 E), CI between adjacent sarcomeres was decreased in association with a decrease in ΔLVP.

Fig. 5 B compares individual ΔSL (maximal SL minus minimal SL) at various ΔLVP. We found that ΔSL was 0.56 ± 0.33 μm at 96.4 mm Hg. The value was decreased by ∼24% to 0.43 ± 0.19 μm (P < 0.01 compared with the value at 96.4 mm Hg) at 135.7 mm Hg and similar at 60.5 mm Hg with 0.55 ± 0.41 μm (P > 0.05). Then, it was decreased by ∼30% to 0.39 ± 0.29 μm (P < 0.001 compared with the value at 96.4 mm Hg) at 40.6 mm Hg. Interestingly, ΔSL was increased by ∼98% to 1.11 ± 0.56 μm (P < 0.001 compared with the value at 96.4 mm Hg) at 7.2 mm Hg, and it remained ∼23% larger at 4.7 mm Hg than at 96.4 mm Hg (P < 0.05). Therefore, ΔSL changes in a nonlinear fashion in response to a change in ΔLVP. Namely, (1) ΔSL decreases in response to an increase in ΔLVP from the normal physiological level to ∼135 mm Hg; (2) similar to this, it decreases when ΔLVP is decreased to ∼40 mm Hg; but (3) it increases when ΔLVP is lowered to <10 mm Hg. Provided that maximal SL was markedly increased when ΔLVP was lowered from the normal physiological level to <10 mm Hg (i.e., 2.03 ± 0.26 μm at 96.4 mm Hg, and 2.70 ± 0.45 μm and 2.37 ± 0.20 μm at 7.2 and 4.7 mm Hg, respectively; Fig. S16), we consider that this SL elongation in diastole predominantly underlies the increased ΔSL at low contractile states. Namely, an increase in maximal SL to greater than ∼2.25–2.3 μm is likely to increase the thick–thin filament sliding distance during contraction. Conversely, shortening of SL in diastole at the high contractile state, albeit by a slight magnitude, is likely to underlie the observed decrease in ΔSL at 135.7 mm Hg.

Here, it is important to discuss the physiological significance of the present findings. It has long been considered that in striated muscle, sarcomeres along a myofibril generate equal levels of active force as well as thick–thin filament sliding during activation under various loaded conditions (see Introduction). In the present study, however, our nanoimaging technology reveals that individual sarcomeres alternatively contributed to myofibrillar dynamics at various levels of ΔLVP (Fig. 1 F; Fig. 3 D; and Figs. S6, S15, and S18) with average CI, which was similar in each cardiac cycle (Table S2), and that there was a linear relationship between ΔLVP and CI (Fig. 4 E). It is therefore suggested that, in the in vivo beating heart, the following occurs: (1) active as well as passive force varies between sarcomeres even along the same myofibril; (2) sarcomeres per se have a property to move asynchronously, but when connected in a series, myofibrils exert stable dynamics; and (3) myocardial contractility is a function of synchrony of sarcomere movements in LV myocytes. Provided that the heart undergoes millions of contractions during a lifetime at various inotropic states, "alternative contribution" of sarcomeres is an intrinsic property of cardiac muscle to prevent potential damage to the thick–thin filament structure during normal cardiac cycles; the "noncontributing sarcomeres" may operate as a "cushion" to absorb external forces (e.g., when myocytes are stretched due to an increase in ventricular filling, thereby protecting the cellular structure).

What is the mechanism of sarcomere synchronization in the heart under normal physiological conditions? We consider that the finding in Fig. 3 F provides a novel insight into the synchrony of sarcomere movements. Namely, the present analysis using heat maps revealed that there was a certain fraction of sarcomeres moving in opposition to their immediate neighbors; along a myofibril, however, sarcomere movements were positively correlated with the ones next to the immediate neighbors (and farther; Fig. 3 F), suggesting that a distal intersarcomere interaction (compare de Souza Leite and Rassier, 2020, and references therein), by taking advantage of the opposite movements of immediate neighbors, operates to synchronize their movements, resulting in CI ∼0.3 at ΔLVP 96.4 mm Hg (Fig. 1 F, Fig. 3 D, and Table 1). In the mouse ventricle, stiff N2B titin, rather

than the more compliant N2BA titin, is expressed (e.g., Wu et al.,1999; Cazorla et al., 2000; Inoue et al., 2013). Therefore, when SL is, on average, elongated to ∼2.0 µm (Fig. S16), it is expected that some sarcomeres will produce inward-oriented, titin-based passive force. As stated above, longer sarcomeres are more sensitive to Ca^{2+} than shorter ones (i.e., they exhibit length-dependent activation), thus enabling actomyosin interaction and thick–thin filament sliding, resulting in the lengthening of shorter sarcomeres, which produce less active force. This is illustrated schematically in Fig. 6 A for a hypothetical circumstance with five sequentially connected sarcomeres along a myofibril in a myocyte with varying diastolic lengths (see Kobirumaki-Shimozawa et al., 2016, for SL variance in diastole). Because of its longer length, the sarcomere at no. 2 shortens more than those at nos. 1, 3, and 5 in response to a rise of the intracellular Ca^{2+} concentration ($[Ca^{2+}]_i$) upon systole. The shortest sarcomere in the myofibril, positioned at no. 4, is lengthened, however. Then, when $[Ca^{2+}]_i$ falls upon diastole, the shortened sarcomeres (nos. 1, 2, 3, and 5) lengthen, presumably due, at least in part, to outward-oriented, titin-based restoring force (shown in sarcomeres at nos. 2 and 5; see, e.g., Helmes et al., 1999; Fukuda et al., 2005b for restoring force). In contrast, because of inward-oriented, titin-based passive force that is developed in the preceding systole, sarcomeres lengthened during systole (e.g., no. 4) will shorten upon diastole, promoting lengthening of neighboring sarcomeres (e.g., nos. 3 and 5). Thus, sarcomeres at nos. 1, 2, 3, and 5 move in synchrony during the cardiac cycle, and, importantly, those distally located at nos. 3 and 5 do so by taking advantage of opposite length changes of the one at no. 4. We hereby propose that the distal intersarcomere interaction operates effectively on a beat-to-beat basis along a myofibril to synchronize sarcomeric movements under normal physiological (and high contractile) conditions. It is likely that sarcomere synchrony regulates the heart's pump function in coordination with myofibrillar contractility.

It is likewise important to discuss the possible mechanism underlying a reduction of synchrony at low contractile states (i.e., ΔLVP 7.2 and 4.7 mm Hg; see Fig. 4, A–D). First, under depressed conditions, maximal (diastolic) SL was shifted toward a longer range (i.e., greater than or equal to ∼2.25–2.3 µm; Fig. S16), coupled presumably with enhanced ventricular filling (as indicated by increased diastolic LVP; see Table 1 and Fig. S17). It has been reported that, at average SL greater than or equal to ∼2.25–2.3 µm, N2B titin-based passive force increases exponentially in mouse myocardium (e.g., Wu et al., 1999). Therefore, it is likely that when only a slight stretch is imposed on elongated sarcomeres, inward-oriented, titin-based passive force will dramatically increase, surpassing the actomyosin-based active force. In a well-controlled study using N2B titin-expressing rat ventricular myocytes, Weiwad et al. (2000) demonstrated that the magnitude of SL variance increased linearly upon stretch under the resting condition in the range between 1.8 and 2.8 µm. Therefore, as illustrated for our example string of sarcomeres placed in a low contractile state (Fig. 6 B), longer sarcomeres (nos. 2 and 4) shorten more extensively upon systole by producing greater active force than shorter sarcomeres (nos. 1, 3, and 5) via length-dependent activation (see above). It is likely that shortening of sarcomeres at nos. 2 and 4 causes lengthening of those at nos. 1, 3, and 5, in which titin-based passive force markedly increases. In turn, upon diastole, high passive force–generating sarcomeres (nos. 1, 3, and 5) will abruptly shorten, resulting in stretching of their neighbors (nos. 2 and 4) and the generation of asynchronous movements between sarcomeres. We consider that despite an increase in ΔSL (Fig. 5 B) coupled with elongation of SL, asynchrony in the movements of sarcomeres along myofibrils, as evidenced by low CI (Fig. 5 A), promotes weakening of myocardial contractile force. Ultimately, we postulate that this asynchrony exacerbates the heart's pump function under depressed conditions.

It is worthwhile discussing the range of maximal (diastolic) SL observed under depressed conditions (Fig. S16). As mentioned above, stiff N2B titin (compared with the more compliant N2BA titin) is expressed in the mouse heart. In N2B titin, the A-band region is composed of relatively simple patterns of Ig-like and fibronectin type 3 repeats. With strong binding to the rod portion of myosin and myosin-binding protein C, this region shows little or no compliance. In contrast, the I-band portion has a complex sequence with distinct extensible segments: the tandem Ig segments, the PEVK segment, and a region that has a unique amino acid sequence called N2B (see Granzier and Labeit, 2002, 2004; Fukuda et al., 2008, 2010). It has been reported that when SL is elongated up to ∼2.25–2.3 µm (i.e., the physiological limit), the PEVK and N2B sequences are straightened and then stretched, resulting in the production of passive force (see Granzier and Labeit, 2002, 2004; Fukuda et al., 2008, 2010). Given the relatively long SL range in myocytes at ΔLVP 7.2 and 4.7 mm Hg (Fig. S16), it is reasonable to consider that N2B titin's individual Ig domains are unfolded in the majority of sarcomeres during diastole. While this issue remains disputed (e.g., Trombitás et al., 1998), mechanical studies have demonstrated that N2B titin-expressing myofibrils (from rats) can be stretched up to ∼2.5–2.6 µm, which unfolds the Ig domains but causes no irreversible damage to the sarcomere structure (Linke et al., 1999; Weiwad et al., 2000). It can therefore be considered that in failing conditions with low ventricular contractility, SL can be stretched beyond the physiological limit to ∼2.5–2.6 µm, with unfolding of titin's Ig domains in the I-band.

One may point out that in the LV myocardium of rats and mice, collagen is well developed, preventing myocytes from stretching beyond the "physiological limit" (e.g., Wu et al., 1999). However, a well-known study using intact rat ventricular trabeculae demonstrated that although average SL is set at ∼2.15 µm in the relaxed state, SL varies from ∼1.70 to ∼2.60 µm. Thus, there is likely a coexistence of myocytes with various ranges of SL at rest, including some that are longer than the "physiological limit" (Kentish et al., 1986), in agreement with our present observations in a myocyte from a heart with reduced contractility (ΔLVP 7.2 mm Hg; see Fig. S16).

Although the majority of sarcomeres were less than ∼2.5–2.6 µm in diastole, some sarcomeres were observed to fall outside this range, especially under depressed contractile conditions (Fig. S16). There could be two reasons for this. First, the myocyte

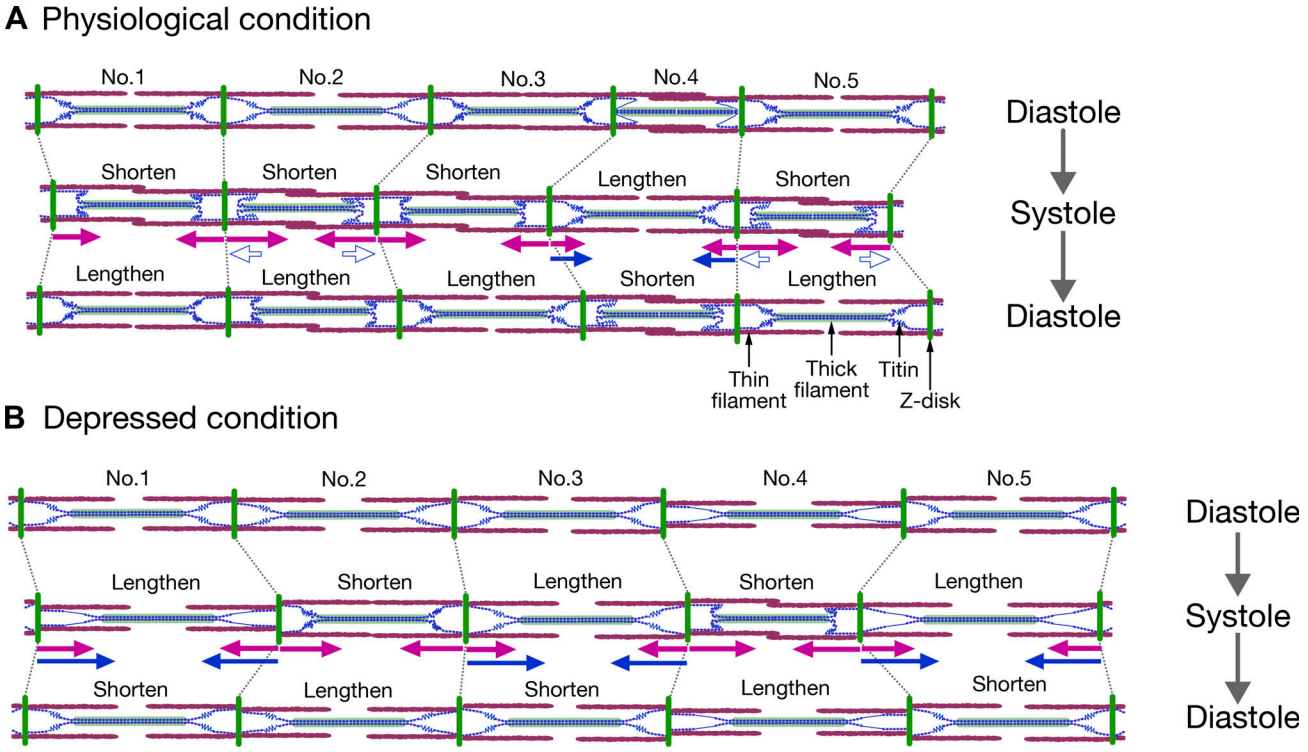

Figure 6. **Schematic illustrating the postulated mechanism of intramyofibril sarcomeric asynchrony in the in vivo beating heart. (A)** Changes in the lengths of five sequentially connected sarcomeres along a myofibril during a cardiac cycle under normal physiological conditions (e.g., ΔLVP 96.4 mm Hg in the present study). Average SL during diastole is ∼2.05 µm (compare Fig. S16 and Kobirumaki-Shimozawa et al., 2016). Upon systole, sarcomeres at nos. 2 and 5 exhibit greater shortening than those at nos. 1 and 3 due to their longer SL (via length-dependent activation, see text; active force shown by pink closed arrows). Concomitantly, the no. 4 sarcomere, which is short during diastole, is lengthened by its neighbors, producing inward-oriented, titin-based passive force (blue closed arrows). Upon diastole, shortened sarcomeres (nos. 1, 2, 3, and 5) lengthen due, at least in part, to outward-oriented, titin-based restoring force (blue open arrows in sarcomeres at nos. 2 and 5), but the one at no. 4 shortens due to inward-oriented, titin-based passive force (produced in systole), causing asynchrony. **(B)** Sarcomere interactions during conditions of depressed contractility (ΔLVP <10 mm Hg; i.e., ΔLVP 7.2 or 4.7 mm Hg in the present study). Average SL is greater than ∼2.25–2.30 µm during diastole (compare Fig. S16). Sarcomeres with longer diastolic lengths (nos. 2 and 4) exhibit greater length-dependent activation (active force shown by pink closed arrows) and shorten upon systole at the expense of shorter sarcomeres, which are lengthened (nos. 1, 3, and 5). Thus, titin-based passive force (blue closed arrows) markedly increases in sarcomeres at nos. 1, 3, and 5, causing them to abruptly shorten upon diastole, stretching their neighbors (nos. 2 and 4). Consequently, sarcomeres move in marked asynchrony under depressed conditions.

relative to the confocal image plane may result in an overestimation of SL (see Bub et al., 2010; Botcherby et al., 2013; Kobirumaki-Shimozawa et al., 2016). Second, compared with normally functioning hearts, myocardium exposed to depressed conditions tends to exhibit unorganized, complex movements due to Ca^{2+} wave–induced contractions in myocytes proximal to the imaging site (see, e.g., Shimozawa et al., 2017 for Ca^{2+} waves). Occasionally, because of resulting movements in the Z-direction, the intensity of AcGFP fluorescence in Z-disks was not sufficiently high to be detected by our custom-made multipeak fitting program (see Kobirumaki-Shimozawa et al., 2016), and, consequently, the length of two sarcomeres would have been detected. It is therefore likely that maximal (diastolic) SL values longer than ∼2.5–2.6 µm, especially in the hearts of ΔLVP 7.2 and 4.7 mm Hg, represent measurements from two adjacent sarcomeres. Likewise, there could be two reasons for the minimal SL values shorter than the A-band length (i.e., ∼1.6 µm), which we observed under all contractile conditions (Fig. S16). First, given the average value of 1.46 ± 0.22 (or 1.54 ± 0.16) µm at ΔLVP 96.4 (or 135.7) mm Hg, sarcomeres, and the A-band in particular, may be reversibly deformed or distorted by the high contractile force exerted under normal physiological or high contractile conditions, resulting in SL values that are shorter than the normal A-band length (i.e., ∼1.6 µm). Second, as mentioned above, noise accompanied by irregular movements of target myocytes can steer our program to yield short SL values under all contractile conditions.

In conclusion, we analyzed the dynamic behaviors of individual sarcomeres along a myofibril in an LV myocyte of a beating in vivo mouse heart under various contractile conditions, and we demonstrated that sarcomere synchronization was correlated with ventricular contractility. Future studies are warranted to quantify how synchronized sarcomere movements occur along a myofibril via distal intersarcomere interactions by carefully measuring the phase of shortening or lengthening of individual sarcomeres under various loaded conditions in isolated single myofibrils (e.g., Shimamoto et al., 2009; Kagemoto et al., 2018; de Souza Leite and Rassier, 2020; Kono et al., 2020; and references therein). Likewise, it is important to investigate whether a heterogeneous rise or fall of local $[Ca^{2+}]_i$ plays a role in the asynchrony of sarcomere movements at a variety of inotropic states (see Results and discussion VI in the supplemental text) in the healthy and diseased heart.

Acknowledgments

Henk L. Granzier served as editor.

We thank Naoko Tomizawa and Michiyo Murata (The Jikei University School of Medicine) for technical assistance.

This work was supported by the Ministry of Education, Culture, Sports, Science and Technology under Grants-in-Aid for Scientific Research on Innovative Areas (23107003 to N. Fukuda), Scientific Research (B; 15H04677 and 20H03421 to N. Fukuda), Scientific Research (C; 18K06878 and 21K06789 to F. Kobirumaki-Shimozawa, 21K08981 to T. Terui), Challenging Exploratory Research (26560225 and 21K19929 to N. Fukuda), and Young Scientists (B; 16K18993 to T. Terui) and by the Japan Society for the Promotion of Science Fellows (15J10205 to K. Oyama). This study was also supported by funding from the Japan Heart Foundation (to F. Kobirumaki-Shimozawa), the Naito Foundation (to F. Kobirumaki-Shimozawa), the European Union's Horizon 2020 Framework Programme research and innovation program (consolidator grant to W.E. Louch) under agreement 647714, and the Norwegian Institute of Public Health (12973 to J. Li).

The authors declare no competing financial interests.

Author contributions: F. Kobirumaki-Shimozawa, T. Shimozawa, K. Oyama, J. Li, T. Nakanishi, T. Terui, W.E. Louch, S. Ishiwata, and N. Fukuda designed the research; F. Kobirumaki-Shimozawa, T. Shimozawa, K. Oyama, S. Baba, J. Li, and T. Terui performed experiments; F. Kobirumaki-Shimozawa, T. Shimozawa, K. Oyama, and N. Fukuda analyzed data; F. Kobirumaki-Shimozawa, T. Shimozawa, K. Oyama, W.E. Louch, S. Ishiwata, and N. Fukuda interpreted the data; Kobirumaki-Shimozawa, T. Shimozawa, K. Oyama, T. Nakanishi, W.E. Louch, S. Ishiwata, and N. Fukuda drafted the manuscript. All authors have approved the final draft of the manuscript, and their contributions qualify them as authors.

Submitted: 14 January 2021
Accepted: 3 September 2021

References

Aguirre, A.D., C. Vinegoni, M. Sebas, and R. Weissleder. 2014. Intravital imaging of cardiac function at the single-cell level. *Proc. Natl. Acad. Sci. USA.* 111:11257–11262. https://doi.org/10.1073/pnas.1401316111

Aschar-Sobbi, R., F. Izaddoustdar, A.S. Korogyi, Q. Wang, G.P. Farman, F. Yang, W. Yang, D. Dorian, J.A. Simpson, J.M. Tuomi, et al. 2015. Increased atrial arrhythmia susceptibility induced by intense endurance exercise in mice requires TNFα. *Nat. Commun.* 6:6018. https://doi.org/10.1038/ncomms7018

Bennett, P.M. 2018. Riding the waves of the intercalated disc of the heart. *Biophys. Rev.* 10:955–959. https://doi.org/10.1007/s12551-018-0438-z

Bennett, P.M., A.M. Maggs, A.J. Baines, and J.C. Pinder. 2006. The transitional junction: a new functional subcellular domain at the intercalated disc. *Mol. Biol. Cell.* 17:2091–2100. https://doi.org/10.1091/mbc.e05-12-1109

Bosnjak, Z.J., F.D. Supan, and N.J. Rusch. 1991. The effects of halothane, enflurane, and isoflurane on calcium current in isolated canine ventricular cells. *Anesthesiology.* 74:340–345. https://doi.org/10.1097/00000542-199102000-00022

Bosnjak, Z.J., A. Aggarwal, L.A. Turner, J.M. Kampine, and J.P. Kampine. 1992. Differential effects of halothane, enflurane, and isoflurane on Ca^{2+} transients and papillary muscle tension in guinea pigs. *Anesthesiology.* 76:123–131. https://doi.org/10.1097/00000542-199201000-00018

Botcherby, E.J., A. Corbett, R.A.B. Burton, C.W. Smith, C. Bollensdorff, M.J. Booth, P. Kohl, T. Wilson, and G. Bub. 2013. Fast measurement of sarcomere length and cell orientation in Langendorff-perfused hearts using remote focusing microscopy. *Circ. Res.* 113:863–870. https://doi.org/10.1161/CIRCRESAHA.113.301704

Bub, G., P. Camelliti, C. Bollensdorff, D.J. Stuckey, G. Picton, R.A.B. Burton, K. Clarke, and P. Kohl. 2010. Measurement and analysis of sarcomere length in rat cardiomyocytes in situ and in vitro. *Am. J. Physiol. Heart Circ. Physiol.* 298:H1616–H1625. https://doi.org/10.1152/ajpheart.00481.2009

Camara, A.K.S., Z. Begic, W.M. Kwok, and Z.J. Bosnjak. 2001. Differential modulation of the cardiac L- and T-type calcium channel currents by isoflurane. *Anesthesiology.* 95:515–524. https://doi.org/10.1097/00000542-200108000-00038

Cazorla, O., A. Freiburg, M. Helmes, T. Centner, M. McNabb, Y. Wu, K. Trombitás, S. Labeit, and H. Granzier. 2000. Differential expression of cardiac titin isoforms and modulation of cellular stiffness. *Circ. Res.* 86:59–67. https://doi.org/10.1161/01.RES.86.1.59

Cazorla, O., Y. Wu, T.C. Irving, and H. Granzier. 2001. Titin-based modulation of calcium sensitivity of active tension in mouse skinned cardiac myocytes. *Circ. Res.* 88:1028–1035. https://doi.org/10.1161/hh1001.090876

Conover, G.M., and C.C. Gregorio. 2011. The desmin coil 1B mutation K190A impairs nebulin Z-disc assembly and destabilizes actin thin filaments. *J. Cell Sci.* 124:3464–3476. https://doi.org/10.1242/jcs.087080

Davies, L.A., C.N. Gibson, M.R. Boyett, P.M. Hopkins, and S.M. Harrison. 2000. Effects of isoflurane, sevoflurane, and halothane on myofilament Ca^{2+} sensitivity and sarcoplasmic reticulum Ca^{2+} release in rat ventricular myocytes. *Anesthesiology.* 93:1034–1044. https://doi.org/10.1097/00000542-200010000-00027

de Souza Leite, F., and D.E. Rassier. 2020. Sarcomere length nonuniformity and force regulation in myofibrils and sarcomeres. *Biophys. J.* 119:2372–2377. https://doi.org/10.1016/j.bpj.2020.11.005

Epstein, N.D., and J.S. Davis. 2003. Sensing stretch is fundamental. *Cell.* 112:147–150. https://doi.org/10.1016/S0092-8674(03)00037-0

Fukuda, N., H. Fujita, T. Fujita, and S. Ishiwata. 1998. Regulatory roles of MgADP and calcium in tension development of skinned cardiac muscle. *J. Muscle Res. Cell Motil.* 19:909–921. https://doi.org/10.1023/A:1005437517287

Fukuda, N., Y. Wu, G. Farman, T.C. Irving, and H. Granzier. 2003. Titin isoform variance and length dependence of activation in skinned bovine cardiac muscle. *J. Physiol.* 553:147–154. https://doi.org/10.1113/jphysiol.2003.049759

Fukuda, N., Y. Wu, G. Farman, T.C. Irving, and H. Granzier. 2005a. Titin-based modulation of active tension and interfilament lattice spacing in skinned rat cardiac muscle. *Pflugers Arch.* 449:449–457. https://doi.org/10.1007/s00424-004-1354-6

Fukuda, N., Y. Wu, P. Nair, and H.L. Granzier. 2005b. Phosphorylation of titin modulates passive stiffness of cardiac muscle in a titin isoform-dependent manner. *J. Gen. Physiol.* 125:257–271. https://doi.org/10.1085/jgp.200409177

Fukuda, N., H.L. Granzier, S. Ishiwata, and S. Kurihara. 2008. Physiological functions of the giant elastic protein titin in mammalian striated muscle. *J. Physiol. Sci.* 58:151–159. https://doi.org/10.2170/physiolsci.RV005408

Fukuda, N., T. Terui, S. Ishiwata, and S. Kurihara. 2010. Titin-based regulations of diastolic and systolic functions of mammalian cardiac muscle. *J. Mol. Cell. Cardiol.* 48:876–881. https://doi.org/10.1016/j.yjmcc.2009.11.013

García-Olloqui, P., J.R. Rodriguez-Madoz, M. Di Scala, G. Abizanda, Á. Vales, C. Olagüe, O. Iglesias-García, E. Larequi, L.P. Aguado-Alvaro, A. Ruiz-Villalba, et al. 2020. Effect of heart ischemia and administration route on biodistribution and transduction efficiency of AAV9 vectors. *J. Tissue Eng. Regen. Med.* 14:123–134. https://doi.org/10.1002/term.2974

Gordon, A.M., A.F. Huxley, and F.J. Julian. 1966. The variation in isometric tension with sarcomere length in vertebrate muscle fibres. *J. Physiol.* 184:170–192. https://doi.org/10.1113/jphysiol.1966.sp007909

Granzier, H., and S. Labeit. 2002. Cardiac titin: an adjustable multi-functional spring. *J. Physiol.* 541:335–342. https://doi.org/10.1113/jphysiol.2001.014381

Granzier, H.L., and S. Labeit. 2004. The giant protein titin: a major player in myocardial mechanics, signaling, and disease. *Circ. Res.* 94:284–295. https://doi.org/10.1161/01.RES.0000117769.88862.F8

Guo, A., C. Zhang, S. Wei, B. Chen, and L.S. Song. 2013. Emerging mechanisms of T-tubule remodelling in heart failure. *Cardiovasc. Res.* 98:204–215. https://doi.org/10.1093/cvr/cvt020

Hanley, P.J., and D.S. Loiselle. 1998. Mechanisms of force inhibition by halothane and isoflurane in intact rat cardiac muscle. *J. Physiol.* 506:231–244. https://doi.org/10.1111/j.1469-7793.1998.231bx.x

Hannon, J.D., and M.J. Cody. 2002. Effects of volatile anesthetics on sarcolemmal calcium transport and sarcoplasmic reticulum calcium content in isolated myocytes. *Anesthesiology*. 96:1457–1464. https://doi.org/10.1097/00000542-200206000-00027

Helmes, M., K. Trombitás, T. Centner, M. Kellermayer, S. Labeit, W.A. Linke, and H. Granzier. 1999. Mechanically driven contour-length adjustment in rat cardiac titin's unique N2B sequence: titin is an adjustable spring. *Circ. Res.* 84:1339–1352. https://doi.org/10.1161/01.RES.84.11.1339

Herland, J.S., F.J. Julian, and D.G. Stephenson. 1993. Effects of halothane, enflurane, and isoflurane on skinned rat myocardium activated by Ca^{2+}. *Am. J. Physiol.* 264:H224–H232. https://doi.org/10.1152/ajpheart.1993.264.1.H224

Huxley, A.F. 1957. Muscle structure and theories of contraction. *Prog. Biophys. Biophys. Chem.* 7:255–318. https://doi.org/10.1016/S0096-4174(18)30128-8

Huxley, A.F., and R.M. Simmons. 1971. Proposed mechanism of force generation in striated muscle. *Nature.* 233:533–538. https://doi.org/10.1038/233533a0

Ibarra, C., J.M. Vicencio, M. Estrada, Y. Lin, P. Rocco, P. Rebellato, J.P. Munoz, J. Garcia-Prieto, A.F.G. Quest, M. Chiong, et al. 2013. Local control of nuclear calcium signaling in cardiac myocytes by perinuclear microdomains of sarcolemmal insulin-like growth factor 1 receptors. *Circ. Res.* 112:236–245. https://doi.org/10.1161/CIRCRESAHA.112.273839

Inoue, T., F. Kobirumaki-Shimozawa, T. Kagemoto, T. Fujii, T. Terui, Y. Kusakari, K. Hongo, S. Morimoto, I. Ohtsuki, K. Hashimoto, et al. 2013. Depressed Frank-Starling mechanism in the left ventricular muscle of the knock-in mouse model of dilated cardiomyopathy with troponin T deletion mutation ΔK210. *J. Mol. Cell. Cardiol.* 63:69–78. https://doi.org/10.1016/j.yjmcc.2013.07.001

Kagemoto, T., K. Oyama, M. Yamane, S. Tsukamoto, F. Kobirumaki-Shimozawa, A. Li, C. Dos Remedios, N. Fukuda, and S. Ishiwata. 2018. Sarcomeric auto-oscillations in single myofibrils from the heart of patients with dilated cardiomyopathy. *Circ. Heart Fail.* 11:e004333. https://doi.org/10.1161/CIRCHEARTFAILURE.117.004333

Kentish, J.C., H.E. ter Keurs, L. Ricciardi, J.J. Bucx, and M.I. Noble. 1986. Comparison between the sarcomere length-force relations of intact and skinned trabeculae from rat right ventricle. Influence of calcium concentrations on these relations. *Circ. Res.* 58:755–768. https://doi.org/10.1161/01.RES.58.6.755

King, N.M.P., M. Methawasin, J. Nedrud, N. Harrell, C.S. Chung, M. Helmes, and H. Granzier. 2011. Mouse intact cardiac myocyte mechanics: cross-bridge and titin-based stress in unactivated cells. *J. Gen. Physiol.* 137:81–91. https://doi.org/10.1085/jgp.201010499

Kobirumaki-Shimozawa, F., T. Inoue, S.A. Shintani, K. Oyama, T. Terui, S. Minamisawa, S. Ishiwata, and N. Fukuda. 2014. Cardiac thin filament regulation and the Frank-Starling mechanism. *J. Physiol. Sci.* 64:221–232. https://doi.org/10.1007/s12576-014-0314-y

Kobirumaki-Shimozawa, F., K. Oyama, T. Shimozawa, A. Mizuno, T. Ohki, T. Terui, S. Minamisawa, S. Ishiwata, and N. Fukuda. 2016. Nano-imaging of the beating mouse heart in vivo: Importance of sarcomere dynamics, as opposed to sarcomere length per se, in the regulation of cardiac function. *J. Gen. Physiol.* 147:53–62. https://doi.org/10.1085/jgp.201511484

Kobirumaki-Shimozawa, F., T. Shimozawa, K. Oyama, Y. Kushida, T. Terui, S. Ishiwata, and N. Fukuda. 2018. Optimization of fluorescent labeling for in vivo nanoimaging of sarcomeres in the mouse heart. *Biomed Res. Int.* 2018:4349170. https://doi.org/10.1155/2018/4349170

Kobirumaki-Shimozawa, F., T. Nakanishi, T. Shimozawa, T. Terui, K. Oyama, J. Li, W.E. Louch, S. Ishiwata, and N. Fukuda. 2020. Real-time in vivo imaging of mouse left ventricle reveals fluctuating movements of the intercalated discs. *Nanomaterials (Basel)*. 10:532. https://doi.org/10.3390/nano10030532

Kono, F., S. Kawai, Y. Shimamoto, and S. Ishiwata. 2020. Nanoscopic changes in the lattice structure of striated muscle sarcomeres involved in the mechanism of spontaneous oscillatory contraction (SPOC). *Sci. Rep.* 10:16372. https://doi.org/10.1038/s41598-020-73247-1

Laver, D.R., J. Attia, C. Oldmeadow, and A.W. Quail. 2017. Cardiac calcium release channel (ryanodine receptor 2) regulation by halogenated anesthetics. *Anesthesiology.* 126:495–506. https://doi.org/10.1097/ALN.0000000000001519

Lindsey, M.L., Z. Kassiri, J.A.I. Virag, L.E. de Castro Brás, and M. Scherrer-Crosbie. 2018. Guidelines for measuring cardiac physiology in mice. *Am. J. Physiol. Heart Circ. Physiol.* 314:H733–H752. https://doi.org/10.1152/ajpheart.00339.2017

Linke, W.A., D.E. Rudy, T. Centner, M. Gautel, C. Witt, S. Labeit, and C.C. Gregorio. 1999. I-band titin in cardiac muscle is a three-element molecular spring and is critical for maintaining thin filament structure. *J. Cell Biol.* 146:631–644. https://doi.org/10.1083/jcb.146.3.631

Lockard, V.G., and S. Bloom. 1993. Trans-cellular desmin-lamin B intermediate filament network in cardiac myocytes. *J. Mol. Cell. Cardiol.* 25:303–309. https://doi.org/10.1006/jmcc.1993.1036

Moo, E.K., T.R. Leonard, and W. Herzog. 2017. In vivo sarcomere lengths become more non-uniform upon activation in intact whole muscle. *Front. Physiol.* 8:1015. https://doi.org/10.3389/fphys.2017.01015

Murat, I., R. Ventura-Clapier, and G. Vassort. 1988. Halothane, enflurane, and isoflurane decrease calcium sensitivity and maximal force in detergent-treated rat cardiac fibers. *Anesthesiology*. 69:892–899. https://doi.org/10.1097/00000542-198812000-00015

Nadadur, R.D., M.T. Broman, B. Boukens, S.R. Mazurek, X. Yang, M. van den Boogaard, J. Bekeny, M. Gadek, T. Ward, M. Zhang, et al. 2016. Pitx2 modulates a Tbx5-dependent gene regulatory network to maintain atrial rhythm. *Sci. Transl. Med.* 8:354ra115. https://doi.org/10.1126/scitranslmed.aaf4891

Sarai, N., Y. Kihara, T. Izumi, T. Mitsuiye, S. Matsuoka, and A. Noma. 2002. Nonuniformity of sarcomere shortenings in the isolated rat ventricular myocyte. *Jpn. J. Physiol.* 52:371–381. https://doi.org/10.2170/jjphysiol.52.371

Serizawa, T., T. Terui, T. Kagemoto, A. Mizuno, T. Shimozawa, F. Kobirumaki, S. Ishiwata, S. Kurihara, and N. Fukuda. 2011. Real-time measurement of the length of a single sarcomere in rat ventricular myocytes: a novel analysis with quantum dots. *Am. J. Physiol. Cell Physiol.* 301:C1116–C1127. https://doi.org/10.1152/ajpcell.00161.2011

Shimamoto, Y., M. Suzuki, S.V. Mikhailenko, K. Yasuda, and S. Ishiwata. 2009. Inter-sarcomere coordination in muscle revealed through individual sarcomere response to quick stretch. *Proc. Natl. Acad. Sci. USA.* 106:11954–11959. https://doi.org/10.1073/pnas.0813288106

Shimozawa, T., E. Hirokawa, F. Kobirumaki-Shimozawa, K. Oyama, S.A. Shintani, T. Terui, Y. Kushida, S. Tsukamoto, T. Fujii, S. Ishiwata, et al. 2017. In vivo cardiac nano-imaging: a new technology for high-precision analyses of sarcomere dynamics in the heart. *Prog. Biophys. Mol. Biol.* 124:31–40. https://doi.org/10.1016/j.pbiomolbio.2016.09.006

Shintani, S.A., K. Oyama, F. Kobirumaki-Shimozawa, T. Ohki, S. Ishiwata, and N. Fukuda. 2014. Sarcomere length nanometry in rat neonatal cardiomyocytes expressed with α-actinin-AcGFP in Z discs. *J. Gen. Physiol.* 143:513–524. https://doi.org/10.1085/jgp.201311118

Terui, T., M. Sodnomtseren, D. Matsuba, J. Udaka, S. Ishiwata, I. Ohtsuki, S. Kurihara, and N. Fukuda. 2008. Troponin and titin coordinately regulate length-dependent activation in skinned porcine ventricular muscle. *J. Gen. Physiol.* 131:275–283. https://doi.org/10.1085/jgp.200709895

Terui, T., Y. Shimamoto, M. Yamane, F. Kobirumaki, I. Ohtsuki, S. Ishiwata, S. Kurihara, and N. Fukuda. 2010. Regulatory mechanism of length-dependent activation in skinned porcine ventricular muscle: role of thin filament cooperative activation in the Frank-Starling relation. *J. Gen. Physiol.* 136:469–482. https://doi.org/10.1085/jgp.201010502

Trombitás, K., M. Greaser, S. Labeit, J.P. Jin, M. Kellermayer, M. Helmes, and H. Granzier. 1998. Titin extensibility in situ: entropic elasticity of permanently folded and permanently unfolded molecular segments. *J. Cell Biol.* 140:853–859. https://doi.org/10.1083/jcb.140.4.853

Tsukamoto, S., T. Fujii, K. Oyama, S.A. Shintani, T. Shimozawa, F. Kobirumaki-Shimozawa, S. Ishiwata, and N. Fukuda. 2016. Simultaneous imaging of local calcium and single sarcomere length in rat neonatal cardiomyocytes using yellow Cameleon-Nano140. *J. Gen. Physiol.* 148:341–355. https://doi.org/10.1085/jgp.201611604

Weiwad, W.K., W.A. Linke, and M.H. Wussling. 2000. Sarcomere length-tension relationship of rat cardiac myocytes at lengths greater than optimum. *J. Mol. Cell. Cardiol.* 32:247–259. https://doi.org/10.1006/jmcc.1999.1069

Wu, Z., K. Wong, M. Glogauer, R.P. Ellen, and C.A. McCulloch. 1999. Regulation of stretch-activated intracellular calcium transients by actin filaments. *Biochem. Biophys. Res. Commun.* 261:419–425. https://doi.org/10.1006/bbrc.1999.1057

Wu, Y., O. Cazorla, D. Labeit, S. Labeit, and H. Granzier. 2000. Changes in titin and collagen underlie diastolic stiffness diversity of cardiac muscle. *J. Mol. Cell. Cardiol.* 32:2151–2161. https://doi.org/10.1006/jmcc.2000.1281

Zhang, J.Q., B. Elzey, G. Williams, S. Lu, D.J. Law, and R. Horowits. 2001. Ultrastructural and biochemical localization of N-RAP at the interface between myofibrils and intercalated disks in the mouse heart. *Biochemistry*. 40:14898–14906. https://doi.org/10.1021/bi0107445

Supplemental material

Materials and methods

Echocardiography

A short-axis M-mode cine loop was recorded at the level of papillary muscles to assess LV end-diastolic and end-systolic internal dimensions, posterior wall end-diastolic and end-systolic thicknesses, and LV function via measurement of fractional shortening (FS) and ejection fraction (EF; based on Nadadur et al., 2016; Lindsey et al., 2018). Images were obtained with the Vevo 3100 High Resolution Imaging System (Visual-Sonics) using the model MX550D scan head designed for mice. Following anesthetic induction with ∼5% isoflurane, mice were placed in the supine position on a heated platform for echocardiography. Body temperature was maintained at 37°C during measurement, and anesthesia was maintained with ∼0.5–1.0% isoflurane. HR was maintained in the range of ∼400–500 bpm.

CellMask treatment

The mouse heart was treated with the plasma membrane stain CellMask Orange (CellMask; Thermo Fisher Scientific) according to our previously published procedure (Kobirumaki-Shimozawa et al., 2018). Namely, animals were anesthetized with ∼2% isoflurane and warmed at 38°C during ventilation. A small piece of gauze was placed on the LV surface of open-chest mice (i.e., second surgery as in the text), and the CellMask solution (dissolved in PBS (−)) at a concentration of 0.1 µg/ml was gently dropped onto it for 5 min using a pipette. CellMask-treated myocytes on the LV surface were excited by a 532-nm laser light (PID-1500; Snake Creek Lasers) and observed under the microscopic system used for AcGFP imaging. The resultant fluorescence signals (emission filter, BA575IF; Olympus Co.) were detected at a 512 × 80–pixel resolution at an exposure time of 4.82 ms.

Results and discussion I

We confirmed by using echocardiography that the first open-chest surgery did not affect macroscopic cardiac functions; namely, echocardiography measurements revealed that the values of LVEF, FS, diastolic and systolic LV internal dimensions, and the thickness of the ventricular wall in diastole and systole in mice 2 d after the surgery were similar to those in mice without surgery (Fig. S1 and Table S1).

Results and discussion II

Recently, García-Olloqui et al. (2020) systematically investigated in mice the expression of cardiac-specific troponin T via adenovirus injections. They demonstrated that viral expression was detected by day 1 and reached a peak by days 3–7. The present result that α-actinin-AcGFP was expressed 2 d after an ADV injection is consistent with the finding of their previous work. Given, however, the short period of time (2 d) between an ADV injection and the second open-chest operation for sarcomere imaging employed in the present study, it is not impossible that local Ca^{2+} homeostasis, or local excitation–contraction coupling, or both, is affected via ADV injection in nearby myocytes, even though the appropriate doses (1×10^{11} to 1×10^{12} viral particles/ml; determined in Kobirumaki-Shimozawa et al., 2018) are used.

Results and discussion III

In order to confirm asynchronous sarcomere behaviors, we performed a control experiment in a CellMask-treated in vivo beating heart because this procedure allows us to avoid the first open-chest surgery and adenovirus infection and hence is less invasive than α-actinin-AcGFP expression. As previously shown by us (Kobirumaki-Shimozawa et al., 2018), clear striation patterns were observed following CellMask treatment (Fig. S13 A and Video 5). First, we analyzed the precision of the single T-tubular distance measurement in a myocyte in the left ventricle of the in vivo mouse heart at rest (Fig. S13 B and Video 5). The precision value for the single T-tubular distance measurement was 110 nm at 197 fps (see Fig. S13 C).

In the in vivo beating mouse heart treated with CellMask, we selected three regions of interest (i.e., M1, M2, and M3) in an LV myocyte when ΔLVP was 73.0 ± 0.3 mm Hg (HR, 492 ± 0.4 bpm; Fig. S14 A and Video 6). The CI values were 0.31 ± 0.18, 0.28 ± 0.11, and 0.39 ± 0.15 for M1, M2, and M3, respectively (average, 0.33 ± 0.15; Table S3). This average value was similar to that at ΔLVP 96.4, 60.5, or 40.6 mm Hg with α-actinin-AcGFP expression (cf. Table 1). Irregular color configurations in the top row of the triangular heat maps are consistent with the notion that the magnitude of contribution of individual sarcomeres (surrogated as the T-tubular distances) to the average myofibrillar movements varies between sarcomeres (Fig. S14 B), as found with α-actinin-AcGFP expression. Likewise, color configurations were disordered in rows below the top, especially in the diagonal portion (i.e., one position right of the leftmost edge), indicating asynchronous movements between adjacent sarcomeres. Moreover, individual sarcomeres alternatively contributed to myofibrillar dynamics during six cardiac cycles (Fig. S14 C). These findings are consistent with those obtained via α-actinin-AcGFP expression in the heart (see text for details). We therefore consider that the apparently low value of CI

(~0.3) is not caused by the procedures for α-actinin-AcGFP expression in Z-disks, such as the first open-chest surgery and adenovirus infection, but rather it represents a fundamental nature of the sarcomere dynamics in LV myocytes of the beating mouse heart in vivo.

Results and discussion IV

In the present study, we used isoflurane to anesthetize mice as well as to depress ventricular contractility. Isoflurane is widely used to anesthetize mice for various types of in vivo experiments, such as pressure–volume loop and echocardiography experiments in the cardiovascular field; it exerts its negative inotropic effect on the heart via alteration of excitation–contraction coupling, as evident by diminished intracellular Ca^{2+} transients (Bosnjak et al., 1992; Hanley and Loiselle, 1998; Davies et al., 2000). Numerous earlier studies have suggested that the negative inotropic effect is caused via inhibition of L-type Ca^{2+} channels (e.g., Bosnjak et al., 1991; Camara et al., 2001), not via an activating effect on cardiac ryanodine receptors (and the resultant depletion of Ca^{2+} in the SR; e.g., Laver et al., 2017). Likewise, isoflurane may decrease myofibrillar Ca^{2+} sensitivity. Some investigators reported data that are consistent with this idea (e.g., Murat et al., 1988; Bosnjak et al., 1992; Davies et al., 2000), whereas others concluded that a reduction in myofilament Ca^{2+} sensitivity plays little or no role in the negative inotropic effects of isoflurane (e.g., Herland et al., 1993). Therefore, it is reasonable to consider that the negative inotropic effect of isoflurane is primarily caused by suppression of Ca^{2+} entry through L-type Ca^{2+} channels and subsequent reduction of the amount of Ca^{2+} release from the SR (Bosnjak et al., 1991; Camara et al., 2001; Hannon and Cody, 2002). Therefore, it may be possible that isoflurane-induced changes in local $[Ca^{2+}]_i$ in myocytes may influence the magnitude of synchrony (CI) in myocytes, especially under deep anesthesia (Fig. 4). Future studies are needed to investigate whether asynchronous sarcomere movements depend on the isoflurane concentration by simultaneously measuring local $[Ca^{2+}]_i$ and individual sarcomere movements in the in vivo beating heart (see Results and discussion VI).

Results and discussion V

As demonstrated in our previous study (Kobirumaki-Shimozawa et al., 2018), an ADV injection allows the expression of α-actinin-AcGFP in a few myocytes in the left ventricle of a mouse, with the fraction of α-actinin-AcGFP–expressing myocytes being ~10%. By taking advantage of this methodological property, we further analyzed SL synchrony in myocytes at ΔLVP in the physiological and near-physiological levels (i.e., mice with ΔLVP 96.4 and 60.5 mm Hg; see, e.g., Figs. 4 and 5 and Table 1). Fig. S20, A and B, shows myocytes in the left ventricle of a mouse with ΔLVP 96.4 mm Hg, but at different pressure points (i.e., ΔLVP 107.7 ± 2.8 mm Hg, HR 464 ± 15.7 bpm; and ΔLVP 90.4 ± 4.1 mm Hg, HR 550 ± 22.6 bpm, respectively). We analyzed two myofibrils at ΔLVP 107.7 ± 2.8 mm Hg and three myofibrils at 90.4 ± 4.1 mm Hg. We found that the average CI values were 0.49 ± 0.14 and 0.26 ± 0.31 for M1 and M2, respectively, at 107.7 ± 2.8 mm Hg (six cardiac cycles), and 0.25 ± 0.19, 0.28 ± 0.20, and 0.31 ± 0.13 for M1, M2, and M3, respectively, at ΔLVP 90.4 ± 4.1 mm Hg (six cardiac cycles). Fig. S20, C and D, shows myocytes of the mouse with ΔLVP 60.5 mm Hg at different pressure points (i.e., ΔLVP 87.2 ± 1.4 mm Hg, HR 595 ± 0.4 bpm; and 70.5 ± 1.7 mm Hg, HR 582 ± 25.3 bpm, respectively). We analyzed three myofibrils at both pressures. It was found that the average CI values were 0.28 ± 0.23, 0.32 ± 0.23, and 0.34 ± 0.30 for M1, M2, and M3, respectively, at 87.2 ± 1.4 mm Hg (seven cardiac cycles), and 0.25 ± 0.15, 0.29 ± 0.22, and 0.23 ± 0.28 for M1, M2, and M3, respectively, at 70.5 ± 1.7 mm Hg (eight cardiac cycles).

Inclusion of these data revealed that there was a significant positive linear relationship (R = 0.75; $P < 0.001$) between ΔLVP and contributing sarcomeres (Fig. S20 E; total 25 myofibrils at 10 pressure points). Similarly, a significant positive linear relationship (R = 0.89; $P < 0.001$) was revealed between ΔLVP and average CI (Fig. S20 F), supporting the notion that ventricular pump function is under the influence of sarcomere synchrony.

Results and discussion VI

We previously developed an experimental system for simultaneous nanoimaging of changes in the $[Ca^{2+}]_i$ at Z-disks and in the lengths of individual sarcomeres along a myofibril in rat neonatal cardiomyocytes (Tsukamoto et al., 2016). Namely, a FRET-based Ca^{2+} sensor yellow Cameleon-Nano140 (k_{on} and k_{off}, ~2.4 $\mu M^{-1}\ s^{-1}$ and ~0.3 s^{-1} at 25°C, respectively) was fused to α-actinin in order to localize to Z-disks. We found that although local Ca^{2+} transients were synchronized along a myofibril, the sarcomere movements were asynchronous (Tsukamoto et al., 2016). This previous finding is consistent with the notion that asynchronous behaviors of individual sarcomere movements in LV myocytes in the in vivo beating heart occur independently of Ca^{2+} but via intrinsic inter-sarcomere interactions. However, Sarai et al. (2002) demonstrated nonuniformity of individual sarcomere dynamics (shortening and lengthening) coupled, presumably, with inhomogeneous local Ca^{2+} transients in isolated adult rat cardiomyocytes. Therefore, future studies are needed to investigate whether asynchronous sarcomere movements are independent of Ca^{2+} by, for example, expressing a fast-kinetics, Ca^{2+}-sensitive fluorescent protein in Z-disks under an advanced microscope allowing simultaneous nanoimaging of local $[Ca^{2+}]_i$ and individual sarcomeric movements in LV myocytes in vivo at physiological heartbeat frequencies. This is likewise because it cannot be ruled out completely that the presently found asynchronous sarcomere movements may be caused by alteration of excitation–contraction coupling in myocytes at the single-sarcomere level due to technical procedures for in vivo cardiac nanoimaging (e.g., coverslip setting, adenovirus infection, and the use of isoflurane).

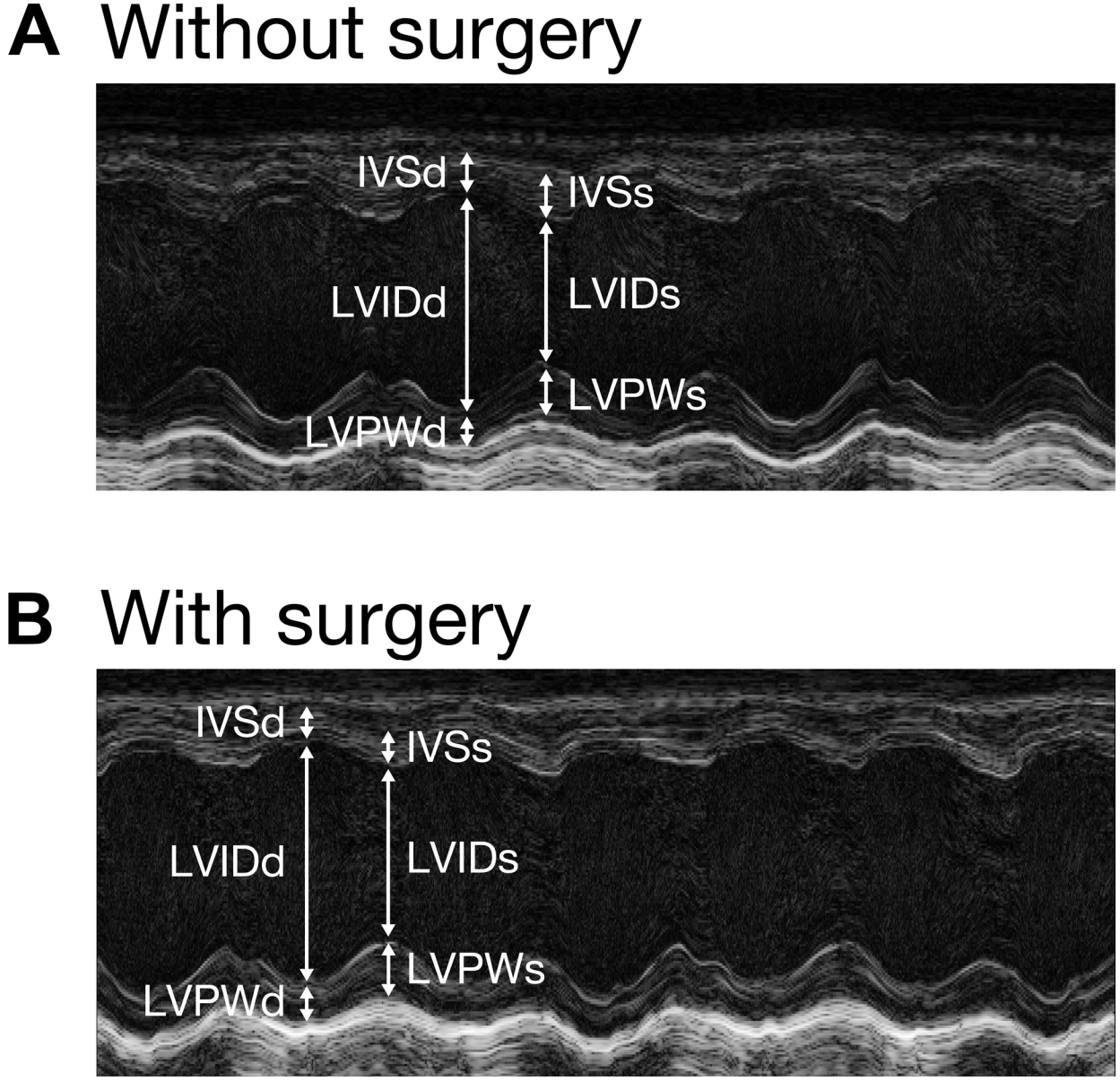

Figure S1. **Echocardiographic evaluation of the LV structure and function in mice with and without the first open-chest surgery. (A and B)** Representative 2-D guided M-mode images of the left ventricle in a mouse without surgery (A) and the age-matched animal with surgery (B) during diastole (d) and systole (s). In B, echocardiographic evaluation was performed 2 d after surgery. IVS, interventricular septum; LVID, LV internal dimension; LVPW, LV posterior wall.

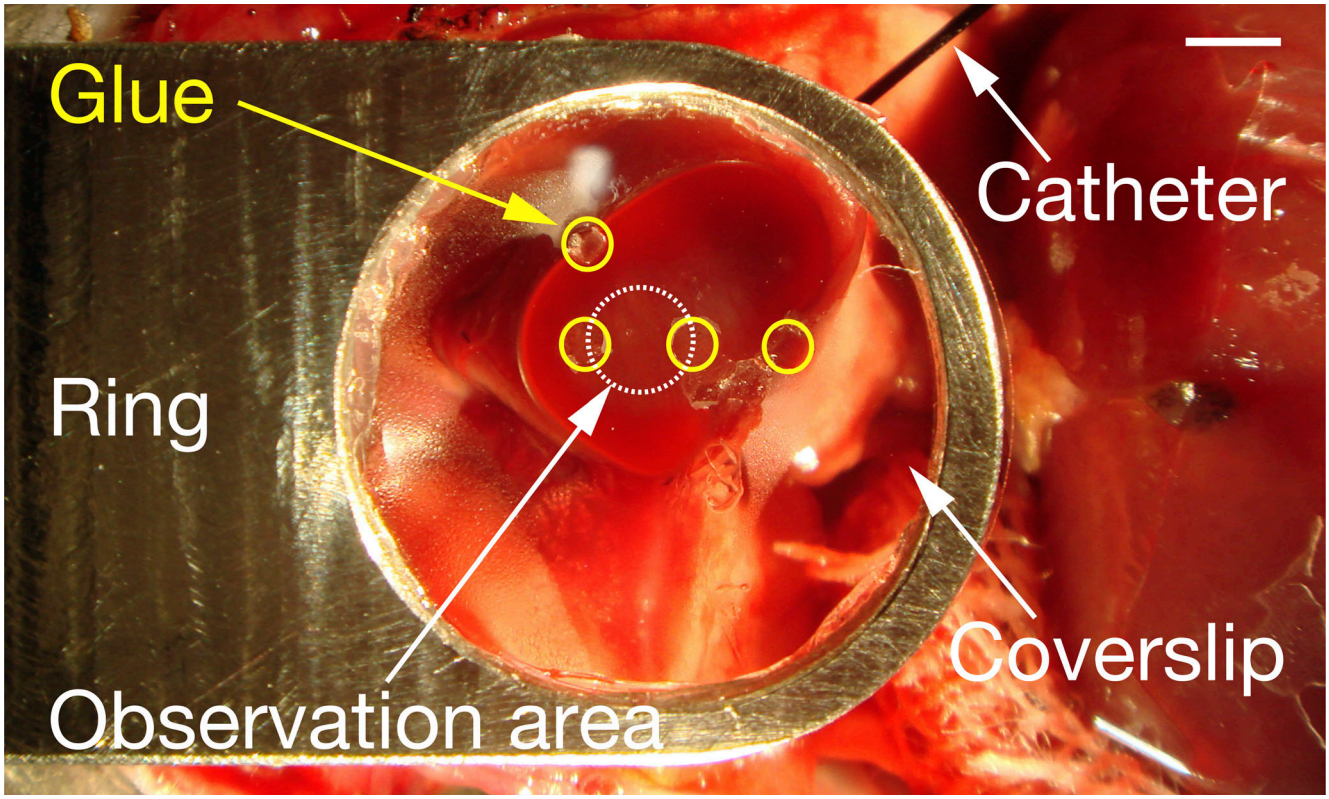

Figure S2. **Coverslip setting for nanoimaging of sarcomeres on the LV surface in an open-chest mouse.** A coverslip set on a metal ring (denoted by Ring; diameter, 12 mm) was gently placed on the LV surface of the heart (see Materials and methods). Animal head position is to the left. The LVP change caused by this procedure is <5% (as in Kobirumaki-Shimozawa et al., 2016). The coverslip and catheter (inserted into the left ventricle via the apex) are indicated by white arrows, and one of four glued areas (yellow circles; diameter, ~1 mm; ~2 mm apart) is indicated by the yellow arrow. An observation area between glued areas (dotted white circle; diameter, ~2 mm) is likewise indicated by a white arrow. Scale bar, 2 mm.

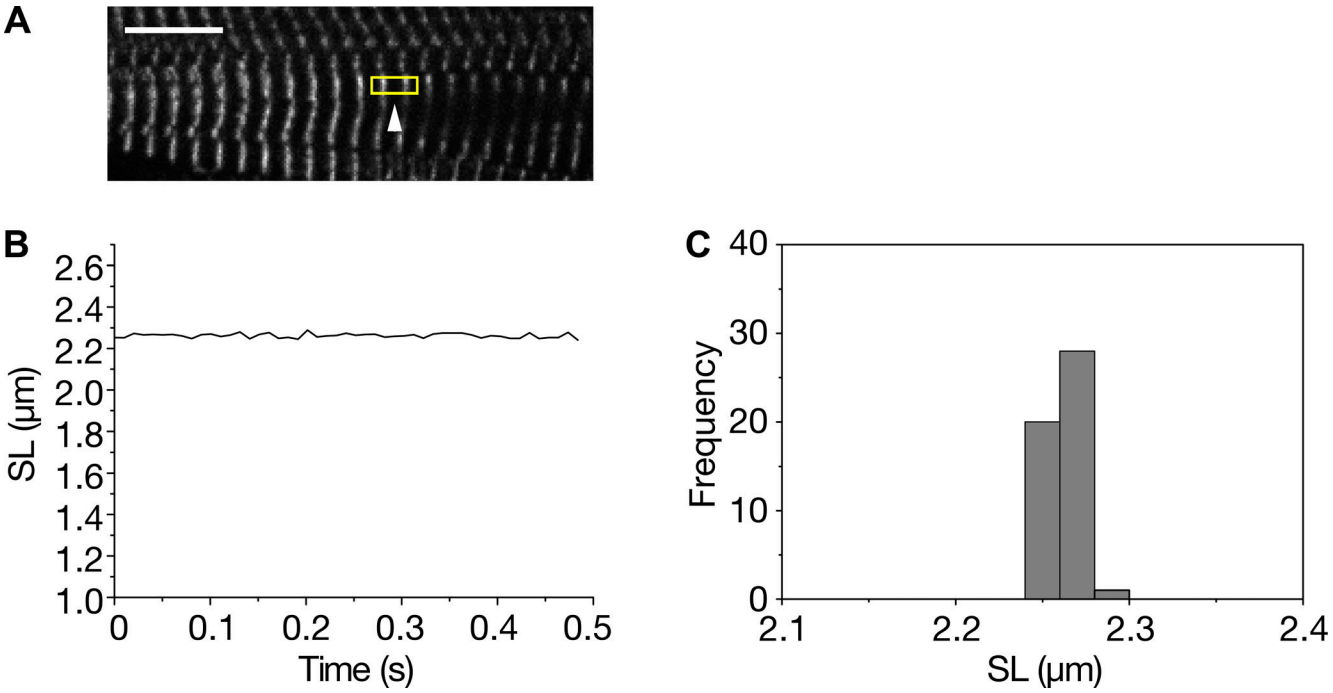

Figure S3. **Fluctuation analysis for the length of a single sarcomere in a myocyte in an in vivo mouse heart at rest. (A)** Confocal image showing a myocyte expressed with α-actinin-AcGFP in Z-disks in the left ventricle of the heart at rest in a mouse (with greater than ∼5% isoflurane). The sarcomere within the yellow-outlined rectangle (indicated by the arrowhead) was analyzed. Scale bar, 10 µm. See Video 1. **(B)** Time course of changes in SL. Imaging was performed at 100 fps. **(C)** Histogram showing the variance of SL. Average SL, 2.260 ± 0.011 µm, indicating that the SD (i.e., index of spatial resolution) was 11 nm.

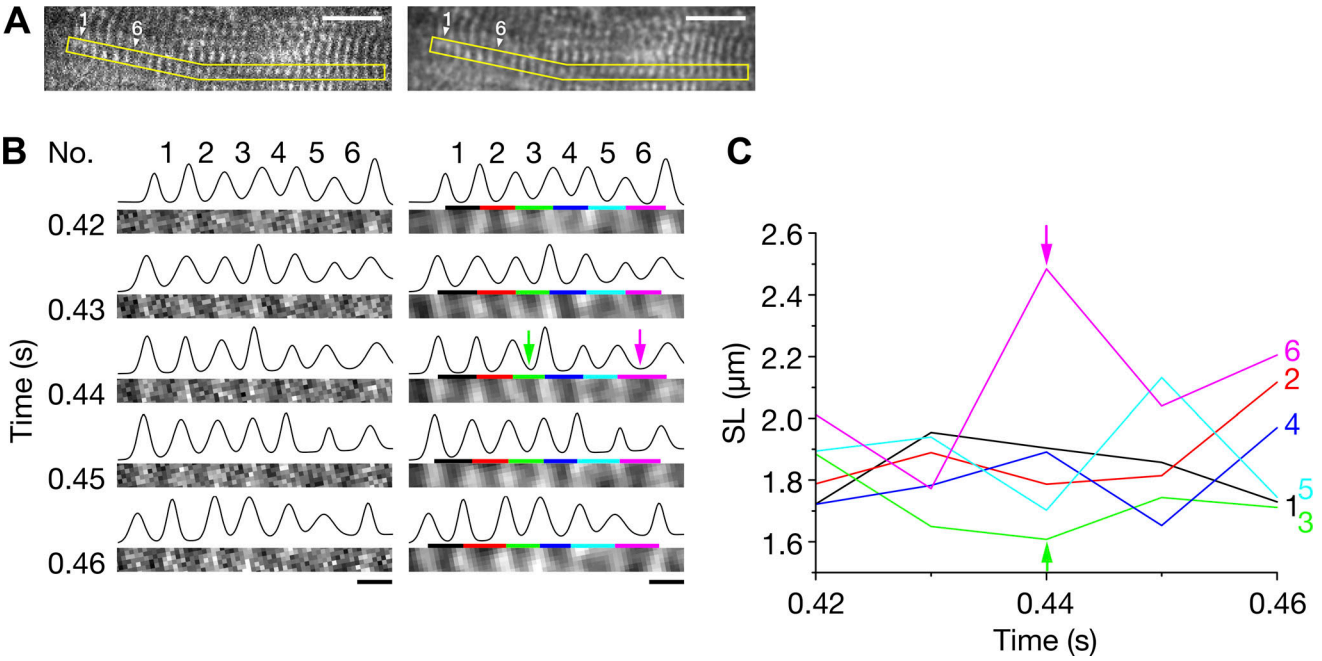

Figure S4. **Representative data showing SL changes in an LV myocyte in a mouse with normal systolic function. (A)** Left: Confocal image of a myofibril used for the analysis of sarcomeres (enlarged view of M1 in the yellow-outlined rectangle in Fig. 1 A). Right: Same as in left image, processed by Gaussian smoothing filter (1 σ). Data on sarcomere nos. 1–6 are shown below. Scale bars, 10 µm. **(B)** Left: Confocal images for sarcomere nos. 1–6 at various time points (i.e., 0.42, 0.43, 0.44, 0.45, and 0.46 s from the onset of imaging; compare Fig. 1 B). Sarcomere numbers are indicated on top and time points on left. Right: Same as in left image, processed by Gaussian smoothing filter (1 σ). Plot profiles were obtained from the raw data (left). Colored lines below the plot profiles indicate individual SLs (derived based on the plot profiles). Scale bars, 2 µm. **(C)** Data showing time course of changes in the lengths of sarcomere nos. 1–6 (sarcomere numbers indicated on right). At the midpoint of 0.44 s, SL values were 1.90, 1.79, 1.61, 1.89, 1.70, and 2.48 µm for sarcomere nos. 1, 2, 3, 4, 5, and 6, respectively (shortest [no. 3] and longest [no. 6] sarcomeres indicated by arrows). Magnitudes of change in SL were 11.8%, 15.6%, 14.7%, 16.1%, 20.2%, and 28.7% for sarcomere nos. 1, 2, 3, 4, 5, and 6, respectively. See Video 2.

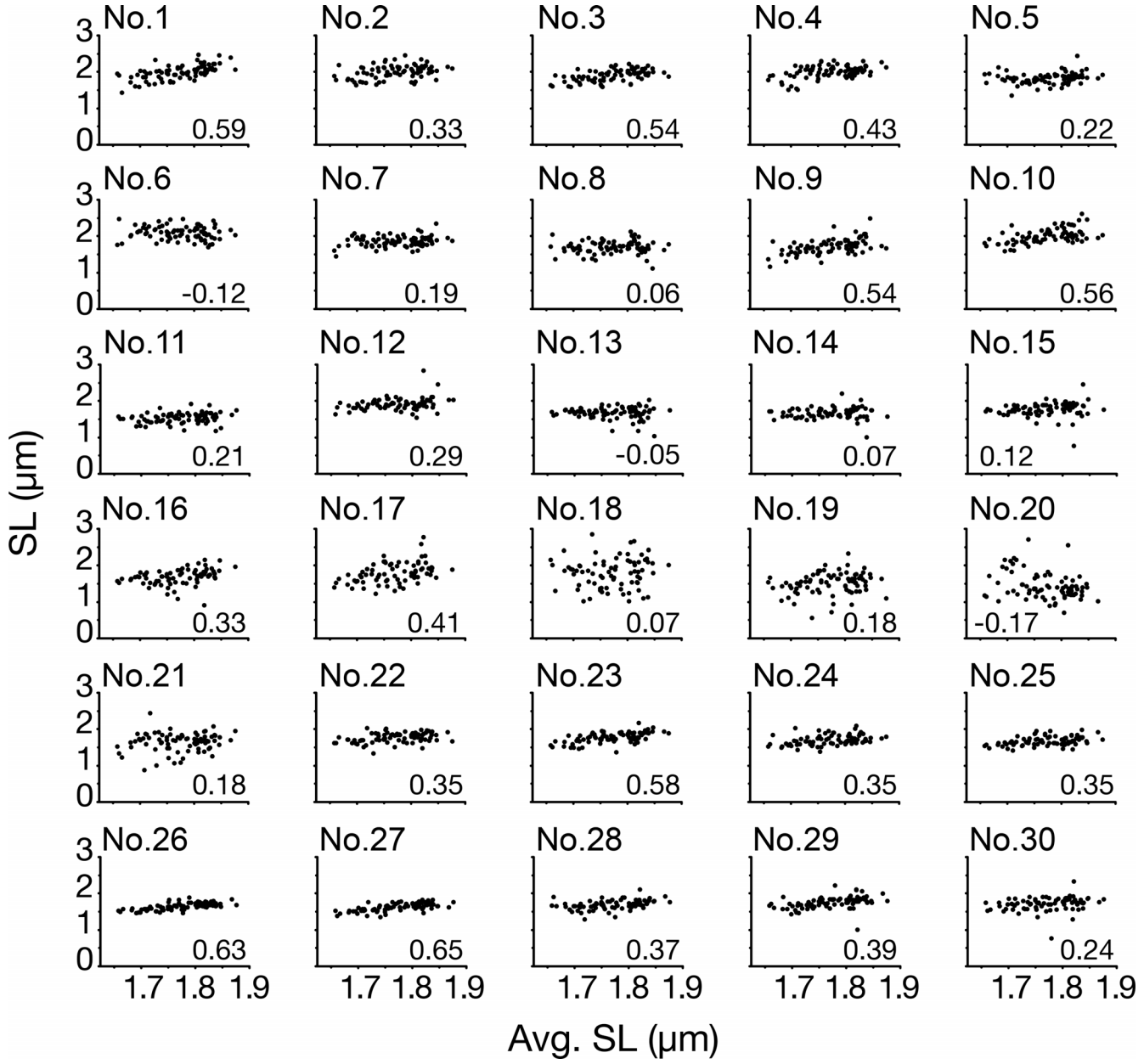

Figure S5. **Scatter plots between average and individual SLs in an LV myocyte of a mouse with normal systolic function.** Data from M1 in Fig. 1 A during six cardiac cycles are shown for sarcomere nos. 1–30 (79 plots for each sarcomere). Sarcomere number is shown on top of each graph. X axis, average SL (average length of 30 sarcomeres); y axis, individual SL. Number in graph indicates CI for each sarcomere (i.e., *R* between average and individual SLs).

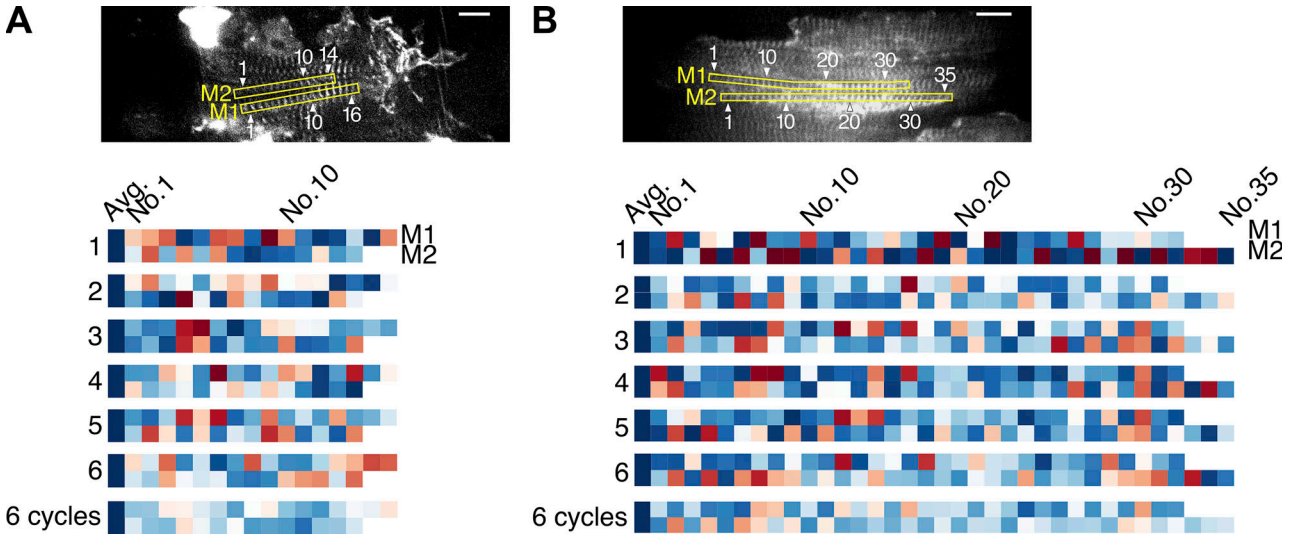

Figure S6. **In vivo tracking of individual sarcomeres in an LV myocyte of a mouse with low systolic function. (A)** Top: Confocal image of a myocyte expressing α-actinin-AcGFP in a mouse with ΔLVP 60.5 mm Hg. During six cardiac cycles, ΔLVP was 60.5 ± 4.2 mm Hg, and HR was 581 ± 6.6 bpm (Table 1). In 2 myofibrils, 16 and 14 sequentially connected sarcomeres (in yellow-outlined rectangles) were analyzed for M1 and M2, respectively. Numbers indicate longitudinal positions of sarcomeres. Scale bar, 10 µm. See Video 3. Bottom: Color diagram showing CI between average and individual SLs during six cardiac cycles for M1 and M2. Sarcomere numbers are indicated on top and cardiac cycle numbers on left. Data on the average of six cycles are shown on bottom. **(B)** Top: Same as in A, in a mouse with ΔLVP 40.6 mm Hg. During six cardiac cycles, ΔLVP was 40.6 ± 2.5 mm Hg, and HR was 347 ± 7.9 bpm (Table 1). In 2 myofibrils, 32 and 35 sequentially connected sarcomeres (in yellow-outlined rectangles) were analyzed for M1 and M2, respectively. Numbers indicate longitudinal positions of sarcomeres. Scale bar, 10 µm. See Video 4. Bottom: Color diagram showing CI between average and individual SLs during six cardiac cycles for M1 and M2. Sarcomere numbers are indicated on top, and cardiac cycle numbers on left. Data on the average of six cycles are shown on bottom.

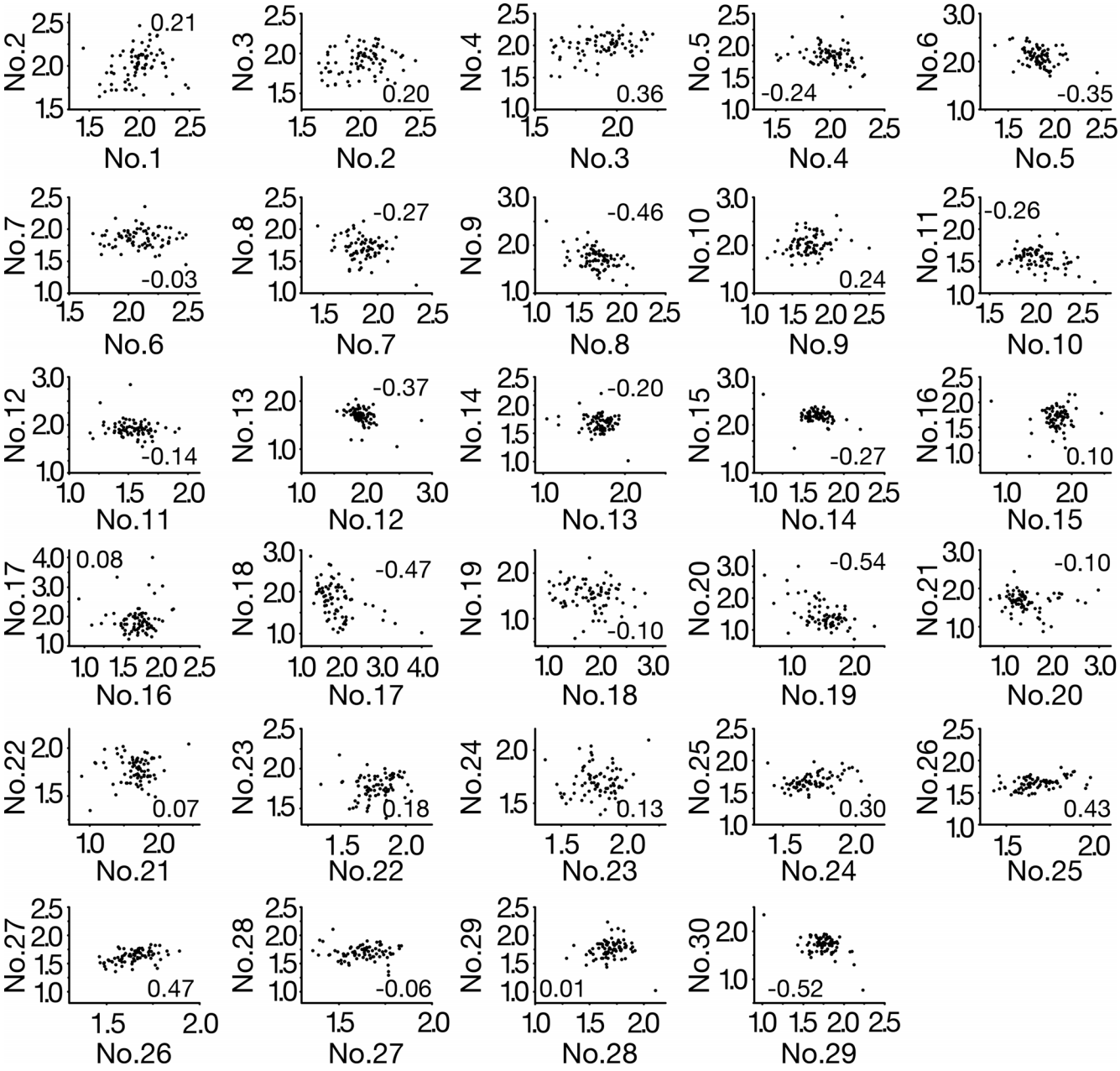

Figure S7. **Scatter plots between adjacent sarcomeres in an LV myocyte of a mouse with normal systolic function.** Data obtained from M1 in Fig. 1 A during six cardiac cycles were plotted for adjacent sarcomeres (i.e., from 1 versus 2 to 29 versus 30). Sarcomere numbers are indicated on x and y axes in each graph. CI is indicated on bottom right in each graph.

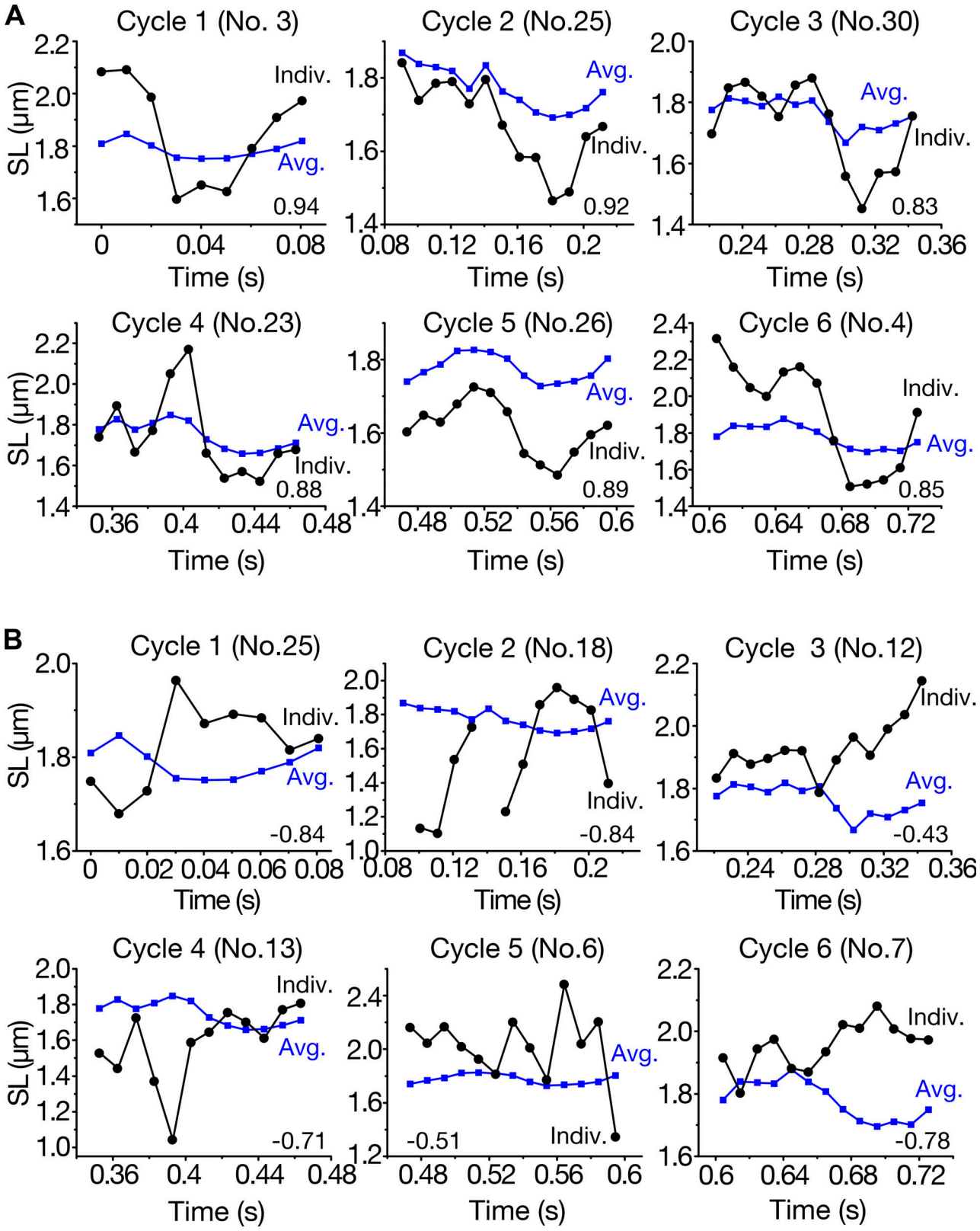

Figure S8. **Representative data showing the time course of changes in individual versus average SLs in an LV myocyte of a mouse with normal systolic function. (A)** Time course of changes in an individual SL versus average SL showing a positive correlation during six cardiac cycles. Cardiac cycle number is shown on top of each graph. Black circles, individual SL; blue squares, average SL. Sarcomere nos. 3, 25, 30, 23, 26, and 4 are shown for cycles 1, 2, 3, 4, 5, and 6, respectively. **(B)** Same as in A, showing a negative correlation during six cardiac cycles. Cardiac cycle number is shown on top of each graph. Black circles, individual SL; blue squares, average SL. Sarcomere nos. 25, 18, 12, 13, 6, and 7 are shown for cycles 1, 2, 3, 4, 5, and 6, respectively. In A and B, data were obtained from M1 in Fig. 1 A. Number in each graph indicates CI.

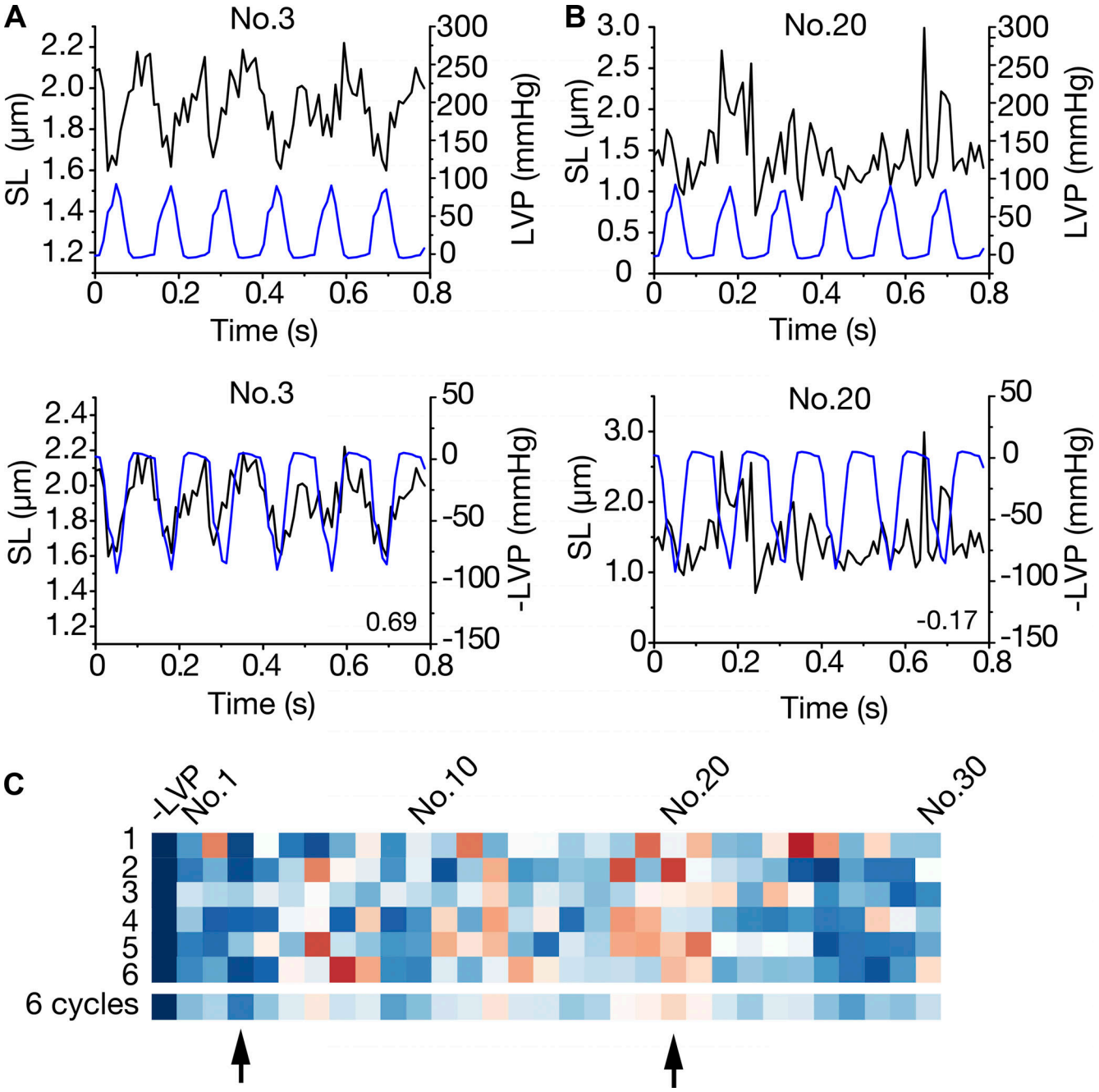

Figure S9. **Representative data for the time course of changes in individual SL versus LVP in an LV myocyte of a mouse with normal systolic function. (A)** Changes in an individual SL versus LVP (top) and an individual SL versus −LVP (bottom) showing a positive correlation. Data on sarcomere no. 3 in M1 (Fig. 1 A) were plotted. Black and blue lines indicate SL and LVP (or −LVP), respectively. **(B)** Same as in A, showing a negative correlation. Data on sarcomere no. 20 in M1 (Fig. 1 A) were plotted. Black and blue lines indicate SL and LVP (or −LVP), respectively. In A and B, number in bottom graph indicates CI. **(C)** Color diagram showing CI between individual SLs (nos. 1–30) and −LVP during six cardiac cycles. Sarcomere numbers are indicated on top and cardiac cycle numbers on left. Data on the average of six cycles are shown on bottom. Sarcomere nos. 3 (positive correlation; A) and 20 (negative correlation; B) are indicated by arrows.

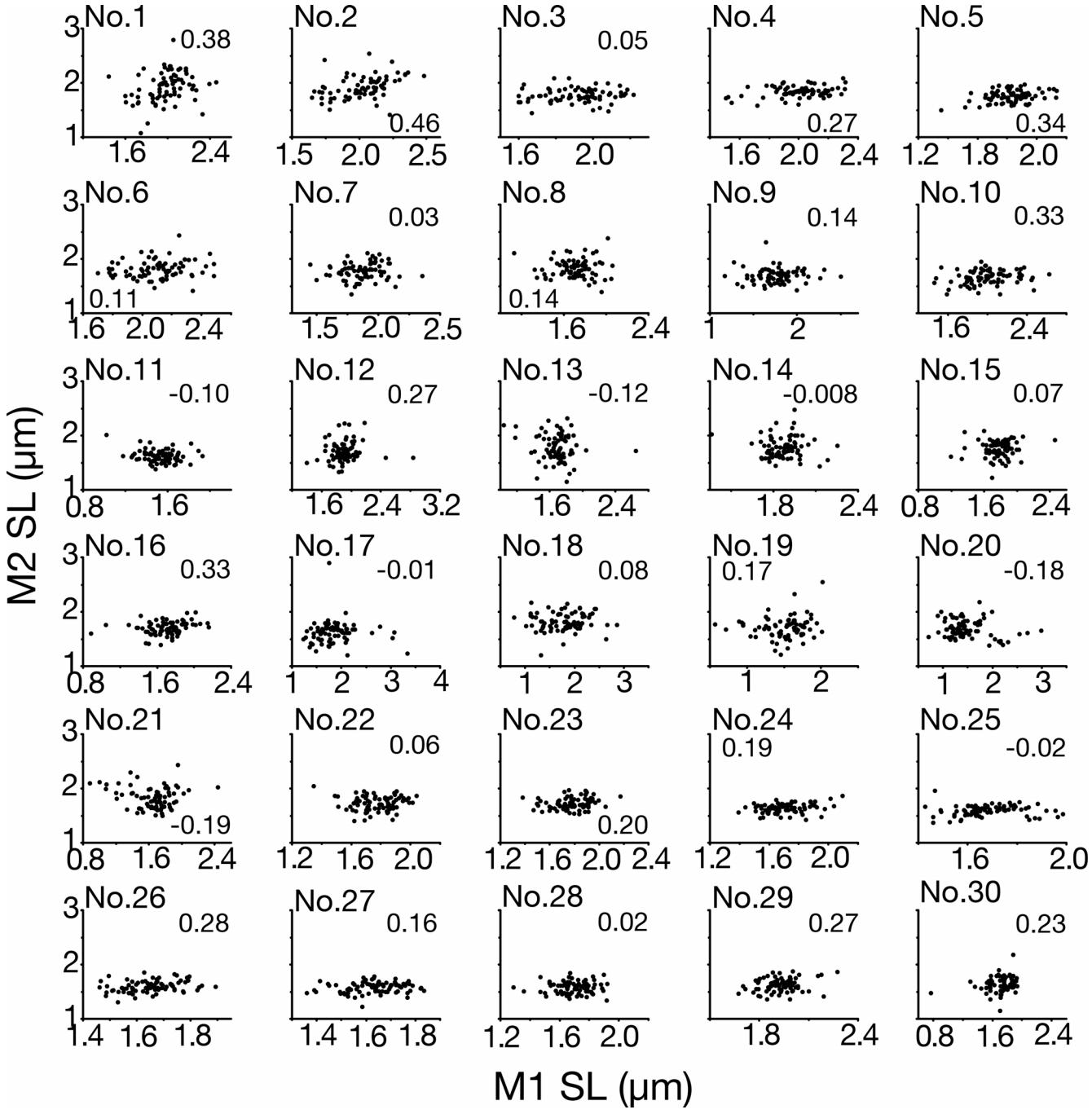

Figure S10. **Scatter plots between sarcomeres at the same longitudinal positions in neighboring myofibrils in an LV myocyte of a mouse with normal systolic function.** Data from M1 and M2 in Fig. 3 A during six cardiac cycles are shown for sarcomeres located at the same longitudinal positions (i.e., nos. 1–30; 79 plots for each sarcomere). Longitudinal position is shown on top of each graph. X axis, individual SL in M1; y axis, individual SL in M2. Number in graph indicates CI.

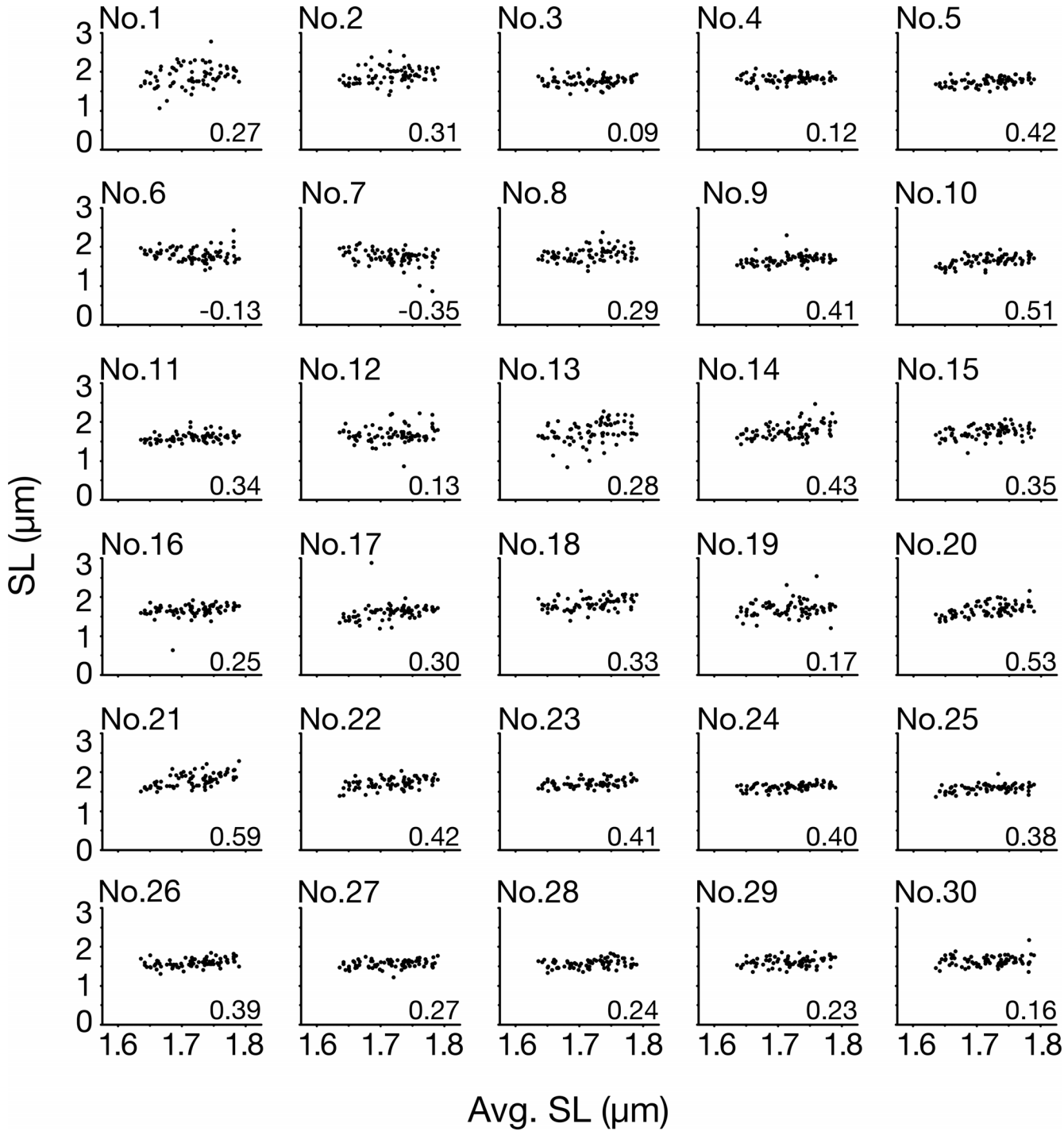

Figure S11. **Scatter plots between average and individual SLs in an LV myocyte of a mouse with normal systolic function.** Data from M2 in Fig. 3 A during six cardiac cycles are shown for sarcomere nos. 1–30 (79 plots for each sarcomere). X axis, average SL (average length of 30 sarcomeres); y axis, individual SL. Sarcomere number is shown on top of each graph. Number in graph indicates CI for each sarcomere (i.e., *R* between average and individual SL).

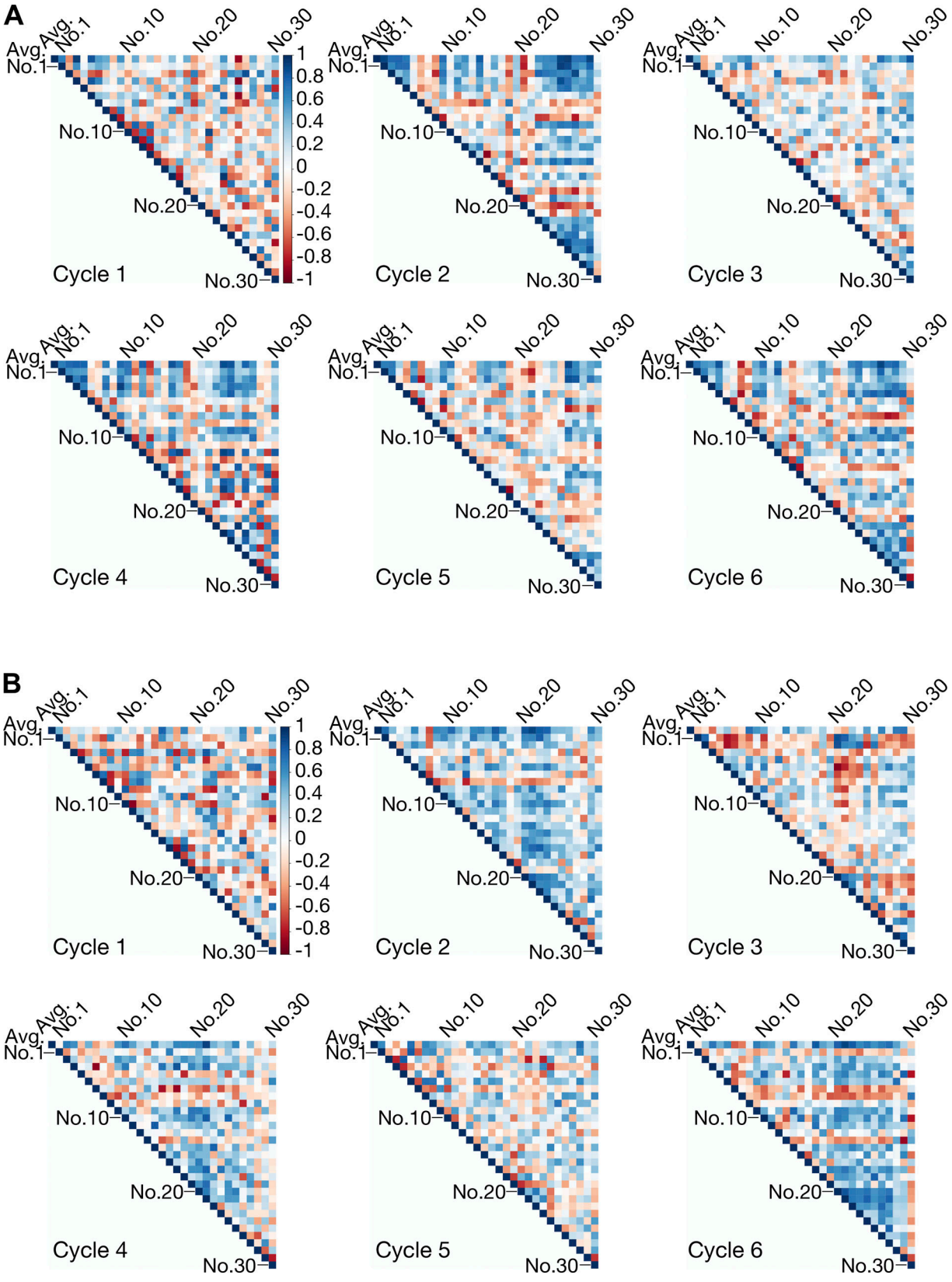

Figure S12. **Triangular heat maps showing correlation between sarcomeres during consecutive cardiac cycles in a mouse with normal systolic function. (A)** Diagrams for M1 in Fig. 3 A (and Fig. 1 A). Correlation between average and individual sarcomeres (top row) and between an individual sarcomere and other sarcomeres (second row and below) are shown. **(B)** Same as in A for M2 in Fig. 3 A. In A and B, CI is displayed on a color scale, as indicated on right (i.e., from 1 [dark blue] to −1 [dark red]), and sarcomere number (i.e., from nos. 1–30 [or average, denoted as Avg.]), as indicated on top and left, of each row. Data on six sequential cardiac cycles are shown.

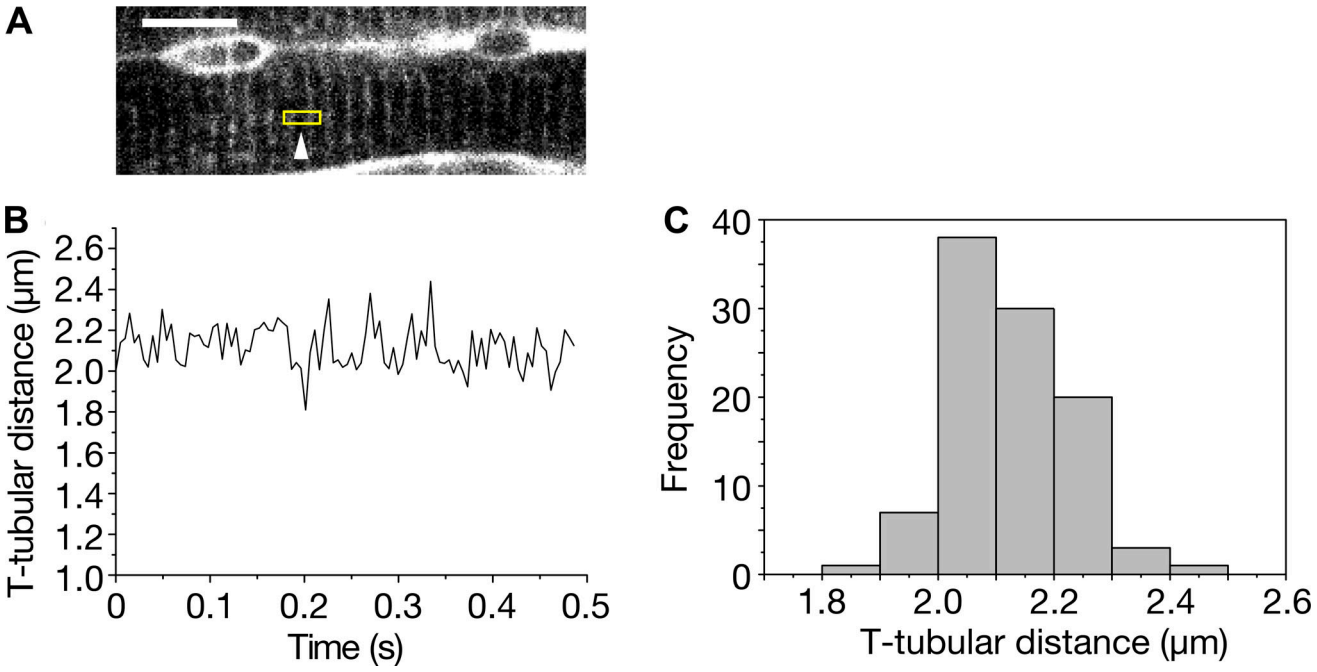

Figure S13. **Fluctuation analysis for the T-tubular distance in a myocyte in an in vivo mouse heart at rest. (A)** Confocal image showing a CellMask-treated myocyte in the left ventricle of the heart at rest in a mouse (with greater than ∼5% isoflurane). The T-tubular distance in the yellow-outlined rectangle (indicated by the arrowhead) was analyzed. Scale bar, 10 µm. See Video 5. **(B)** Time course of changes in the T-tubular distance. Imaging performed at 197 fps. **(C)** Histogram showing the variance of the T-tubular distance. Average T-tubular distance was 2.11 ± 0.11 µm, indicating that the SD (i.e., index of single T-tubular distance measurement resolution) was 110 nm.

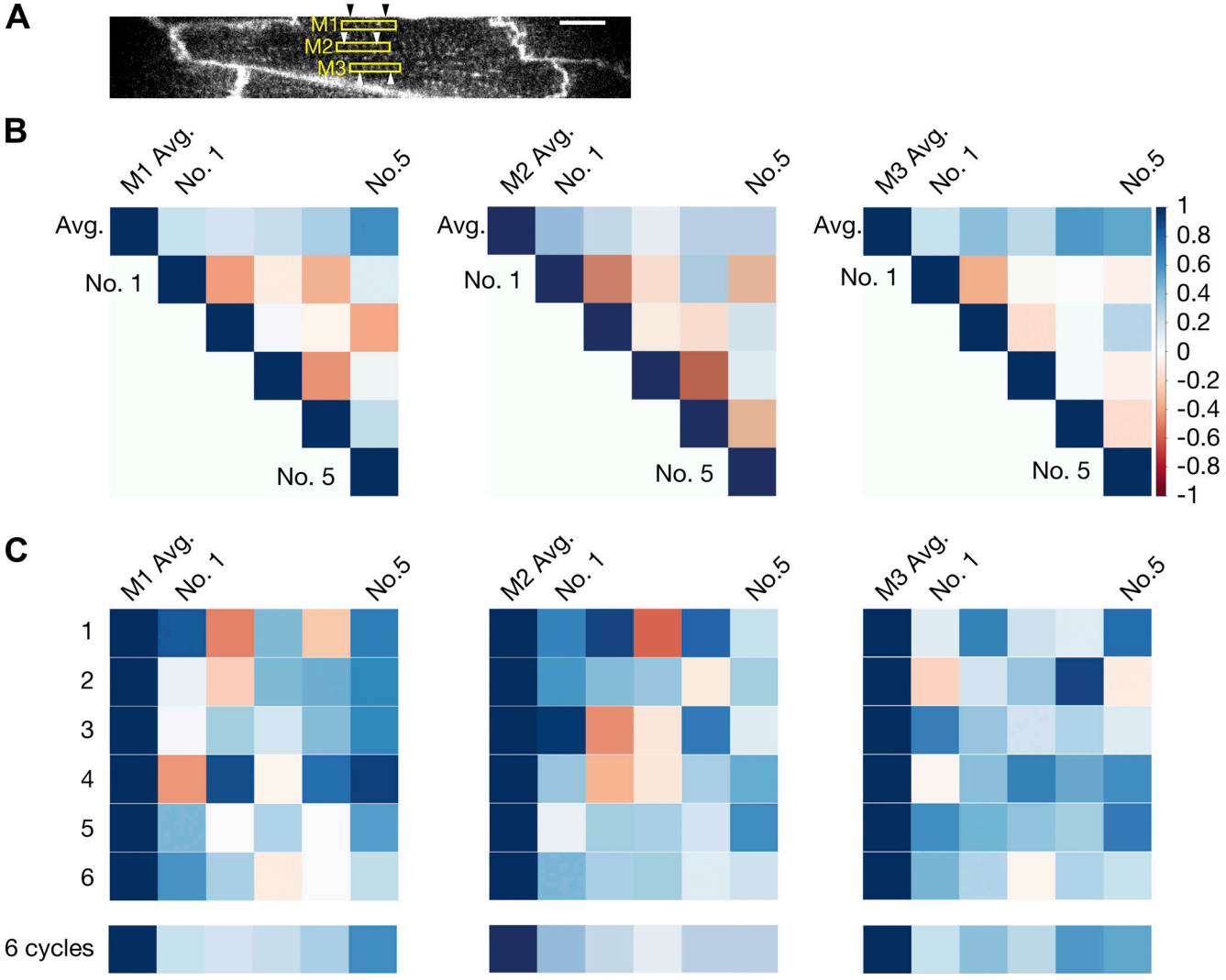

Figure S14. **In vivo analysis of individual T-tubular distances in an LV myocyte of a mouse. (A)** Confocal image of a CellMask-treated LV myocyte in a heart of a mouse. ΔLVP, 73.0 ± 0.3 mm Hg; HR, 492 ± 0.4 bpm. In three myofibrils, five sequentially connected T-tubular distances (within yellow-outlined rectangles) were analyzed (M1, M2, and M3). Arrowheads indicate T-tubule nos. 1 and 5, respectively. Scale bar, 10 µm. See Video 6. **(B)** Triangular heat maps showing correlation between average and individual T-tubular distance (top row) and between an individual T-tubular distance and others in M1 (left), M2 (middle), and M3 (right; second row and below). Numbers for T-tubular distances are indicated on top and left of each row. **(C)** Color diagram showing CI between average and individual T-tubular distances during six cardiac cycles for M1 (left), M2 (middle), and M3 (right). Cardiac cycle numbers are shown on left. Numbers for T-tubular distances, same as in B. Bottom: Average of six cycles (i.e., same as top row in B) for each myofibril. In B and C, CI is shown based on a color scale (i.e., from 1 [dark blue] to −1 [dark red]).

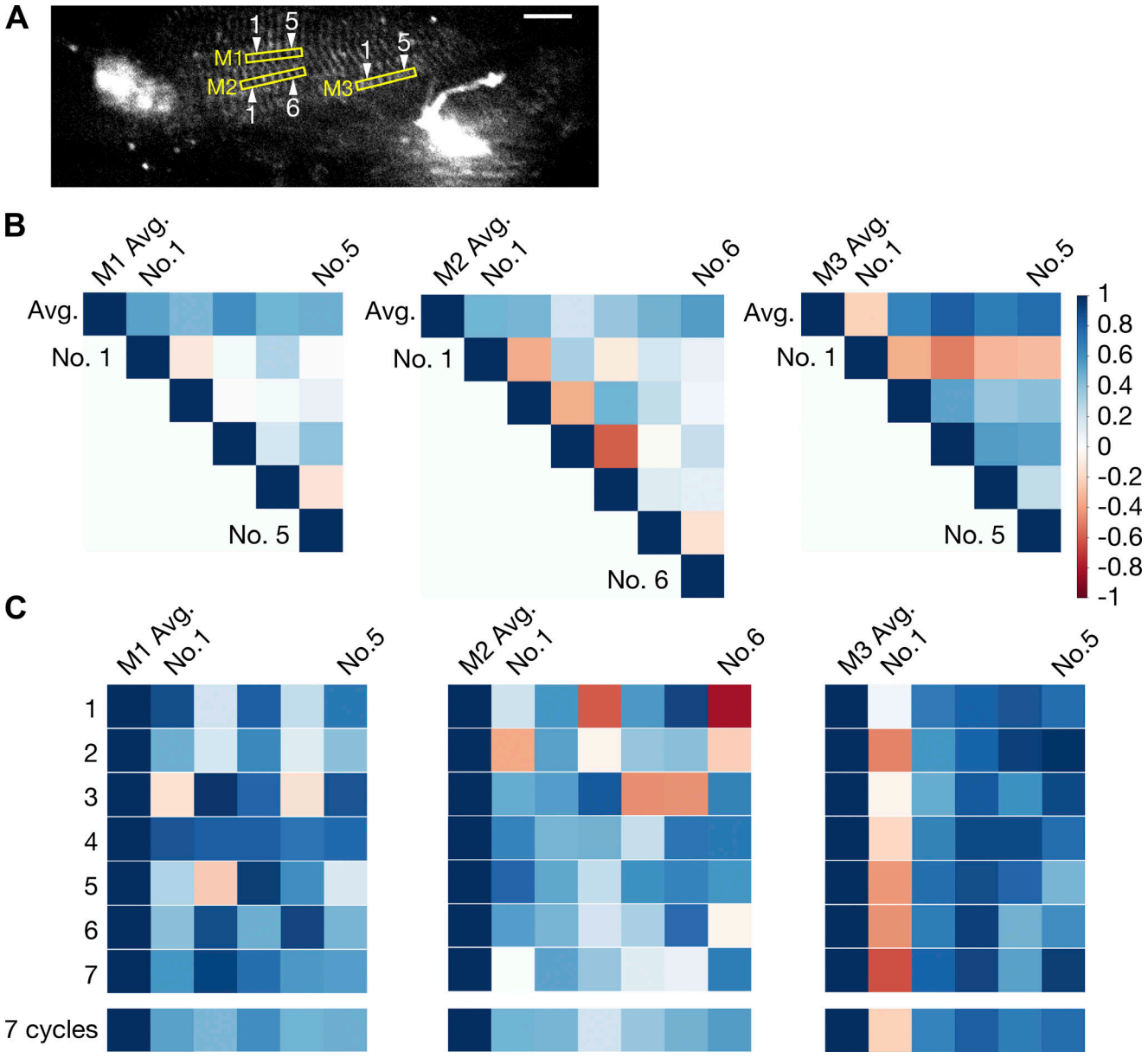

Figure S15. **In vivo tracking of individual sarcomeres along myofibrils in an LV myocyte of a mouse with high ΔLVP. (A)** Confocal image of a myocyte expressing α-actinin-AcGFP. ΔLVP, 135.7 ± 1.5 mm Hg; HR, 496 ± 0.4 bpm. Within the yellow-outlined rectangles, five, six, and five sequentially connected sarcomeres were analyzed for M1, M2, and M3, respectively. Numbers indicate longitudinal positions of sarcomeres. Left and right arrowheads indicate sarcomere nos. 1 and 5 (or 6), respectively. Scale bar, 10 µm. See Video 7. **(B)** Triangular heat maps showing correlation between average and individual SLs (top row) and between an individual sarcomere and other sarcomeres in M1 (left), M2 (middle), and M3 (right; second row and below). **(C)** Color diagram showing CI between average and individual SLs during seven cardiac cycles for M1 (left), M2 (middle), and M3 (right). Cardiac cycle numbers are shown on left. Sarcomere numbers, same as in B. Bottom: Average of seven cycles (i.e., same as top row in B) for each myofibril. In B and C, CI is shown based on a color scale (i.e., from 1 [dark blue] to −1 [dark red]).

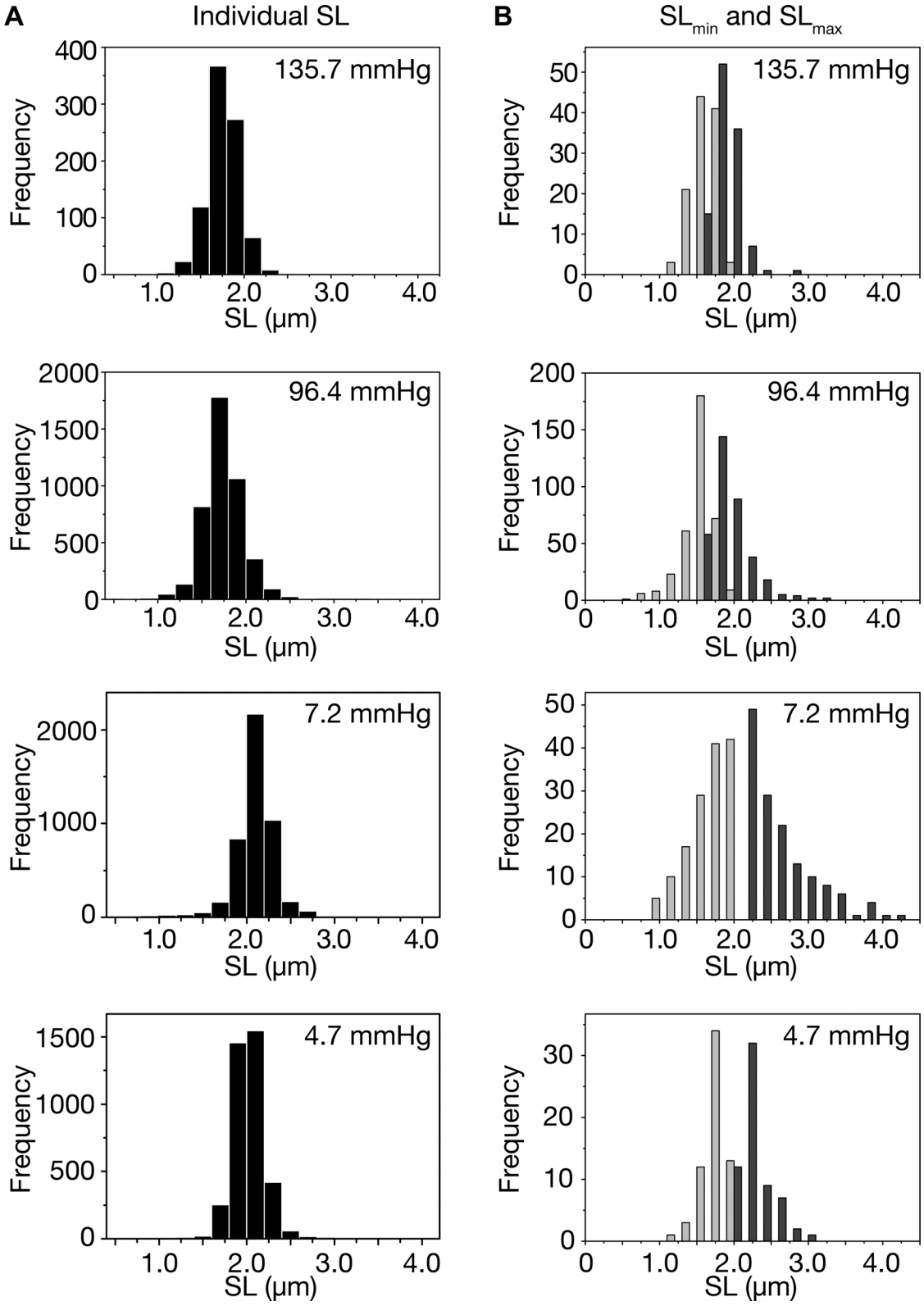

Figure S16. **Individual SL distributions in LV myocytes of mice with normal and depressed systolic functions. (A)** Histograms showing individual SL distributions in mice with ΔLVP 135.7, 96.4, 7.2, and 4.7 mm Hg (from top to bottom). SL: 1.76 ± 0.18 (Fig. S15 A), 1.74 ± 0.24 (Fig. 3 A), 2.11 ± 0.24 (Fig. 4 A, top left), and 2.03 ± 0.17 (Fig. 4 A, top right) μm for ΔLVP 135.7, 96.4, 7.2, and 4.7 mm Hg, respectively. **(B)** Same as in A, but the individual maximal SL (SL_{max}) and minimal SL (SL_{min}) data from mice with ΔLVP 135.7, 96.4, 7.2, and 4.7 mm Hg (from top to bottom) were plotted. SL_{min}, light gray; SL_{max}, dark gray. SL_{min}: 1.54 ± 0.16, 1.46 ± 0.22, 1.60 ± 0.28, and 1.67 ± 0.18 μm for ΔLVP 135.7, 96.4, 7.2, and 4.7 mm Hg, respectively. SL_{max}: 1.97 ± 0.17, 2.03 ± 0.26, 2.70 ± 0.45, and 2.37 ± 0.20 μm for ΔLVP 135.7, 96.4, 7.2, and 4.7 mm Hg, respectively. In A and B, two myofibrils were analyzed for 96.4 and 7.2 mm Hg and three myofibrils for 135.7 and 4.7 mm Hg.

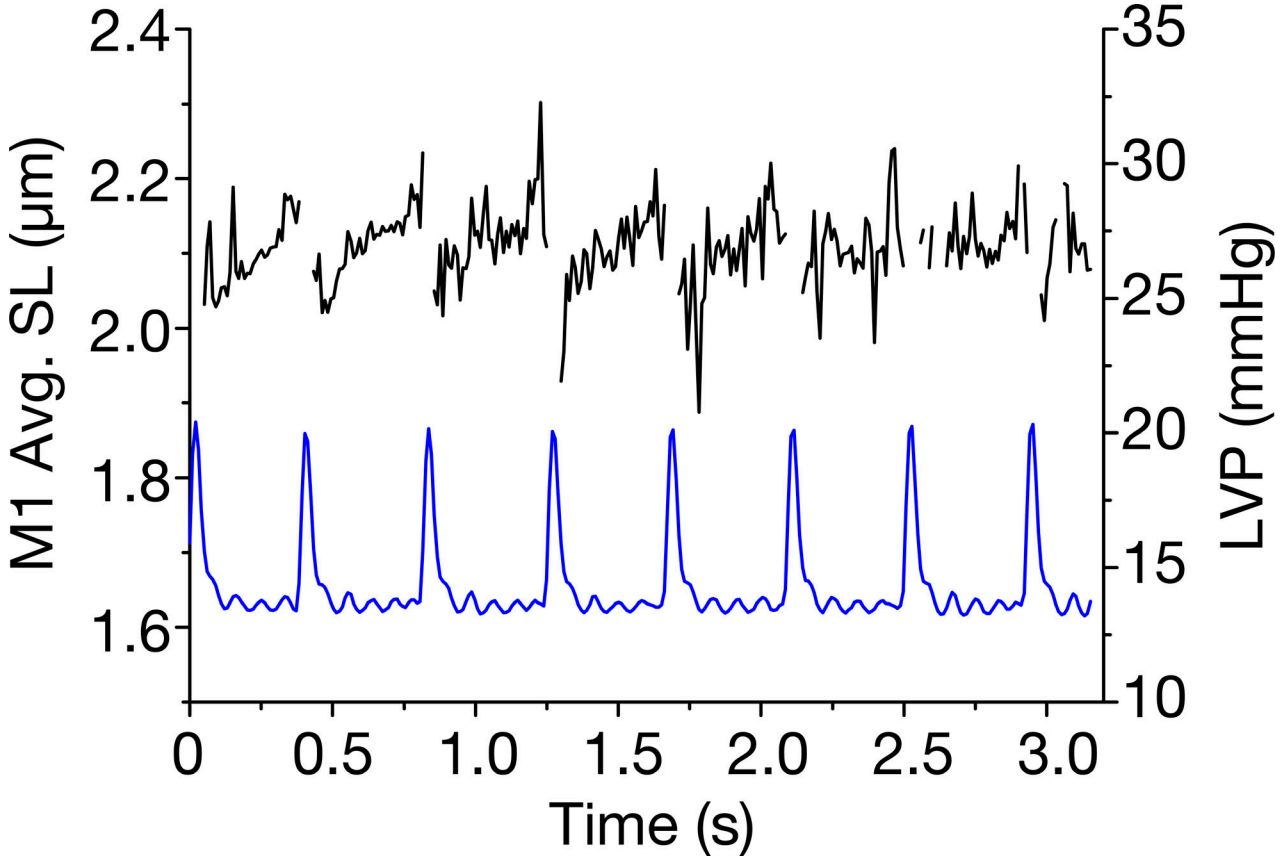

Figure S17. **Time course of changes in LVP and average SL in an LV myocyte in a mouse under deep anesthesia.** The mouse was anesthetized with ∼5% isoflurane. Black line indicates changes in the average length of nine sarcomeres in M1 (M1 Avg. SL) in Fig. 4 A, top left. Blue line indicates changes in LVP. In contrast to the mouse under normal physiological condition (ΔLVP 96.4 mm Hg), the LVP and average SL signals tended to be less coupled (compare Fig. 1 B).

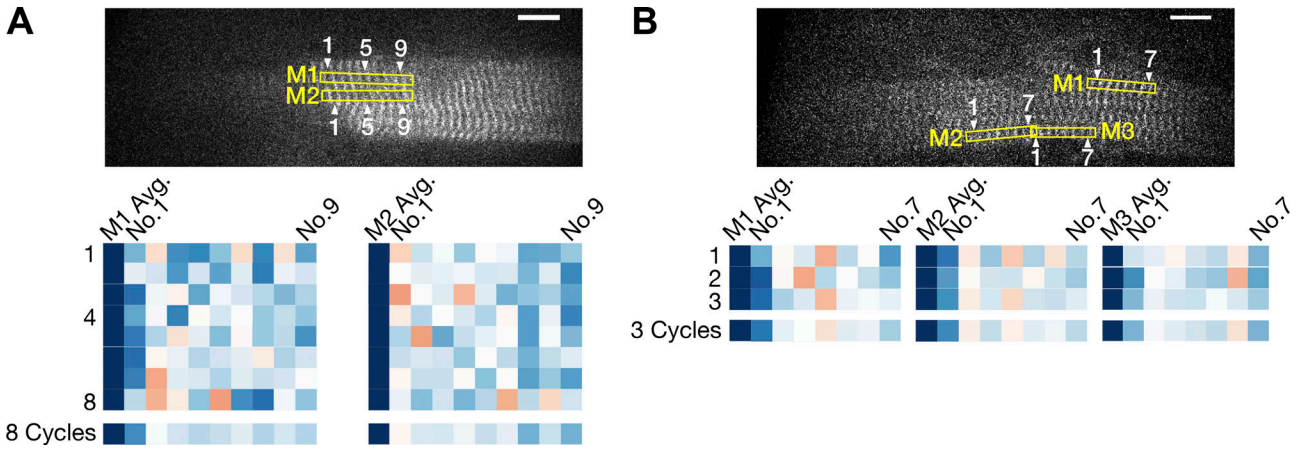

Figure S18. **In vivo tracking of individual sarcomeres in an LV myocyte of a mouse under deep anesthesia. (A)** Top: Confocal image of a myocyte expressing α-actinin-AcGFP in a mouse with ΔLVP 7.2 mm Hg. During eight cardiac cycles, ΔLVP was 7.2 ± 0.1 mm Hg, and HR was 159 ± 45.4 bpm (Table 1). In the yellow-outlined rectangle, nine sequentially connected sarcomeres were analyzed for both M1 and M2. Numbers indicate longitudinal positions of sarcomeres (i.e., nos. 1–9 for both M1 and M2). Scale bar, 10 μm. See Video 8. Bottom: Color diagram showing CI between average and individual SLs, from nos. 1 to 9, during eight cardiac cycles for M1 (left) and M2 (right). Sarcomere numbers are indicated on top and cardiac cycle numbers on left. Data on the average of eight cycles are shown on bottom. **(B)** Top: Same as in A, in a mouse with ΔLVP 4.7 mm Hg. During three cardiac cycles, ΔLVP was 4.7 ± 0.2 mm Hg, and HR was 80 ± 14.2 bpm (Table 1). In the yellow-outlined rectangle, seven sequentially connected sarcomeres were analyzed for M1, M2, and M3. Numbers indicate longitudinal positions of sarcomeres (i.e., nos. 1–7 for M1, M2, and M3). Scale bar, 10 μm. See Video 9. Bottom: Color diagram showing CI between average and individual SLs, from nos. 1 to 7, during three cardiac cycles for M1 (left), M2 (middle), and M3 (right). Sarcomere numbers are indicated on top and cardiac cycle numbers on left. Data on the average of three cycles are shown on bottom. Arrowheads (with numbers) indicate longitudinal positions of sarcomeres.

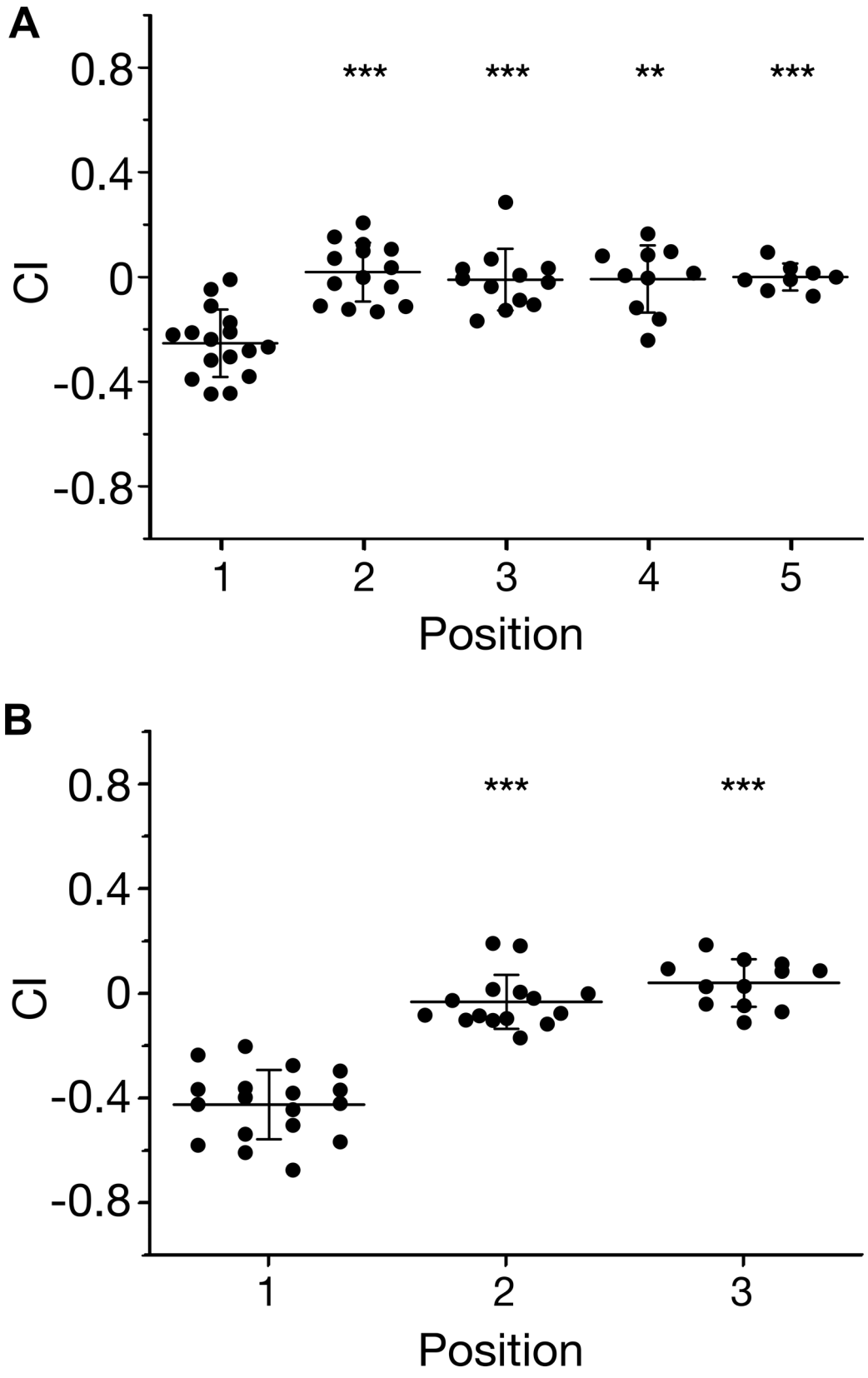

Figure S19. **Interplay between sarcomeres connected in series in an LV myocyte of a mouse under deep anesthesia. (A)** Graph showing CI for sarcomeres located at positions 1–5 in a mouse with ΔLVP 7.2 mm Hg. Data from M1 and M2 in Fig. S18 A were pooled. Horizontal bars, average; vertical bars, SD. **, P < 0.01; and ***, P < 0.001 compared with position 1. **(B)** Same as in A for sarcomeres located at positions 1–3 in a mouse with ΔLVP 4.7 mm Hg. Data from M1, M2, and M3 in Fig. S18 B are pooled. Horizontal bars, average; vertical bars, SD. ***, P < 0.001 compared with position 1. In A and B, sarcomeres at position 1 are adjacent to the ones at position 0. See Fig. 3 F for sarcomere geometry.

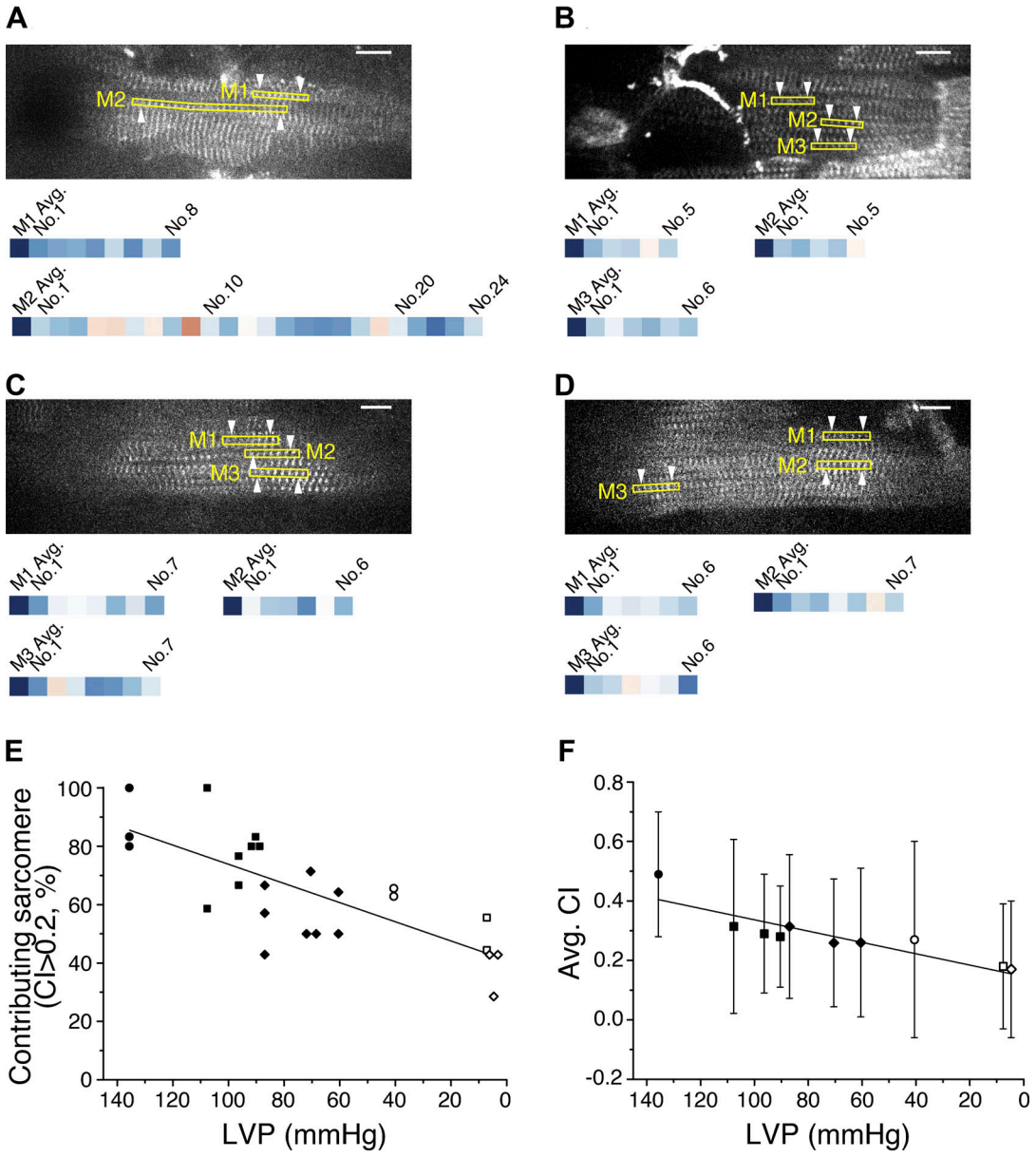

Figure S20. **In vivo tracking of individual sarcomeres along myofibrils in LV myocytes of mice at various systolic states. (A)** Top: Confocal image of a myocyte expressing α-actinin-AcGFP in the left ventricle of a mouse at ΔLVP 107.7 mm Hg (same myocyte as in Figs. 1 A and 3 A). Within the yellow-outlined rectangles, 8 and 24 sequentially connected sarcomeres were analyzed for M1 and M2, respectively. Left and right arrowheads indicate sarcomere nos. 1 and 8 (or 24), respectively. Bottom: Color diagram showing CI between average and individual SLs during six cardiac cycles for M1 and M2. Average of six cycles is shown. **(B)** Top: Same as in A, with ΔLVP at 90.4 mm Hg (~0.5 mm distal to the myocyte in A from the same mouse). Within the yellow-outlined rectangles, five, five, and six sequentially connected sarcomeres were analyzed for M1, M2, and M3, respectively. Arrowheads indicate sarcomere nos. 1 and 5 (or 6), respectively. Bottom: Same as in A, during six cardiac cycles for M1, M2, and M3. Average of six cycles is shown. **(C)** Confocal image of a myocyte expressing α-actinin-AcGFP in the left ventricle of a mouse at ΔLVP 87.2 mm Hg (~0.5 mm distal to the myocyte shown in Fig. S6 A). Within the yellow-outlined rectangles, seven, six, and seven sequentially connected sarcomeres were analyzed for M1, M2, and M3, respectively. Arrowheads indicate sarcomere nos. 1 and 7 (or 6), respectively. Bottom: Color diagram showing CI between average and individual SLs during seven cardiac cycles for M1, M2, and M3. Average of seven cycles is shown. **(D)** Same as in Cat ΔLVP 70.5 mm Hg (~0.5 mm distal to the myocyte in C or that in Fig. S6 A from the same mouse). Within the yellow-outlined rectangles, six, seven, and six sequentially connecting sarcomeres were analyzed for M1, M2, and M3, respectively. Arrowheads indicate sarcomere nos. 1 and 6 (or 7), respectively. Bottom: Same as in C, during eight cardiac cycles for M1, M2, and M3. Average of eight cycles is shown. In A–D, CI is shown based on a color scale (i.e., from 1 [dark blue] to −1 [dark red]). Scale bars, 10 µm. **(E)** Relationship between ΔLVP and the fraction of contributing sarcomeres in myofibrils from mice at various ΔLVP values. Closed circles, myofibrils in Fig. S15 A (135.7 mm Hg); closed squares, myofibrils in A (107.7 mm Hg), Fig. 3 A (96.4 mm Hg) and B (90.4 mm Hg); closed diamonds, myofibrils in C (87.2 mm Hg) and D (70.5 mm Hg) and Fig. S6 A (60.5 mm Hg); open circles, myofibrils in Fig. S6 B (40.6 mm Hg); open squares, myofibrils in Fig. S18 A (7.2 mm Hg); open diamonds, myofibrils in Fig. S18 B (4.7 mm Hg). Contributing sarcomeres are defined as those with CI >0.2 in the average data of three to eight cardiac cycles. A significant linear relationship was observed (R = 0.75; $P < 0.001$). **(F)** Relationship between ΔLVP and the average values of CI (Avg. CI) in myofibrils from mice with various ΔLVP values. Symbols, same as in E. Error bars indicate SD of Avg. CI (compare Fig. 4 D). A significant linear relationship (R = 0.89; $P < 0.001$) was observed. In E and F, two myofibrils were analyzed for ΔLVP 107.7, 96.4, 60.5, 40.6, and 7.2 mm Hg, and three myofibrils were analyzed for 135.7, 90.4, 87.2, 70.5, and 4.7 mm Hg (see above for corresponding figures).

Video 1. **Image sequence of a myocyte in the left ventricle of a mouse at rest.** A myocyte expressing α-actinin-AcGFP in the central part of the left ventricle was imaged (see Fig. S3 A). Scale bar, 10 µm. Imaging performed at 100 fps.

Video 2. **Image sequence of a myocyte in the left ventricle of a mouse with normal systolic function.** ΔLVP 96.4 mm Hg. A myocyte expressing α-actinin-AcGFP in the central part of the left ventricle was imaged (see Figs. 1 A and 3 A and Table 1). Scale bar, 10 µm. Imaging performed at 100 fps.

Video 3. **Image sequence of a myocyte in the left ventricle of a mouse with low systolic function.** ΔLVP 60.5 mm Hg. A myocyte expressing α-actinin-AcGFP in the central part of the left ventricle was imaged (see Fig. S6 A and Table 1). Scale bar, 10 µm. Imaging performed at 100 fps.

Video 4. **Image sequence of a myocyte in the left ventricle of a mouse with low systolic function.** ΔLVP 40.6 mm Hg. A myocyte expressing α-actinin-AcGFP in the central part of the left ventricle was imaged (see Fig. S6 B and Table 1). Scale bar, 10 µm. Imaging performed at 100 fps.

Video 5. **Image sequence of a CellMask-stained myocyte in the left ventricle of a mouse at rest.** A CellMask-stained myocyte in the central part of the left ventricle was imaged (see Fig. S13 A). Scale bar, 10 µm. Imaging performed at 197 fps.

Video 6. **Image sequence of a CellMask-stained myocyte in the left ventricle of a mouse.** ΔLVP 73.0 mm Hg. CellMask-stained myocyte in the central part of the left ventricle was imaged (see Fig. S14 A and Table S3). Scale bar, 10 µm. Imaging performed at 197 fps.

Video 7. **Image sequence of a myocyte in the left ventricle of a mouse with high systolic function of ΔLVP 135.7 mm Hg.** Myocyte expressing α-actinin-AcGFP located in the central part of the left ventricle was imaged (see Fig. S15 A and Table 1). Scale bar, 10 µm. Imaging performed at 100 fps.

Video 8. **Image sequence of a myocyte in the left ventricle of a mouse under deep anesthesia with ΔLVP 7.2 mm Hg.** Myocyte expressing α-actinin-AcGFP located in the central part of the left ventricle was imaged (see Figs. 4 A and S18 A and Table 1). Scale bar, 10 µm. Imaging performed at 100 fps.

Video 9. **Image sequence of a myocyte in the left ventricle of a mouse under deep anesthesia with ΔLVP 4.7 mm Hg.** Myocyte expressing α-actinin-AcGFP located in the central part of the left ventricle was imaged (see Figs. 4 A and S18 B and Table 1). Scale bar, 10 µm. Imaging performed at 100 fps.

Provided online are four tables. Table S1 summarizes echocardiographic data of mice with and without the first open-chest surgery. Table S2 summarizes the average values of CI in sequential cardiac cycles under various contractile conditions. Table S3 summarizes CI, LVP, and HR with CellMask treatment. Table S4 summarizes CI, LVP, and HR under physiological and near-physiological contractile conditions.